Quantitative analysis of incorporation dynamics of conserved centriole proteins in *Drosophila* early embryos

MSc By Research Molecular Cell Biology in Health and Disease

Tess Harrison

St Cross College

Contents

Abstract

To divide efficiently, cells of animals and many other higher eukaryotes, rely upon centrosomes to help nucleate the bipolar mitotic spindle. At each division, two centrosomes are required, such that one centrosome is ultimately inherited by each daughter cell. Consequently, centrosomes must duplicate precisely once during each cycle of cell division. At the core of each centrosome is a mother centriole that can duplicate by growing a new daughter centriole off its side, which will later mature into a mother and nucleate its own centrosome. The core components of the centriole are highly conserved across higher eukaryotes, despite this there is still a lack of detail regarding their function and their hierarchy of assembly.

In this thesis, I perform a comparative analysis of the incorporation dynamics of several conserved centriole proteins, using both standard and super-resolution microscopy, and the *Drosophila* early embryo as a model. I show that the daughter centrioles in the *Drosophila* early embryo appear to begin assembling earlier than previously reported. Further, I provide evidence that several core centriole proteins may be recruited into a transient centrosomal primordial "soup" in addition to the centriole proper. In addition, I refine the order of assembly of the centriole - allowing incorporation of Sas-6, Ana2, Ana3, CEP135, Ana1 and Asl to be placed on a continuous timeline alongside the cell cycle. Finally, through the use of CEP135 mutants, I show that, CEP135 does not appear to be necessary to recruit Ana1 into centrioles, in contrast to previous findings.

In summary, my work redefines the initial incorporation dynamics of centriole assembly, challenging several previous assumptions and providing new avenues for interrogation of the specific functions of the core centriole proteins.

Abbreviations

Asl – Asterless

FRAP – Fluorescence recovery after photobleaching

GFP – Green fluorescent protein

M/A – Metaphase/Anaphase Transition

MCPH - Autosomal recessive primary microcephaly

MT – Microtubule

MTOC – Microtubule Organising Centre

NEB – Nuclear Envelope Breakdown

NG – mNeonGreen

PCM – Pericentriolar material

PLK – polo-like kinase

Chapter 1: Introduction

Cell division is a key process in the development and maintenance of multicellular organisms. In animals, efficient cell division relies on the coordination of two centrosomes acting as microtubule organising centres (MTOCs). The core of a centrosome contains a mother centriole, structural centriolar microtubules (MTs), and a growing daughter centriole. The mother centriole links to an extended scaffold which in turn recruits pericentriolar material (PCM). PCM provides function to the centrosome, through PCM client proteins which enable centrosomal functions such as nucleating and organising the mitotic spindle (*Figure 1.1*) [1]. Both the number of centrosomes and the amount of PCM must be tightly regulated such that cell division remains bipolar and symmetric [1,2]. As cells go through division, to maintain the number of centrosomes, more centrioles must be assembled. This assembly must be coordinated with the cell cycle, as to be ready for further division. Furthermore, the length of the

centriole is thought to define the number of PCM scaffold proteins that can directly bind, thus the amount of PCM that can be recruited total [2–4]. Overall, this sets up centriolar assembly as a process of high regulatory and biological significance in dividing cells and developing organisms.

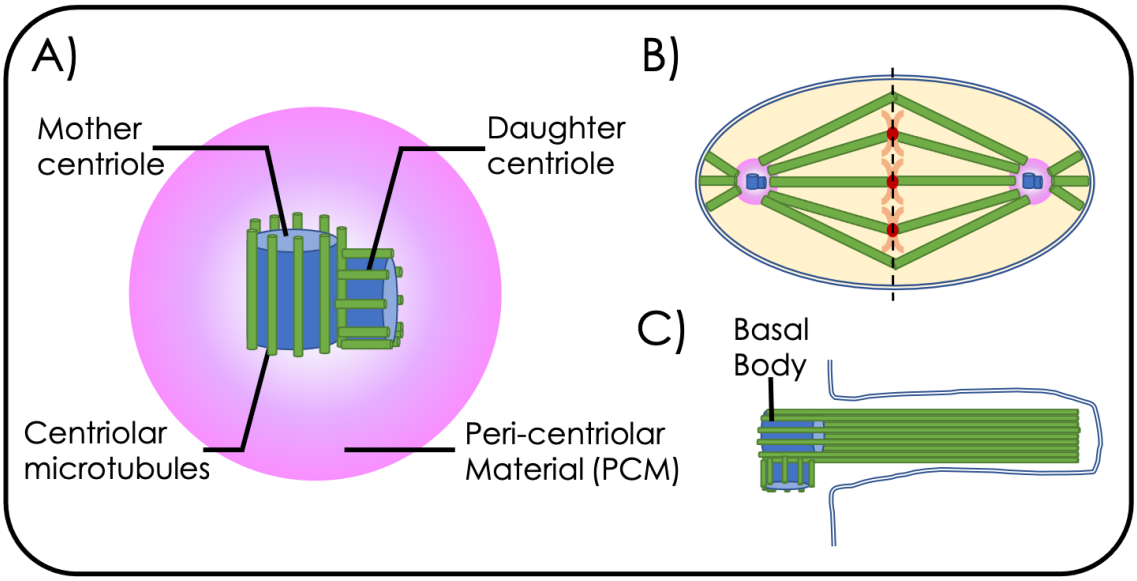

Figure 1.1: Centrosome Gross Structure and Related Functions A) The gross structure of the centrosome. At the core of the centrosome is formed of a mother centriole, surrounded by 9-fold radially symmetric centriolar microtubules. A daughter centriole is grown, alongside its microtubules, perpendicularly from the mother. Peri-centriolar material is recruited by the mother to in turn recruit client proteins allowing centrosome function. B) The roles of the centrosome in generating the mitotic spindle. As the cell divides, the centrosome organises microtubules to align chromosomes then separate sister chromatids across the metaphase plate (dashed line), enabling efficient, reliable segregation of DNA into daughter cells. C) A basal body, formed from a centriole pair, found at the proximal end of cilia. The centriolar microtubules from the mother extend into the cilia, providing structure and the substrate for locomotion

1.1 The Life Cycle of the Centrosome

The duplication of the centrosome is coordinated with the cell cycle (*Figure 1.2*) and highly conserved across the animal kingdom[5,6]. Following cell division, each new daughter cell begins with a pair of centrioles consisting of a mother and a daughter, originating from the centrosome at its respective spindle pole. Within the daughter cell, these

centrioles disengage and the daughter is converted to a new-mother, which can then recruit PCM to become another centrosome [1]. During interphase, depending on cell type, centrosomes recruit relatively little PCM [1]. As a cell moves into S-phase, polo-like kinase 4 (PLK4; aka Sak), accumulates on the mother centriole and symmetry breaks forming a single focus on the side at the proximal end (*Figure 1.3)* [7,8]. Activated PLK4 then phosphorylates STIL/Ana2 (Humans/*Drosophila*) to enable its oligomerisation with Sas-6 and the assembly of a Sas-6/Ana2 central cartwheel, perpendicular to the mother, forming the centre of the growing daughter centriole [9,10]. An additional set of conserved proteins are then incorporated around the central cartwheel, including: CPAP/SAS4, CEP135, CEP295/Ana1, Rotatin/Ana3, PPP1R35/Rcd4 (Humans/*Drosophila*) [11–23]. As the cells prepare to enter mitosis, the centrosomes undergo PCM expansion where, through the activity of PLK1/Polo (Humans/*Drosophila*), further PCM scaffold is recruited to mother centrioles and the overall PCM swells to allow nucleating of the mitotic spindle [19,24,25]. The centrosomes then begin to migrate to opposing sides of the nucleus where they develop spindles and position themselves with respect to the axis of division [26,27]. As mitosis comes to an end, two major centriolar events occur: the mother and daughter centrioles disengage, and the daughter begins recruitment of CEP152/Asl (Humans/*Drosophila*) [1,12]. These events mark the conversion of the

daughter to a new-mother, licencing it to be able to both recruit PCM and grow its own daughter [1,12]. In humans this event is further punctuated by the central STIL/Sas-6 cartwheel being lost. Overall, this results in a pair of centrioles present at both spindle poles, so that both daughter cells inherit a single centrosome containing two centrioles.

Outside of roles in centrosomes, centrioles are also used in the formation of cilia, where they form basal bodies. In this case centrioles migrate to the cell cortex and their inner doublet/doublet (human/*Drosophila)* centriolar MTs extend to form the microtubule structure forming the axoneme of the cilia[28,29]. Interestingly, some evidence suggests basal bodies may not be essential for the prolonged stability of cilia, as CEP135 mutant *Drosophila* show phenotypically functional cilia yet can be observed lacking associated basal bodies[17]. Centriole conversion to cilia is particularly prevalent in mammals, where in quiescent cells are further 'locked' from division by the sequestering of their centrioles as a basal body in primary cilia[29]. Furthermore, highly ciliated cells can utilise alternative centriole assembly pathways, using the same conserved proteins, to acquire the number of basal bodies required[30,31].

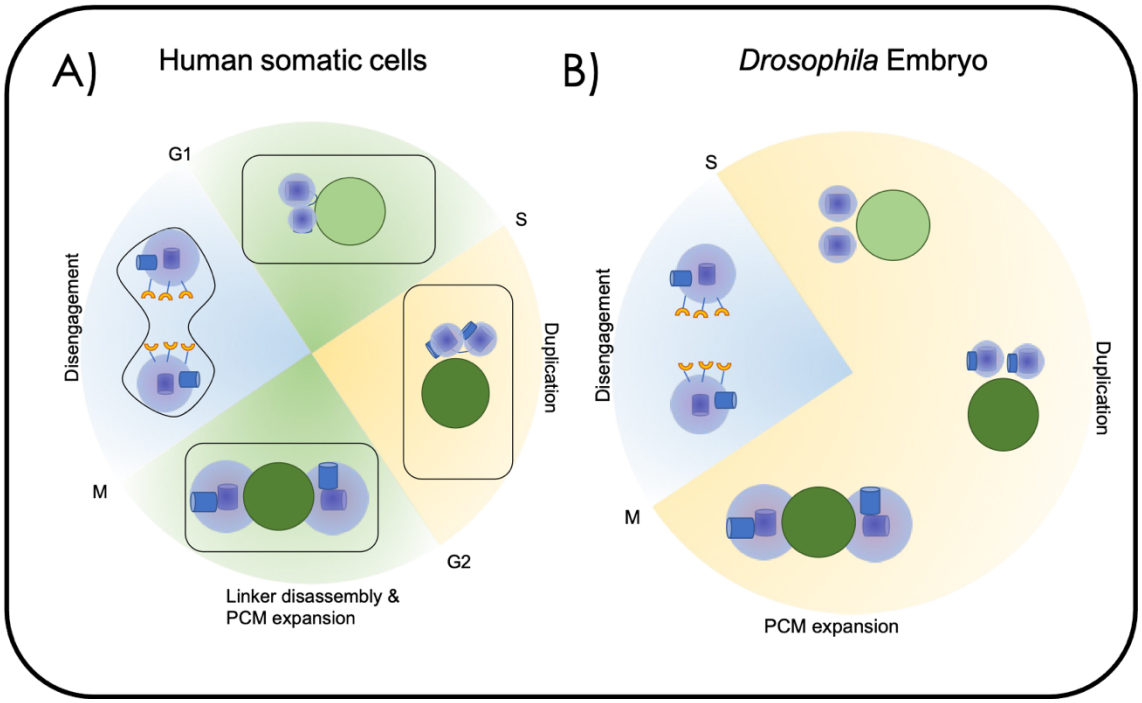

Figure 1.2: The Centrosome through the Cell Cycle *A) Centrosomes in human somatic cells. Cells enter the cell cycle with two centrosomes, each containing a mother centriole nucleating interphase PCM. As cells move into S-phase the mother centrioles ,within centrosomes, each begin to grow a daughter centriole off their side. Before entering mitosis, the mother centrioles expand their PCM to the full mitotic PCM capable of organising the spindle. At the same time the two centrosomes migrate to either side of the nucleus, where they will form spindle poles. Through mitosis the two centrosomes lead the sister chromatids to segregate into either daughter cell. At each pole, the daughter centriole disengages from its mother and is converted to a new-mother, allowing it to recruit PCM and form a centrosome. At this point each daughter cell contains two centrosomes, one with the new-mother, the other with the old, both competent to grow new daughters and carry on the cycle. B) Centrosomes in Drosophila early embryos. In the early embryo the cell cycle lacks G1 and G2 phases, instead being divided into S-phase where centriole growth is permitted and a restricted M-phase which prevents centriole assembly. Upon exiting mitosis, the old and new-mother rapidly split and distance themselves, both nucleating relatively small interphase PCM. Both mother centrioles rapidly assemble new daughters during the S-permissive phase. Before mitosis, PCM expansion occurs and both centrioles move to poles. In mitosis a mitotic spindle is generated and chromosomes are separated, shortly after centrioles separate and the cycle continues.*
Adapted from [1]

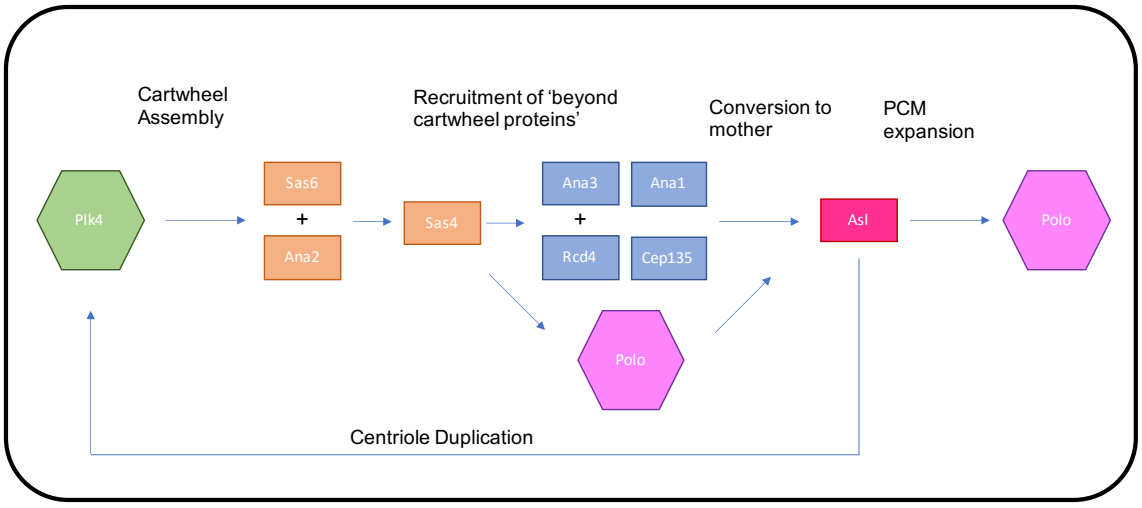

Figure 1.3: The Conserved Pathway of Centriole Assembly in Drosophila *The growth of a new centriole is initiated by recruitment of Plk4 to mother centrioles by Asl* [7,9]. *Plk4 then phosphorylates Ana2, allowing oligomerisation of Sas6 and Ana2 to form a central cartwheel* [9,10]. *This leads to the recruitment of further proteins: Sas4, Ana3, Rcd4, Ana1 and Cep135* [16,18–21,32]. *Ana1 and the polo recruitment of Sas4, recruit Asl to the centriole finalising its conversion to a new-mother* [12,18]. *Once a new-mother, it can recruit Plk4 to further duplicate and Polo to recruit and expand its PCM* [19,33].

1.2 Centriole Assembly in Disease

Defects in centriole assembly in humans are most notably genetically linked to developmental diseases such as autosomal recessive primary microcephaly (MCPH) and dwarfism (*Table 1.1*). MCPH is characterised by significantly smaller heads and brains at birth, caused by a reduction of neuronal progenitor cells (NPCs) during development [34,35]. Investigating centriole defects in MCPH has an extra level of difficulty, as NPCs are affected both by their ability to divide, but also heavily rely upon cilia, for which structural defects in basal bodies formed from centrioles have been shown to affect both neuronal survival and development, thus convoluting the picture [36,37]. Defects in centriole proteins, such as the mutation of CEP63 or deletion of Sas4 prolong mitoses of NPCs, which can

then trigger the 53BP1-US28-P53 surveillance pathway, leading to increased apoptosis directly reducing NPC numbers, and later cranial mass [38]. Interestingly, overactive centriole assembly can also have a microcephaly phenotype from loss of neural stem cells (NCSs). This can occur following PLK4 overexpression induced centriole/centrosome amplification resulting in multi-polar cell division producing aneuploid progeny unable to further proliferate or differentiate, often dying shortly after [39]. Aneuploidy mechanisms also link to primary dwarfisms such as Seckel syndrome, where defects in either CPAP and CEP152 can result in increased frequencies of multipolar spindles and aneuploidy, again leading to premature cell death [40,41].

Table 1.1: Overview of molecular roles and disease phenotypes associated with core centriole proteins

HUMAN GENE	DROSOPHILA GENE	FUNCTION	DISEASE PHENOTYPES	REFERENCES
SAS-6	Sas-6	Central cartwheel	Microcephaly	[42–44]
STIL	Ana2	Central cartwheel	Microcephaly	[15,45–47]
CPAP	Sas4	Structural stabilisation, potential connection to integral MTs, cilia	Microcephaly, Dwarfism (Seckel Syndrome)	[14,41,48–52]
CEP135	CEP135	Centriole structure, stability, cilia	Microcephaly, Subcortical heterotopia	[16,17,53–55]
ROTATIN	Ana3	Centriole structure, cilia	Microcephaly, intellectual disability, cerebral microgyria, dwarfism	[21,56–59]
PPP1R35	Rcd4	Centriole structure, cilia	Microcephaly, ciliopathies	[21,59]
CEP152	Asl	Centriole structure, daughter-mother conversion, daughter growth	Microcephaly, Dwarfism (Seckel Syndrome)	[40,60,61]

Centriole assembly has long been a topic of interest in cancer biology. This initially came from the potential of centrosome amplification to lead to genome instability following multipolar divisions [62]. This initial theory is controversial as cancerous transformation following centriole amplification appears inconsistent depending on tissue and the status of P53 [39,63,64]. This scepticism is furthered by the evidence supporting centrosome amplification induced cell death as a mechanism for dwarfism/microcephaly, suggesting cell death as a more likely outcome than the unregulated propagation innate to cancers [39–41]. More promising theories linking centriole assembly to cancers involve the cell trying to rescue itself from exhibiting multipolar spindles by clustering its centrosomes [65]. In this case, the cell can end up with different numbers of centrosomes and thus different amounts of PCM at each spindle pole, leading to asymmetric dysregulated spindles. Aberrant spindles, may fail to equally or sufficiently pull their respective chromosomes, this can lead to segregation defects such as aneuploidies or damage due to chromatids being trapped in the cleavage furrow [66,67]. Spindle dysregulation can also disrupt canonical asymmetric divisions, in the *Drosophila* neuroblast this prevents proper differentiation away from proliferative tissue, which can lead to tumour formation [68,69]. Despite this, centriole assembly has remained an active area in cancer biology, however, instead as a drug target. Due to its significant role in mitosis, drugs have been developed targeting key centrosomal kinases such as

AuroraA or PLK1, inhibiting the growth and maturation of centrioles with the intention to cause mitotic delay, arrest, or apoptosis [35,70].

1.3 Centriole Structure and Assembly

Centriole structure is highly conserved across species, relying on a consistent conserved core of proteins in higher mammals such as humans, insects such as *Drosophila*, and protoctists such as *Paramecium* [5,6,71]. In a simplified view, the centrosome can be split into three zones [1,72]: the innermost centriole central cartwheel, a wide outer zone of PCM and associated scaffold proteins, then stretching the gap between these an intermediary zone of "beyond the cartwheel" centriole proteins (*Figure 1.4*). The central cartwheel is the first part to be assembled containing Sas-6, STIL/Ana2 and CPAP/Sas4, forming the critical initial scaffold upon which the rest of the centriole is built [1,3,73]. The central cartwheel then defines the gross architecture for the remainder of the centriole, defining the 9-fold radial symmetry characteristic of mammalian and *Drosophila* centrioles [3,44,74,75]. While assembly of the central cartwheel has been widely studied, our knowledge of the function and incorporation dynamics of the beyond the cartwheel zone remains rudimentary. Of note is the further subdivision of conserved beyond the cartwheel proteins into two modules. First, CEP135, CEP295/Ana1 and CEP152/Asl extend to form radial spokes in-phase with the symmetry of the cartwheel. Spatially these are arranged inside to outside CEP135-CEP295/Ana1-CEP152/Asl and as

such have been suggested to be key to the maturation of the centriole towards motherhood, bridging to the PCM and daughter assembly [32,33,72,76–78]. In addition, this axis may be involved in connecting the centriolar MTs to the centriole, as will be discussed later [72]. The second module consists of Rotatin/Ana3 and PPP1R35/Rcd4, these are thought to be found further towards the distal pole of the centriole while maintaining similar but out of phase symmetry with respect to the central cartwheel [20,21,72]. The Ana3-Rcd4 module has primarily been suggested to stabilise the cartwheel and is potentially required for Ana1 loading [21].

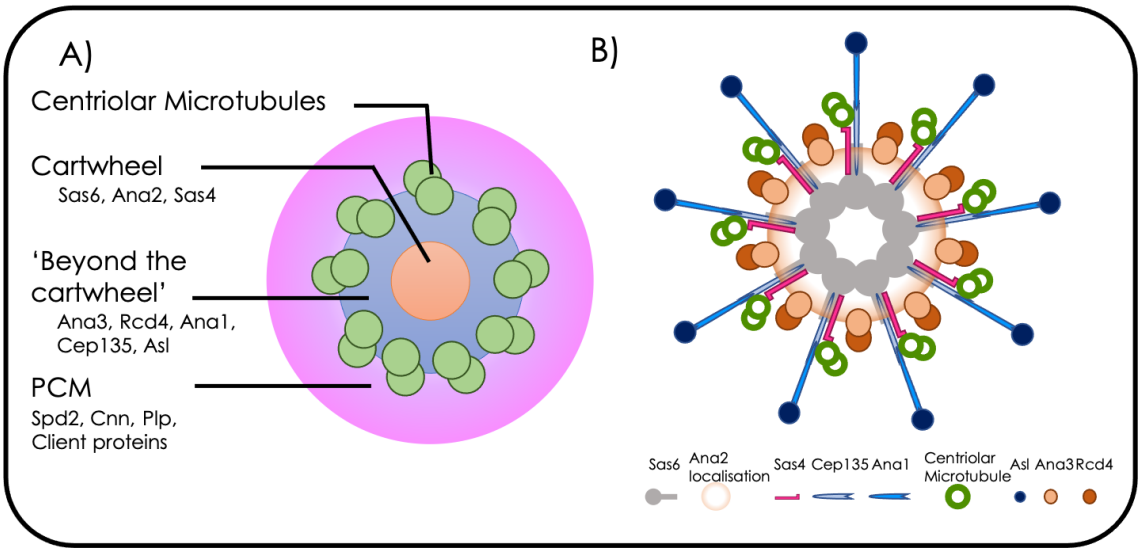

Figure 1.4: Drosophila Centriole & Centrosome Structure *A) Gross centriole structure. Centrosome proteins can be roughly divided into 3 main categories: proteins forming the inner most cartwheel, proteins forming the wider PCM, and proteins "beyond the cartwheel" found bridging to PCM, centriolar microtubules, and implicated in functionalising the centriole* [17–21,33,55]. *Centriolar microtubule doublets are arranged in 9-fold radial symmetry around the centriole. B) Detailed centriole structure. At the core of the Drosophila centriole is a Sas6 cartwheel, which associates with Ana2 and Sas4* [11,74]. *The Sas6 cartwheel forms 9-fold radially symmetric spokes, Cep135 and Sas4 extend from these spokes to attach centriolar microtubules onto the centriole structure* [16,52,55,72,79]. *Further outward, Ana1 then Asl also localise in-phase with these spokes* [32,72].*Ana3 and Rcd4 localise in anti-phase with the spokes, extending outwards from the Ana2 band of localisation* [72]. *Adapted from* [72].

1.3.1 The Central Cartwheel

The central cartwheel provides the core scaffold of the developing centriole [44]. It is assembled from a PLK4 foci within which Sas-6 and STIL/Ana2 monomers oligomerise to form a 9-fold-symmetric ring structure [9,10]. In humans and *Drosophila* these rings display 9-fold radial symmetry and are composed of 9 Sas-6 dimers and an undefined number of STIL/Ana2 tetramers, essential for *in-vivo* ring formation [45]. Interestingly, the 9-fold symmetry of the Sas-6 ring appears to be, at least partly, encoded in the Sas-6 protein specifically, as shown by in-vitro studies demonstrating self-assembling 9-fold symmetrical Sas-6 rings and the ability to alter ring symmetry through various Sas-6 mutations [74,80].

CPAP/Sas4 is also required for centriole and basal body biogenesis, likely at the point of cartwheel construction [11,15,81]. CPAP/Sas4 is known to interact with MTs and is considered the most likely candidate connecting the centriolar MTs to the cartwheel [52]. This suggests a potential mechanism for CPAP/Sas4 to stabilise the assembling cartwheel by enabling linkages to centriolar MTs, indirectly bracing Sas-6 stacks together[49]. In addition to MT-based bracing, this role may be integral to CPAP itself, as structures suggest the capacity for vertically adjacent CPAP molecules to bind one another via a C-terminal domain known as the G-box[52].

A significant question is how these rings physically assemble: are individual rings assembled then bonded together, do structures such as the mother centriole or previous Sas-6 rings nucleate further rings etc. Computational modelling has made a reasonable argument in favour of a nucleating structure, showing that without a surface to form the rings about, ring closure requires a high external source of free energy [82]. This could be further supported as in *Drosophila* Sas-6 has been shown to incorporate at the proximal end of the daughter centriole [83], which would allow Sas-6 to be in contact with the wall of the mother centriole and to be surrounded by the PLK4 plaque, giving two potential nucleation structures in addition to the earlier formed rings of the daughter.

The dynamics of cartwheel growth are central to centriole function, as centrioles of specific consistent lengths must be produced reliably before mitosis, when this period can be hugely variable [83,84]. Cartwheel growth dynamics are fundamentally controlled by centriolar PLK4 [83]. As PLK4 rises above a threshold, Sas-6 incorporation into a daughter is permitted, then as PLK4 levels drop Sas-6 incorporation ceases (*Figure 1.5*). PLK4 oscillations are then timed to the cell cycle, such that as cycles get progressively longer oscillations become elongated. Aydogan et al. further showed that PLK4 oscillations not only follow increasing cycle lengths as found in progressive cycles of *Drosophila* early embryos, but measure cycle lengths as they shorten/lengthen also in response to

genetic backgrounds altering S-phase length [83]. Interestingly, if the cell cycle is perturbed sufficiently suddenly, such as through RNAi depletion of cyclins, PLK4 oscillations continue, demonstrating the system's autonomy of, despite alignment with, cdk/cyclins[84].

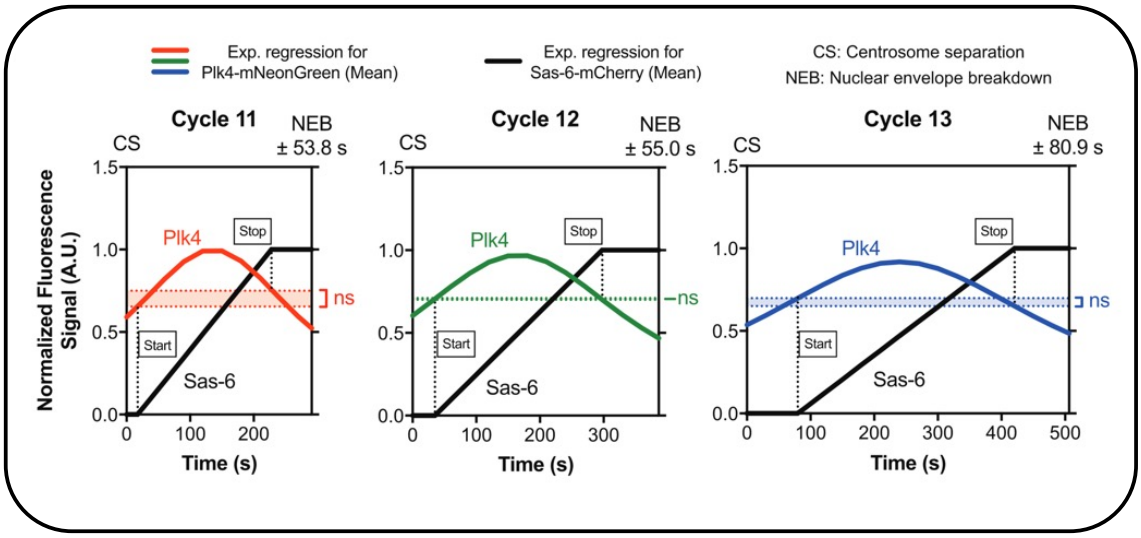

Figure 1.5: Plk4 oscillations regulate Sas6 incorporation into the centrosome *Regression fitted trends for centrosomal Plk4 and Sas6 accumulation across cycles of nuclear divisions in Drosophila early embryos. As cycles increase in length the wavelength of the Plk4 oscillation increases. A threshold of centrosomal Plk4 correlates with the incorporation of Sas6 into the centrosome, suggesting a mechanism for Plk4 control of centriole growth. Figure taken from* [83]

Recently, the cdk1-dependent phosphorylation state of Ana2 has also been implicated in maintaining the growth dynamics of the central cartwheel[46]. This, cdk1-dependent phosphorylation of Ana2, was partially responsible for increased Ana2 diffusion rates about NEB and it was suggested that this was required for efficient Sas-6 incorporation into the growing cartwheel. Conversely, the inability for phosphomimetic Ana2 to localise efficiently at the centriole, while phospho-null Ana2 exhibited prolonged incorporation, suggesting further cdk1-dependent

phosphorylation of Ana2 adds further cell cycle control to centriole assembly by only promoting Ana2 centriolar function at specific cyclin B levels[46].

1.3.2 Functionalising the Centriole

Mother centrioles have two main functional roles at centrosomes: first they must be able to organise PCM by recruiting PCM "scaffold" proteins, which in turn recruit the client proteins necessary for centrosome function; second, they must be able to build daughter centrioles. How a new-born daughter centriole matures to be able to carry out these functions is currently a hot topic of research, primarily focusing on a consistent group of proteins: CPAP/Sas4, CEP135, CEP295/Ana1, CEP152/Asl and PLK1/Polo. At the centre of this is the kinase PLK1/Polo, which has been both implicated in the assembly of the centriole and the expansion/maintenance of PCM [12,19,25]. To assemble new centrioles PLK4 must be recruited to a mother centriole by CEP152/Asl [33,60], so incorporation of CEP152/Asl into the new-born centriole is key. In *Drosophila,* Asl is thought to be recruited and maintained by Ana1 which is itself thought to be recruited by CEP135, forming radial spokes out from the central cartwheel(*Figure 1.4*) [18,32]. This, however, is controversial, as previous data shows far less severe phenotypes in *Drosophila* with CEP135 mutations than those with Ana1 or Asl [17,18,22]. In addition to this, Asl recruitment relies upon Cdk1 phosphorylated Sas4-dependent recruited

Polo [12], and has been shown to interact directly with Sas4 [78,85], suggesting more complexity in the recruitment pathway. The CEP135-Ana1-Asl axis is also implicated in the recruitment of PCM to the centriole. Most notably, Ana1 recruits Polo to the centriole [19,24], which is thought to kickstart a positive feedback system among PCM scaffold proteins leading PCM expansion as discussed in Alvarez-Rodrigo et al. (2019) [25]. Surprisingly, the exact nature of the attachment of the PCM scaffold to the centriole remains unknown. Candidates for PCM attachment include, Asl, Sas4, and CEP135, each being plausibly localised and demonstrated to have links to reduced PCM phenotypes, however, these could be reasonably explained as upstream effects as no conclusive recruitment link has been shown [13,22,86,87].

1.3.3 Beyond Cartwheel Stability

The Rotatin/Ana3-PPP1R35/Rcd4 module is an important and conserved part of centriole structure [22], and if Rotatin/Ana3 is mutated in humans, MCPH and ciliopathies can occur [57,58]. Early studies suggested that Rotatin/Ana3 has in stabilising centriole structure and maintaining mother-daughter cohesion, despite not being essential for PCM nor daughter formation [20]. Interestingly, recently Rotatin/Ana3 has been implicated in further roles, such as cell signalling, cell survival and mitotic spindle orientation [88,89]. Significantly, Ana3 has been shown to recruit Rcd4, leading to these proteins to be considered as a "module". This is further

supported in humans with Rotatin and PPP1R35, however, PPP1R35 appears to further stabilise Rotatin incorporation at the centriole in human models [90]. The specific relationship between Ana3 and Rcd4 appears to be complex, however, as *Rcd4* mutants have been shown to have more severe phenotypes in centriole assembly than previously reported for Ana3, which suggests Rcd4 may also have Ana3-indepedent centriole activities [20,21]. This more severe Rcd4 phenotype is specific to somatic cell types, and excludes spermatocytes [21] which in *Drosophila* have distinct centrioles with much larger structures than in other cell types and unusually (for *Drosophila)* triplet centriolar MTs, perhaps explaining why Rcd4 may be non-essential in this tissue.

Outside of roles at the centriole, Rcd4 and Ana3 are both required for proper cilia assembly through their role at basal bodies, this appears to be a characteristic trait of centriole/basal body proteins involved in structural stability [20,21], likely due to the increased physical stress conferred by the centriolar MT extending into the cilia structure. Similarly involved in centriole stability are CPAP/Sas4 and CEP135, which both have been shown to be able to interact each other and with MTs [16,52,55], thus enabling the potential for a highly stable triangle brace between them. In many organisms, CPAP/Sas4 and CEP135 homologues have been shown to be important for cilia and flagella assembly and functionality [48,91–93]. Conversely, in *Drosophila*, *CEP135* mutants show only mild cilia

phenotypes, despite EM showing destabilised or even absent basal bodies [17]. It should, however, be noted that *Drosophila* contain a relatively small number of functional cilia across their cell types, largely with reduced mechanical roles as opposed to other organisms [17], which may mask the phenotype.

1.4 Methods for Investigating Centriole Assembly

1.4.1 Experimental Systems

As the centriole structure, and its assembly are highly conserved [5], there is a large amount of flexibility in the choice of model organisms and experimental systems available for research. While human cells inherently provide the most disease relevant model for centriole assembly, they come with significant caveats to study. Most significantly, the cell cycle length in human cells is approximately 24h long [94] which significantly restricts usage of live-cell imaging approaches due to photobleaching and phototoxicity. Further to this, human centrosomes are more complex than those of simpler organisms such as *Drosophila*, due to the additions of distil appendages, a G2 extension of microtubules beyond the core centriole, and further redundancy across the system [95,96]. At the other end of the spectrum, simpler organisms, such as *Paramecium* and *Chlamydomonas* have been investigated, particularly in respect to basal body structure due to the number and consistency of cilia produced [92,97,98]. While many papers will refer to this as centriole assembly, it is

important to note that, while basal bodies are produced from mature centrioles, they are functionally distinct with differing roles, and so may not be ideal models of the archetypal human centriole. In animal models, *C. elegans* have been used as they have a highly simplified core centriole structure, while retaining most of the core assembly components, many of which first identified within this system [99–103]. Despite this, *C. elegans* centrioles appear to not conform to the general structure of a central cartwheel, instead their Sas-6 homologue may form spirals, and thus be dissimilar to the human case [73,75]. *Drosophila* have thus emerged as a useful middle ground, lacking the complexity and redundancy of the human system while retaining strong structural homology, despite *Drosophila* retaining the central cartwheel in the mother, lacking distal and subdistal appendages, having doublet microtubules (rather than triplets), and do not undergo G2 extension in human cells [6].

A major advantage for *Drosophila* as a model organism for studying centrioles, is the nature of its early embryos. First, during early embryogenesis the cell cycle is incredibly rapid, with nuclear division taking approximately 10-20 minutes [104] which allows for live-cell imaging with high temporal resolution so that multiple cycles can be captured without notable photobleaching/phototoxicity. Second, as the early embryo is structured as a single giant cell (syncitum), the nuclei occupy the same connected cytoplasm and the cell cycle, thus the assembly of

centrioles, is synchronous across the embryo [105]. This is particularly powerful as it allows for the simultaneous capture of data from >100 centrioles which can be individually tracked then combined to provide reliability and further depth to the information extracted. Finally, for approximately nuclear division 10 through 14, centrioles are tightly associated with the cortex of the embryo [104], which enables the use of super-resolution imaging techniques which limitations on focal depth would otherwise prohibit (see next section).

1.4.2 Microscopy

Since the discovery of the centriole, the diffraction limit of light has posed a significant challenge in experimental design. As each centriole is approximately 200nm in diameter [6], below the diffraction limit of commonly used wavelengths, tight spacing between the mother and the daughter leads to the pair convoluting into an unresolvable dot[106,107]. This has made interrogating the localisation of components around the centriole, particularly difficult as with conventional light microscopy the centriole pair cannot be differentiated, let alone structural domains across individual centrioles [22,107]. To combat resolution limits, EM studies have been used to get higher resolution maps of the centriole as a whole, however, due to the overall density of the centriole and lack of structures of its constituent proteins, they provide only limited insight to the mechanisms behind assembly at a protein level [17,52,73,75,108]. While

EM structures provide high resolution detail of the overall protein complex, specific identification of individual proteins remains more difficult than in light microscopy where fluorescent proteins can be tagged onto proteins of interest. Consequently, for studying the roles of individual proteins incorporating into the centrioles, the ideal would be fluorescence approach with increased resolution. One way this has been achieved is through expansion microscopy where the substrate is fixed to a dehydrated scaffold which, when rehydrated, expands uniformly, increasing the physical separation between species thus reducing the resolution needed to resolve expanded structures [109–111]. This drastically increases the detail visible, allowing resolution of the mother-daughter pair but also the 9-fold symmetry of centriolar MTs [111,112]. Unfortunately, similar to EM, expansion microscopy requires fixed samples, strictly prohibiting live-cell imaging, and excluding temporal data. In order to solve this, instead of fixing the sample, the resolution of captured images must be increased beyond the natural wavelength of light. This can be achieved through a variety of super-resolution techniques now available such as stimulation emission depletion (STED), direct stochastic optical reconstruction microscopy (dSTORM) and structured illumination microscopy (SIM)[113–116]. These utilise the inherent properties of fluorophores and/or of light to further refine the location of fluorophores beyond the natural diffraction limit of light. This is not without trade off, however, as generally these techniques require increased excitation light,

leading to increased photobleaching and phototoxicity, essentially limiting the number of images/length of movies taken [117]. Despite this, these techniques, can be combined with expansion microscopy to compound resolution gains to maximise the resolution of light microscopy in fixed samples [72,117,118].

Due to the lack of feasibility in true live imaging, previous super-resolution studies into centriole assembly have been limited to sampling "snapshots" of centrioles at different points in the cell cycle [72], limiting the temporal resolution and accuracy in defining precisely when events occur. However, as this relies on achieving sufficient signal to noise to detect against the background, this can be sensitive to the relative amounts of each individual protein at the centriole verses the cytoplasm, potentially leading to inaccuracies. Recently, new super-resolution spinning disk (SoRa) microscopes have become available, providing 1.37x increased lateral resolution with a comparatively low increase in laser power delivered to the sample [119]. SoRa microscopes differ from standard spinning disk microscopes by having lenses over each pinhole on the spinning disk. This allows more emission light from the sample to be captured and focused through each pinhole, which enables pinholes to be smaller and resolutions to be higher for a given amount of light. Finally, image resolutions can be further computationally enhanced through deconvolution algorithms which try to revert points of intensity from a point

spread function back to a point emitter based on the known behaviour of light. Super-resolution imaging with lower power lasers opens the door to practical super resolution live imaging over short time courses compatible with *Drosophila* early embryo nuclear divisions enabling true live-cell imaging of mother/daughter centriole development, giving unprecedented temporal resolution and precision.

1.4.3 Image processing

A significant advantage of the *Drosophila* early embryo, is the number of synchronously assembling centrioles that can be observed at once [83,104]. However, to properly exploit this, the analysis of centriole must be automated. This is important so that measurements remain consistent across large sample sizes, but also so that the analysis process can be done efficiently. The question of efficiency becomes particularly important when considering larger datasets, which require very large numbers of centrioles to be measured.

Automated centriole analysis first requires the identification of centrioles on a frame-by-frame basis. To do this, an algorithm must differentiate locally intense centriolar blobs from random points of intensity making up the background and the structured intensity from autofluorescence. This relies heavily upon the contrast of the image [120–122], and is harder when fluorophores are dim or the tagged protein shows weaker

localisation. This is further impeded by the continual photobleaching, both reducing the bit-depth of the centrioles and reducing contrast [123]. While contrast can be improved through background correction methods [124–127], often inherently poor starting conditions (e.g., low Signal-to-Noise ratios) limit the amount of information recoverable.

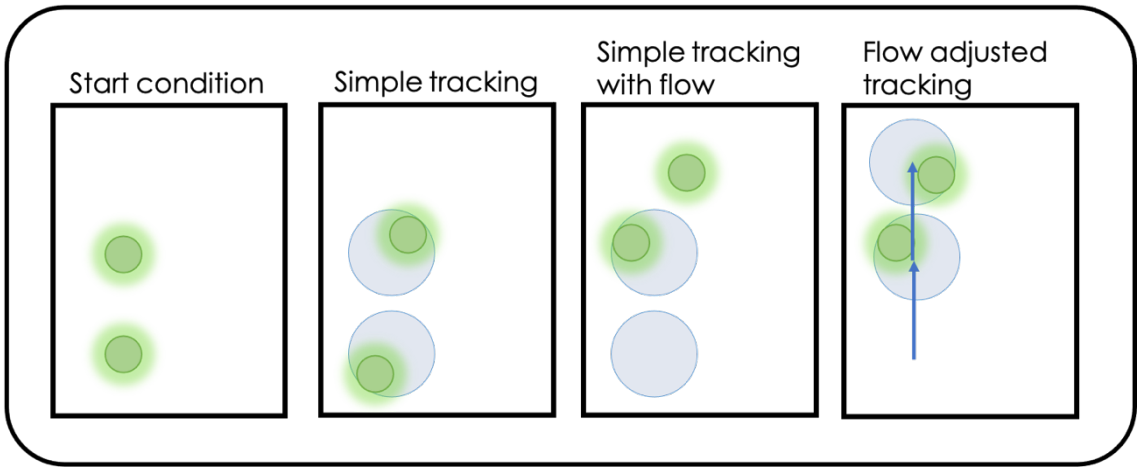

Figure 1.6: Simple Particle Tracking *Simple particle tracking methods rely on looking for a particle in an area around where it was in the previous frame. In cases with significant particle flow, this can lead to particles being improperly assigned to tracks as a neighbouring particle is now closest to the search area. A method to avoid this is to approximate the average flow of particles across an image, then use this as an offset to the search area to realign between frames.*

Purely identifying centrioles, on a frame-by-frame basis is sufficient to allow automated analysis aggregating centrioles within an embryo or even identifying subpopulations, however, it lacks information as to the centriole's fates. To build fate data, centrioles must be further tracked such that a centriole instead consists of multiple snapshots of parts of frames across an entire time course. At a basic level this can be achieved

by connecting similarly located centrioles from one frame to the next *(Figure 1.6)*.

Fundamentally, this relies upon the time between frames being sufficiently small such that individual centrioles remain closest to their previous locations. For this reason, significant centriolar flows in embryos, as caused by asynchrony in nuclear divisions [105], can lead to incorrect linkages that must be accounted for by considering flow from one image to the next. In addition to flow complications, as the embryo is a 3d environment, it is possible for centrioles to move out of the confocal volume, thus being lost from individual frames, to prevent this a memory is required as to reconnect lost centrioles if they reappear. Furthermore, as centrioles divide, blobs split into two at which point they must be assigned as new tracks or into a hierarchy to preserve data. As the tracking environment becomes increasing complex, so must the linkage reasoning and the data storage [128,129].

While complex image analysis has been around for over two decades, it has taken longer to robustly filter through into biology [128–131]. In recent years, the advent of Trackmate [129], an addon to the popular image analysis platform Image J/Fiji [132], has drastically lowered the barrier to entry enabling accessible identification and tracking of centrioles. Utilising Trackmate, previous studies have been able to extract quantitative

intensity data mapping the incorporation profiles of proteins into centrioles across the cell cycle [83,84]. This so far has provided significant insight into the mechanisms and regulation behind centriole assembly, but has yet to be expanded to the fainter proteins in the beyond the cartwheel zone.

1.5 Aims

Overarching goal:

To better understand how conserved centriole proteins are assembled into the centriole

Specific Goals:

1. Generate a high-quality dataset of the incorporation profiles of the main core conserved centriole proteins with respect to the cell cycle during nuclear cycles 11-13 in the *Drosophila* early embryo
2. Optimise and develop an analysis pipeline to combine and align multi-embryo datasets to allow cross-protein comparisons
3. Develop analysis tools to enable the quantification and comparison of centriole assembly as seen on conventional verses super-resolution timelapses, so as to potentially distinguish incorporation between the mother and daughter
4. Use these datasets and methods to investigate the potential role of CEP135 in recruiting Ana1, and so potentially resolve this controversial issue.

Chapter 2: Cartwheel Assembly Dynamics - Sas-6 & Ana2

In this chapter I will investigate the incorporation profiles of Sas-6 and Ana2, while also developing and validating tools to aggregate incorporation data between multiple embryos. I show, that during S-phase Sas-6 and Ana2 exhibit similar incorporation profiles to those that have been previously reported [46,83,84]. However, by extending the time period of imaging, I reveal more complex incorporation patterns that occur during mitosis. Further, by quantifying super-resolution timelapses resolving the appearance of the daughter centriole, I show that daughter centriole assembly appears to begin earlier than previously reported.

2.1 Centrosomal incorporation of Sas-6 and Ana2

In order to reliably compare and contrast the incorporation profiles of various proteins at the centriole, ideally one should be able to directly overlay the profiles atop one another. In practice, there is reasonable variation in cycle length from embryo to embryo, consequently one must be able to compensate for this to reliably align profiles. A potential solution is to directly compare cycles that end have similar lengths, however, this biases results by excluding large amounts of data; better is to generate aggregate datasets then align those.

In prior work [46,83], the centrosomal incorporation of Sas-6-GFP transgenically expressed from its endogenous promoter [83] or Ana2-NeonGreen (Ana2-NG) expressed as a CRISPR knock-in [46], had been independently quantified via their centrosomal fluorescence in *Drosophila* early embryos. To develop methods to accurately compare incorporation profiles, I collected data from the same Ana2-NG line and a previously uncharacterised Sas-6-NG CRISPR knock-in line, generated in parallel (supp. Table 1&2). These experiments were conducted with the homozygous lines, so in absence of untagged endogenous protein, and in the presence of Jupiter-mCherry microtubule marker. This was used to give cell cycle context (e.g. the timing of nuclear envelope breakdown (NEB), and the metaphase/anaphase transition (M/A)) that could subsequently be used to aid alignment of datasets between embryos (*Figure 2.1*).

Figure 2.1 Overview of Embryo Alignment Procedure (next page) *A) Example of the mean centrosome fluorescence intensity (±SEM, and all subsequent error bars) from one embryo separated into nuclear cycles 11, 12 and 13 (yellow, green, blue respectively). Cycles are defined by computed local fluorescence intensity minima associated with centriole separation (dotted lines). This minima occurs because the average centriole fluorescence intensity drops dramatically when the centriole pairs separate and become resolvable as two individual centrioles. B) Stages of alignment of standard resolution centrosome mean fluorescence intensity vs time (seconds) data (Sas-6-NG shown here) from multiple embryos. i) Middle 90th percentile means of individual embryo fluorescence intensity at centrosomes; ii) As top left, cropped to the cycle of interest; iii) Time normalised middle 90th percentile means of aligned cycles; iv) As top right, amplitude normalised; v) mean aggregate of bottom left; vi) As bottom middle, re-dimensionalised. C) Examples of visual scoring for cell cycle events using the microtubule reporter Jupiter-mCherry. Frames are taken from a typical embryo expressing Sas-6-NG (Green) and Jupiter-mCherry (Red). Nuclear envelope break down is defined by the invasion of microtubules into the nucleus, Metaphase/Anaphase by the spindle beginning to elongate, and Midbody breakdown by when the spindle midbody is no longer visible.*

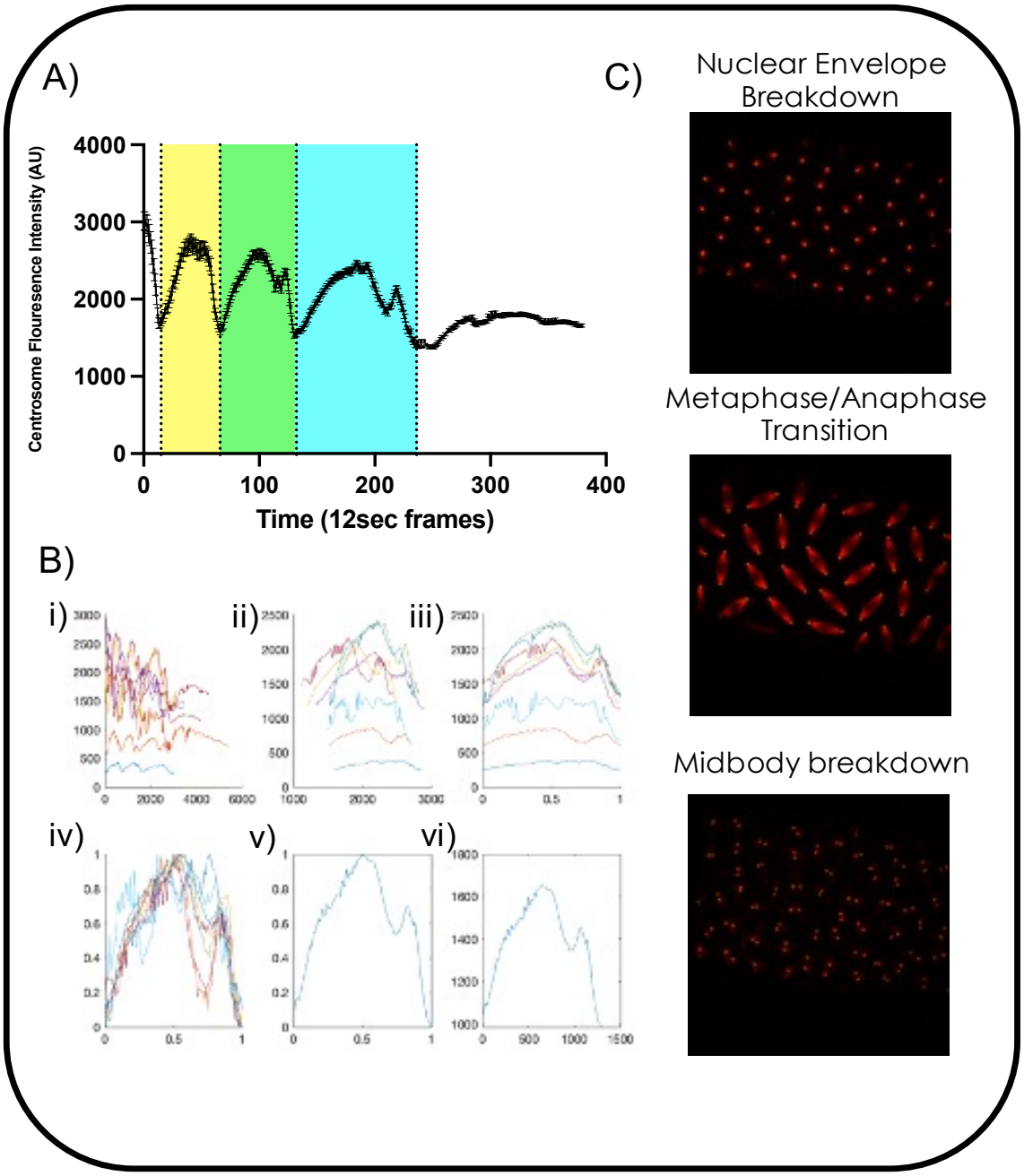

Time-lapses of Sas-6-NG or Ana2-NG embryos expressing Jupiter-mCherry were collected and centrosome fluorescence was quantified over time in each embryo on an individual centrosome basis (*Figure 2.1A*). Most movies encompassed nuclear cycles 11-13 (*Figure 2.1B.i*), so the data from each cycle was obtained by extracting the data between the local fluorescence minima's corresponding to the separation of the centrioles

at the end of each cycle (*Figure 2.1A)*. Cropped cycles from each embryo within a dataset were first normalised to time, then by amplitude (Figure 2.1B.iii and 2.1B.iv respectively) allowing alignment and generation of a composite trend. This data could be re-dimensionalised based on dataset averages for amplitude and time *(Figure 2.1B.vi)*. These composite datasets could then be used to compare the behaviour of the same protein across different nuclear cycles (Figures 2.2-2.3) or of different proteins across the same nuclear cycles (Figure 2.4). As the number of centrioles double with each cycle, the SEM does naturally decrease between cycles, consequently, this should not be confused with a change in amplitude variation across cycles.

Sas-6 and Ana2 both show a similar initial rise in centrosomal fluorescence intensity following centriole separation, this likely corresponds to the proteins associating with the growing cartwheels of the daughter centrioles. Alignments suggest centrosomal Ana2 peaks slightly earlier, implying its recruitment may precede that of Sas-6. Ana2 shows a shorter peak followed by a drastic drop in centrosomal levels before NEB. This is striking as it suggests that nearly all the Ana2-NG recruited to the centrosome in S-phase is lost during mitosis. In contrast, Sas-6 levels remain near their peak for longer, then show a more minor dip beginning around NEB with a minima centred around M/A (discussed in more detail below). Fractions of both protein's start to leave the centrosome during mitosis, but

they both begin to accumulate again, towards the end of mitosis, before a final drop off. This final drop off is due to centriole separation - as old and new-mother centrioles physically separate, they can increasingly be resolved, so a greater proportion are identified by the tracking software as comprising two entities rather than one. In this case the spot that was once two mother centrioles now becomes two spots each with one mother centriole, inherently with a reduced concentration of Sas-6 or Ana2 and thus lower fluorescence intensity.

Figures 2.2-2.3 Centrosome Incorporation Profile of Sas-6-NG and Ana2-NG (next two pages) Mean centrosome fluorescence intensity plotted against time (composite & overlayed – seconds; individual - 12 second frames) across nuclear cycles. Nuclear cycles are defined by the computed fluorescence intensity minima caused by centriole separation. Composite & overlayed graphs consist of multiple embryo tracks aggregated via mean averaging of time and amplitude normalised aligned individual tracks. Nuclear envelope breakdown and the Metaphase/Anaphase transition are shown with blue/yellow and red/orange bands denoting the distribution of event timing within datasets. Standard error of the mean is shown as dashed lines or error bars. Composite/overlayed number of embryos: Sas6 Cycle 11 – 9, Cycle 12 - 15, Cycle 13 – 8; Ana2 Cycle 11 – 3, Cycle 12 - 6, Cycle 13 - 4

Figure 2.4 Comparison of Sas6-NG and Ana2-NG incorporation profiles (3rd page) Overlayed incorporation trends showing the mean normalised centrosome fluorescence intensity verses progression of cycle of Ana2 and Sas6 across nuclear cycles. Nuclear cycles are defined by the computed fluorescence intensity minima caused by centriole separation. Timings of nuclear envelope breakdown and the metaphase/anaphase transition within the dataset are shown by yellow and orange distribution bands respectively. Graphs consist of multiple embryo tracks aggregated via mean averaging of time and amplitude normalised aligned individual tracks.
Composite number of embryos: Sas6 Cycle 11 – 9, Cycle 12 - 15, Cycle 13 – 8; Ana2 Cycle 11 – 3, Cycle 12 - 6, Cycle 13 - 4

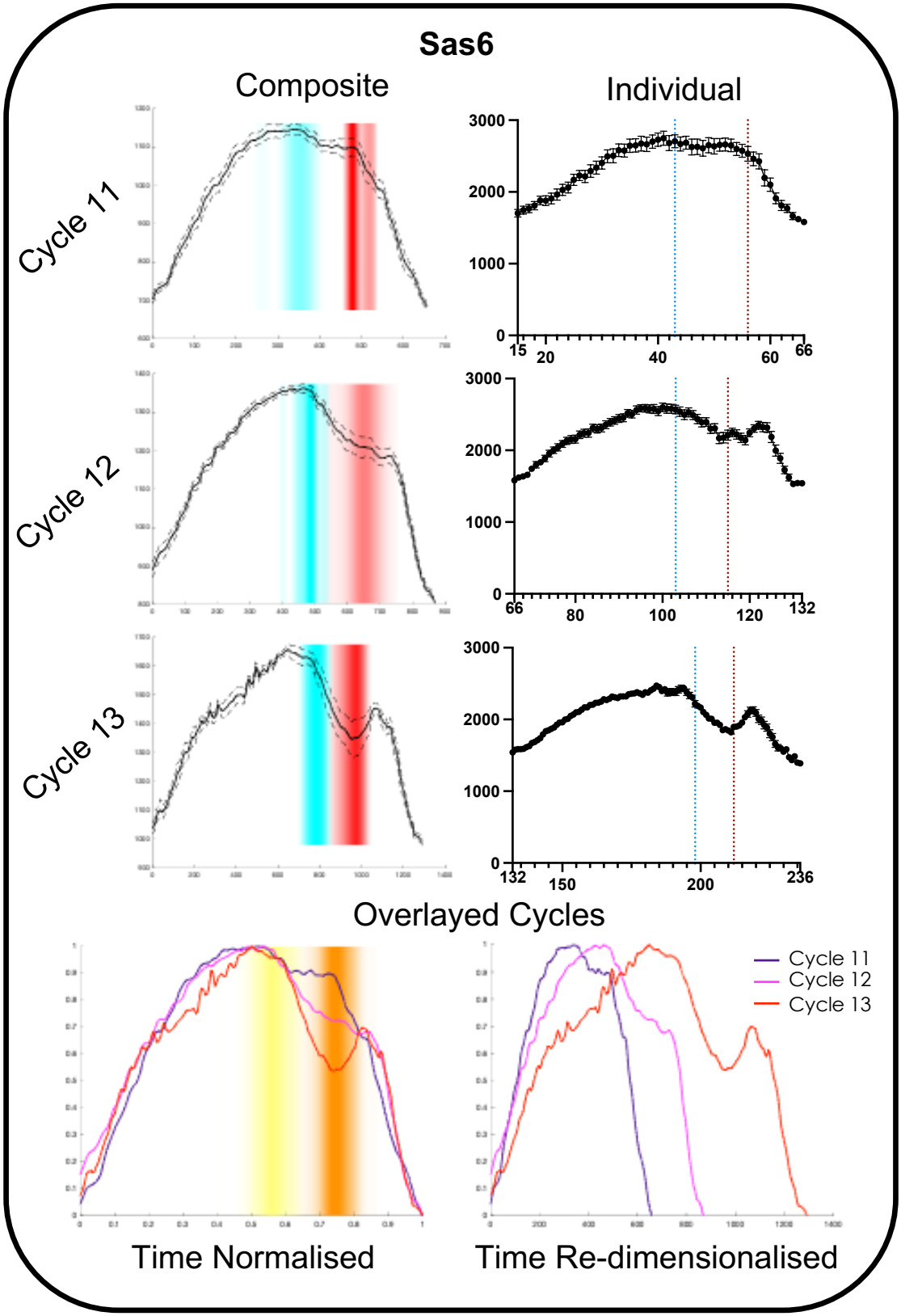
Sas6
Composite
Individual
Cycle 11
Cycle 12
Cycle 13
3000
2000
1000
0
15
20
40
60
66
80
100
120
132
150
200
236
Overlayed Cycles
Cycle 11
Cycle 12
Cycle 13
Time Normalised
Time Re-dimensionalised

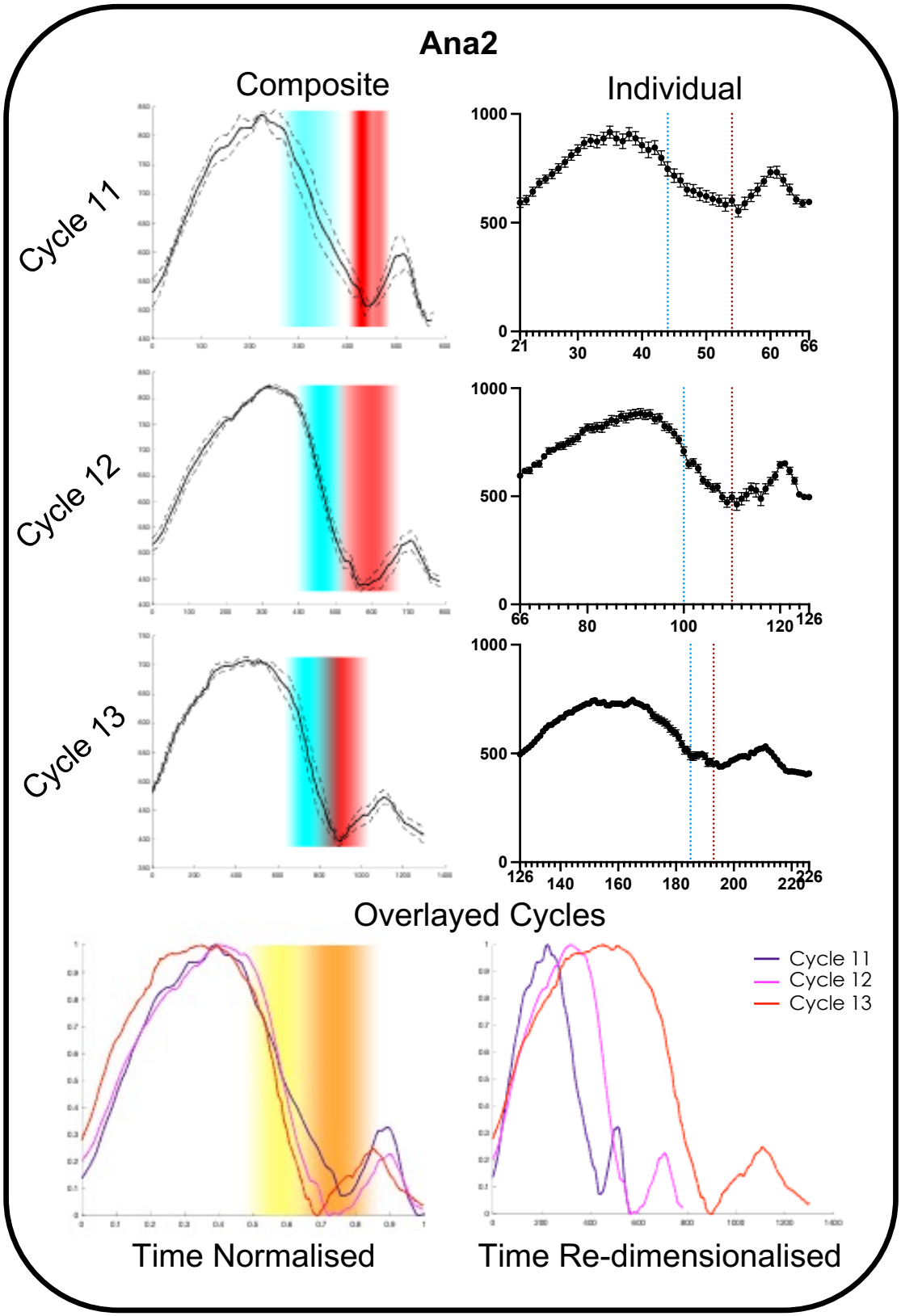
Ana2
Composite
Individual
Cycle 11
Cycle 12
Cycle 13
1000
500
0
21
30
40
50
60
66
66
80
100
120
126
126
140
160
180
200
220
226
Overlayed Cycles
Cycle 11
Cycle 12
Cycle 13
Time Normalised
Time Re-dimensionalised

Cycle 11

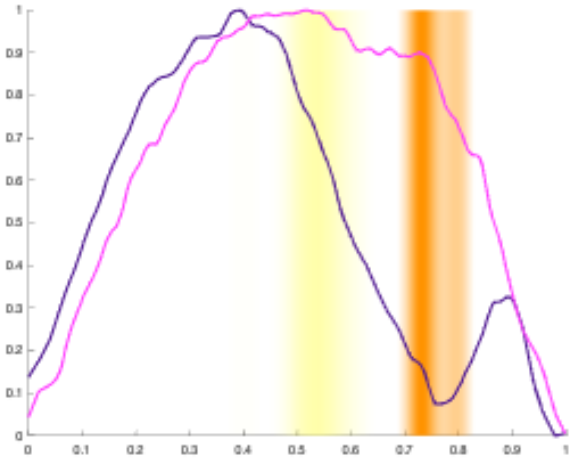

Cycle 12

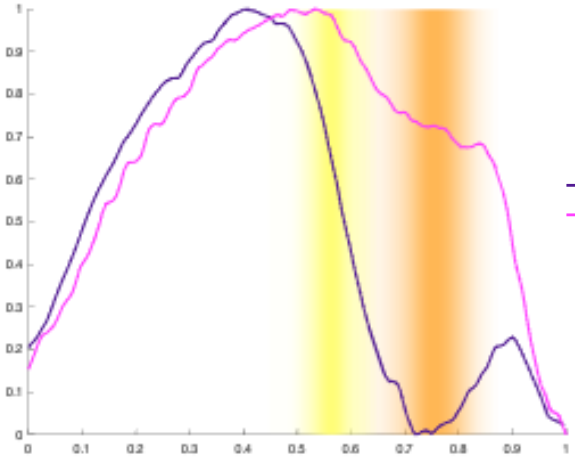

Cycle 13

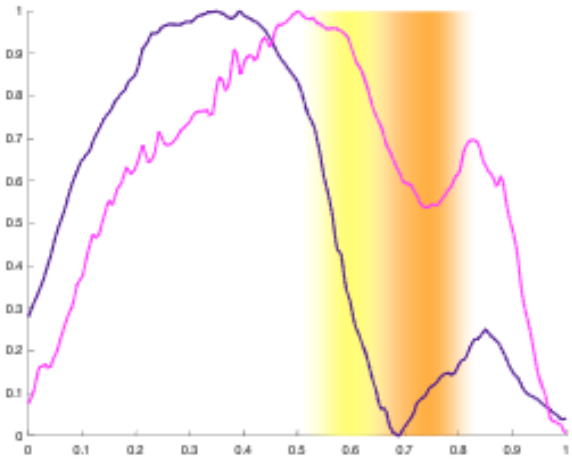

Overall, both the Sas-6 data (Figure 2.2) and the Ana2 data (Figure 2.3) shows a high quality of alignment (Figure 2.4). All the major trend elements appear broadly well-maintained and temporally localised between individual and composite tracks. Furthermore, the distributions of when NEB and M/A occurs within cycles appear tight, this implies that the cycles are uniform and thus also aligned.

Interestingly, when comparing the time normalised vs re-dimensionalised, trends of Ana2 and Sas-6 between cycles, the overlay aligns very tightly. This suggests that, for both proteins, their accumulation profile stretches with the cycle length and is most likely tied to cell cycle events. Between cycles the only major difference appears to be the degree of dip seen, where in later cycles the dip is more pronounced. This is unlikely to be due to a lack of temporal sampling as individual cycles show a large number of data points spanning the respective dip sections.

The sharp drop in centriolar Ana2-NG levels just prior to NEB (*Figure 2.3*) is in agreement with previous studies [46]. The behaviour of Sas-6-NG (*Figure 2.2)*, however, is somewhat different to that reported previously with a transgenic line expressing Sas-6-GFP [83,84]. Although Sas-6-NG levels broadly plateaued prior to NEB in nuclear cycle 11 - as reported previously for Sas-6-GFP - a decrease in centriolar Sas-6-NG levels at or shortly after NEB became progressively more pronounced in cycles 12 and 13 (*Figure*

2.2), and this contrasts with the Sas-6-GFP data where centriole levels largely plateaued at the end of S-phase and in to early mitosis in cycles 12 and 13. A close inspection of the previous data revealed a slight downward trend in centriolar Sas-6-GFP levels after NEB in some embryos, and it is worth noting that these embryos were only followed for a short time after NEB (not throughout mitosis and into the next cycle as reported here). This difference is potentially important, as it suggests that a substantial fraction of the Sas-6-NG recruited to the centrioles during S-phase is not being directly and irreversibly incorporated into the daughter centrioles and is capable of leaving the centrioles during mitosis.

2.2 The drop in centriole intensity as embryos enter mitosis does not appear to be artificial

Interestingly, a similar dip in centriole fluorescence intensity was observed with all the other centriole proteins that were subsequently tested (see section 3.2). This includes, Ana2, however, in this case the "dip" appears convoluted with another large drop in fluorescence before NEB. This convolution has been supported prior, as this large drop is removed in Cdk1-phospho-null mutants, where Cdk-1 phosphorylation sites have been mutated to alanine, yet a dip process between NEB an M/A remains [46]. As this phenomenon was so widespread, an initial hypothesis was that this might be due to a systematic error.

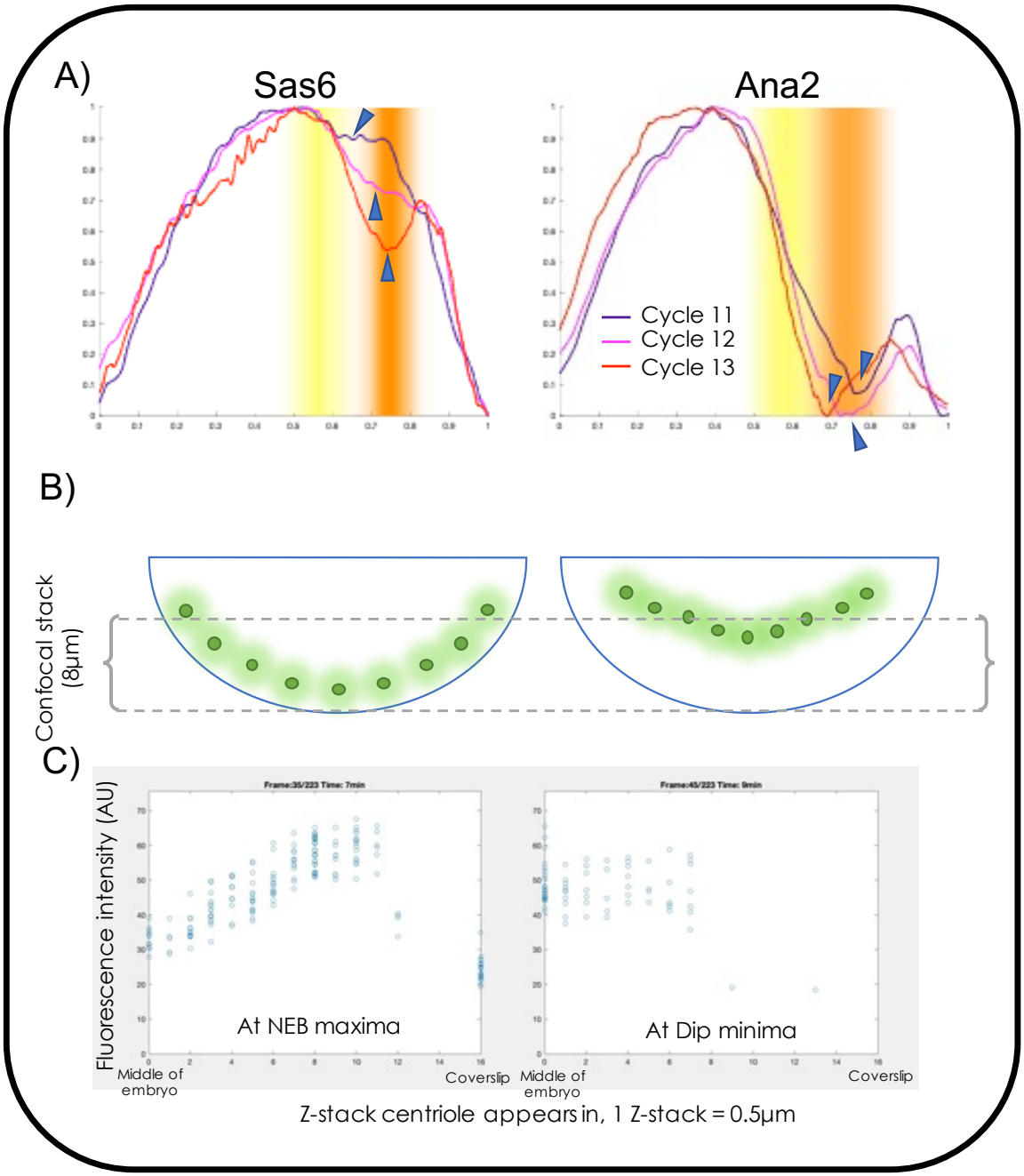
A)
Sas6
Ana2
Cycle 11
Cycle 12
Cycle 13
B)
Confocal stack (8µm)
C)
Fluorescence intensity (AU)
At NEB maxima
At Dip minima
Middle of embryo
Coverslip
Middle of embryo
Coverslip
Z-stack centriole appears in, 1 Z-stack = 0.5µm

Figure 2.5 Evaluation of the dip in fluorescence intensity following NEB (previous page) *A) Overlayed incorporation trends of Sas6 and Ana2 cycles showing the mean normalised fluorescence centrosome intensity verses cycle progression. Nuclear cycles are defined by the computed fluorescence intensity minima caused by centriole separation. Timings of nuclear envelope breakdown and the metaphase/anaphase transition within the dataset are shown by yellow and orange distribution bands respectively. Graphs consist of multiple embryo tracks aggregated via mean averaging of time and amplitude normalised aligned individual tracks. The "dip" is highlighted in each cycle by blue arrowheads. B) Potential mechanism leading to the dip via systematic error. For the majority of the cycle, centrosomes are found lining the cortex of the embryo (left), during mitosis, centrosomes move inwards (right). As the confocal stack is fixed, inward movement of centrosomes leads to point-spread functions of the centrosomes becoming only partially captured within the stack, thus reducing average intensity. C) Comparison of individual centrosome fluorescence intensity of Ana2-NG expression embryos, verses Z-stack height at which the centrosomal intensity is maximal. Graphs are shown both at NEB (maximal mean intensity before the dip) and at the trough of the dip Composite number of embryos: Sas6 Cycle 11 – 9, Cycle 12 - 15, Cycle 13 – 8; Cycle 11 – 3, Cycle 12 - 6, Cycle 13 - 4*

During mitosis, the centrosomes in *Drosophila* early embryos, move away from the embryo cortex by approximately 5µm to form the poles of the mitotic spindle, before returning to the cortex as the embryos exit mitosis. As this coincides with the dip in fluorescence intensity, I hypothesised that this movement of the centrosomes could be responsible. A simple mechanism for this would be that as the centrosomes move further from the cortex, the laser light exciting the fluorophores and the fluorescent light to be captured would have to travel through more cytoplasm, leading to more absorption and less transmission as predicted by the Beer-Lambert law. Alternatively, as the confocal volume of stacks do not move with the centrosomes, as the centrosomes move, they could begin to partially fall out of the confocal volume, such that only a portion of their vertical point-spread function would remain within the confocal volume and be able to be captured, also reducing the fluorescence intensity recorded (*Figure. 2.5.B*). This would lead to the dataset containing

centrosomes where a reduced proportion of their total fluorescence was captured during mitosis, leading to a perceived drop in average fluorescence. To test these hypothesises, I compared the centrosomes Z-positioning, analogous to their depth in the embryo, to their recorded fluorescence in Ana2-NG movies (*Figure 2.5.C)*. If the dip in fluorescence was due to Beer-Lambert law absorption, then there should be a constant linear relationship between fluorescence intensity and Z-positioning, then as the centrosomes move, the population should maintain the gradient and just slip down the slope. Alternatively, if it is due to centrosomes slipping out of the confocal volume, as the centrosomes move a second population with drastically lower fluorescence intensity should appear in the last Z-stack. Interestingly, neither appeared to be the case as while some Beer-Lambert law esc effect appeared present at NEB, at the minima there was negligible difference in fluorescence recorded at centrosomes based on height (*Figure 2.5.C)*. This suggested that the Z-positioning of the of centrosomes was not driving the dip effect, and that it may be biologically relevant.

2.3 Super-resolution characterisation of Sas-6 & Ana2 daughter loading

A significant limitation of standard confocal imaging is the lack of resolution sufficient to identify the daughter and the mother centrioles within the centrosome. To combat this, I analysed super-resolution movies

from embryos expressing Jupiter-mCherry and either Sas-6-NG or Ana-2-NG, captured by Alan Wainman using a SoRa spinning disc confocal super-resolution microscope. While this minimised photobleaching vs general superresolution techniques, deconvolution is required to reach sufficient resolutions resulting in the inability to faithfully quantify fluorescence changes over time with this system.

Instead, I wanted to identify when the fluorescence of the daughter centriole could be first detected on the super-resolution system, and compare that to the fluorescence data acquired from my standard resolution imaging. Initially this was done manually via individual alignments of cycles with similar lengths, the initial appearance of the daughter centriole was timed around the computed point of centriole separation. Individual manual alignments, showed appreciable variance, however, and due to being compared vs other embryos imaged on different microscopes are somewhat unreliable (*Figure 2.6.A&B*).

To improve on this method, I utilised Trackmate [129] to identify centrioles in these super-resolution time-lapses, but I analysed the data twice using two different sizes of structuring factors for each time-lapse. In the first instance, I would use a small structuring factor that was capable of recognising two closely spaced objects (i.e. the mother and daughter centriole) as two independent objects. This would allow me to calculate

the total number of "centrioles" detectable in each image. In the second instance I would use a larger structuring factor approximating to the size of a centrosome; this would identify a closely spaced mother and daughter centriole as a single object, so allowing me to calculate the number of centriole pairs in each image (hereafter termed the number of "centrosomes").

By comparing the ratio of centrioles-to-centrosomes in each image, I could estimate when daughter centrioles first start to become detectable in each time series. For example, even if a centriole marker was loaded onto centrioles at the very start of S-phase, the daughter centriole would be very dim at this time, so I would expect the centriole/centrosome ratio to be close to 1.0 - as Trackmate would usually be unable to distinguish a clear daughter centriole, even using the smaller structuring factor. By the end of S-phase, however, the daughter centriole would be much brighter, so I would expect the centriole/centrosome ratio to be closer to 2.0, as Trackmate would likely to be able to distinguish a clear mother and daughter centriole, and so detect two centrioles for every centrosome. Note that I would not expect this ratio to ever reach 2.0, as some centriole pairs in these embryos are oriented in such a way that it is not possible to spatially distinguish separate mothers/daughters even if the daughter is very bright [84].

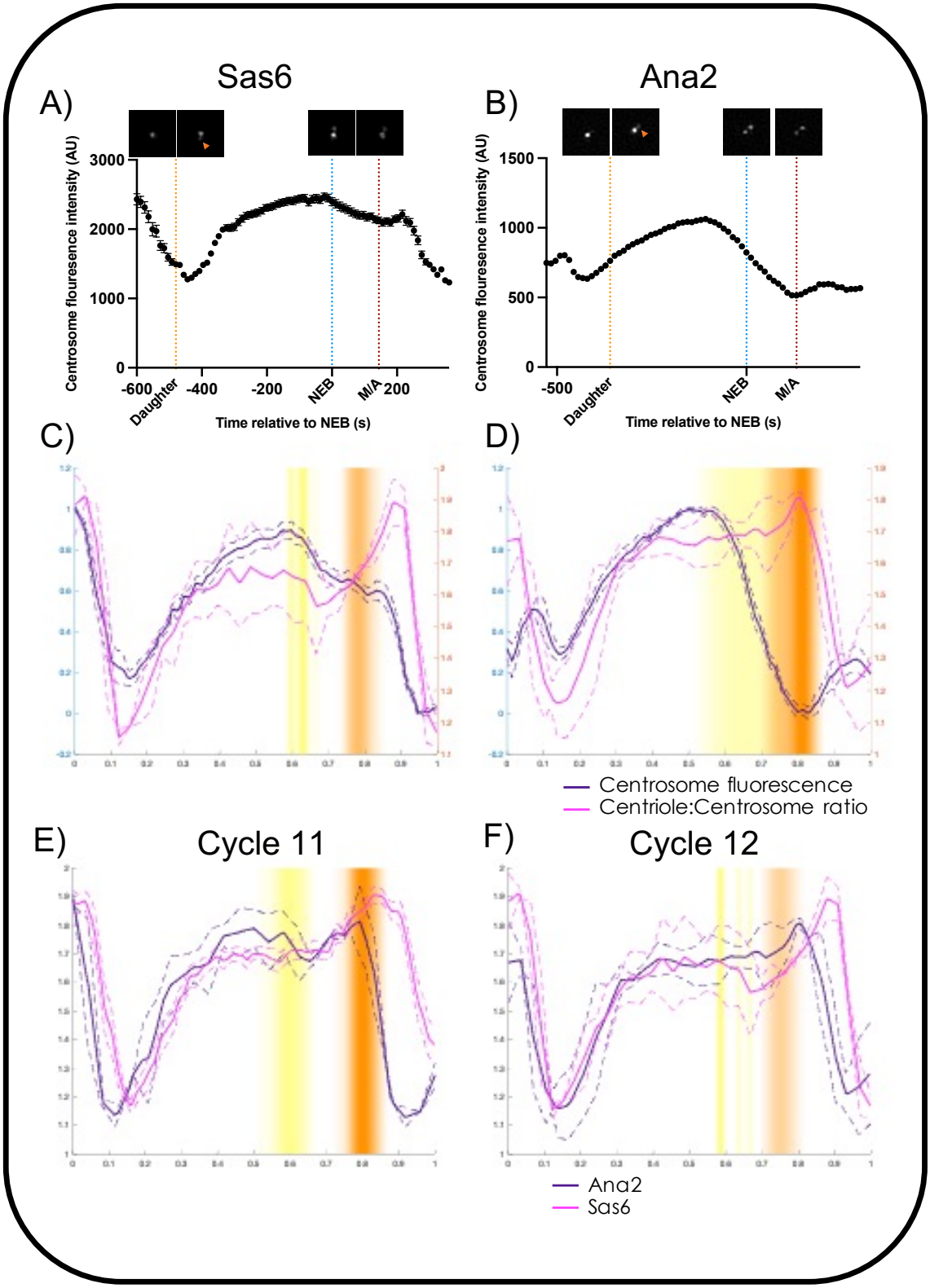
Sas6
A)
Centrosome flouresence intensity (AU)
3000
2000
1000
0
-600
-400
-200
NEB
M/A
200
Daughter
Time relative to NEB (s)
Ana2
B)
Centrosome flouresence intensity (AU)
1500
1000
500
0
-500
Daughter
NEB
M/A
Time relative to NEB (s)
C)
D)
Centrosome fluorescence
Centriole:Centrosome ratio
E)
Cycle 11
F)
Cycle 12
Ana2
Sas6

Figure 2.6 Super-resolution quantification of Sas6 & Ana2 appearance on the daughter *A&B) Sas6 & Ana2 mean centrosomal incorporation (±SEM) across individual cycle 12 embryos, showing the centrosome fluorescence intensity over time in seconds, with nuclear envelope breakdown and the metaphase/anaphase transition annotated. Tracks are shown between M/A of cycle 11 and the midbody breakdown in cycle 13. Similar length cycle 12 super-resolution images have been aligned relative to NEB with the frame before and after the visual appearance of the daughter shown (Yellow, Orange arrowhead) as well as the centriole state at NEB and M/A. C&D) Sas6 & Ana2 aggregated cycle 12 centrosomal fluorescence intensity (left axis) overlayed with the super-resolution centriole:centrosome ratio (right axis) between M/A of cycle 11 and the midbody breakdown in cycle 13. Standard error of the mean is shown by the dashed lines and NEB & M/A distribution is represented by the yellow and red distribution bars respectively. E&F) Comparison between Sas6 and Ana2 cycle 11 & cycle 12 quantifications of centriole:centrosome ratio shown between M/A the previous cycle and the midbody breakdown in the next. Standard error of the mean is shown by the dashed lines and NEB & M/A distribution is represented by the yellow and red distribution bars respectively.*
Composite number of embryos: Sas6 Standard Resolution Cycle 12 – 7, Super-Resolution Cycle 11 – 14, Cycle 12 - 2; Ana2 Standard Resolution Cycle 12 – 5, Super-Resolution Cycle 11 – 2, Cycle 12 – 3

From these types of measurements, I could calculate the proportion of mother centrioles with a daughter at each given time point - this relates to the probability of being able to resolve the daughter and thus to the extent of which the protein that I am examining has assembled onto the daughter at said time point. I aggregated and aligned this centriole:centrosome data (pink, *Figure 2.6.C&D*) to my previous data from standard resolution confocal imaging and super-resolution datasets (purple, *Figure 2.6.E&F*). For these experiments, I used the microtubule-defined events of NEB, M/A and midbody disassembly to standardise and align the confocal and super-resolution datasets. As described above, this allows more statistically valid conclusions and streamlines the process of alignments between different datasets.

By overlaying these two datasets for Ana2-NG and Sas-6-NG, the timing of the loading of each protein onto the daughter became very clear (*Figure* 2.6). For both Ana2-NG and Sas-6-NG, the daughter is resolved in the super-resolution images (i.e. the centriole:centrosome ratio starts to rapidly increase) at the start of S-phase when the two parental centrioles have just separated at the end of mitosis (ie. coincident with the minima associated with centriole separation in the standard resolution data). Interestingly, and in agreement with the fluorescent intensity data, Ana2-NG appears to be detected on the daughter slightly before Sas-6-NG (*Figure 2.6.E/F)*. After this point the centriole:centrosome ratio rises to a plateau of ~1.6-1.7 (as described above, we would not expect this ratio to reach 2.0 for closely spaced mother/daughters). At about the time of the M/A transition, there is a rise in the centriole:centrosome ratio as the mother and daughter centrioles disengage and start to move apart (peaking at ~1.8-1.9), meaning that even non-favourably oriented mother and daughter centrioles can now be distinguished. Finally, at the end of mitosis, the centrioles have moved far apart enough that they can be distinguished as separate objects even by the larger Trackmate scaling factor (that identifies "centrosomes" rather than "centrioles") and so the ratio rapidly drops back to ~1.2.

Interestingly, this ratio appears to decrease earlier for Ana2-NG than Sas-6-NG in cycle 11, suggesting the separation of Sas6-NG marked

centrosomes are easier to detect than Ana2-NG marked centrosomes. It should be noted, that due to imaging constraints with regard to photobleaching, cycle 11 had notably more data than cycle 12 and so may be more representative. Further, in both Sas-6-NG and Ana2-NG there is a slight up inflection in the centriole:centrosome ratio before the sudden drop corresponding to centriole separation. This suggests that during M/A the mother and daughter centrioles become notable easier to individually resolve. As this coincides with the loss of material from the centrosome this could refer to a loss of transiently centrosomal material leaving the remaining highly localised cartwheel intensities. Alternatively, this could suggest that the distance between centrioles increases before centriole separation proper, which would suggest multiple levels of separation processes.

2.4 Discussion

Overall, my Sas-6 and Ana2 standard resolution fluorescence intensity data largely agrees with existing data on timing of incorporation into the centriole [46,83]. As touched on earlier, however, there is a slight difference in the Sas-6 incorporation data. Previously, Sas-6-GFP has been described as having a phase of linear accumulation then that plateaus in late S-phase and into early mitosis [83]. This also appears to be the case for Sas-6-NG up to NEB. However, following NEB the dip clearly breaks this pattern and, especially in later cycles, doesn't recover to pre-dip levels.

These differing findings are likely very compatible as previous Aydogan (2018) study [83] didn't record data through to the end of the cycle and then based on the trend up to NEB assumed a plateau phase, which became the model further studies fit to [46]. Additionally, as the previous studies used transgenically expressed Sas-6-GFP whereas I have used a Sas-6-NG knock-in at the endogenous gene locus, consequently my data likely benefits from an improvement of sensitivity due to lower background, better photobleaching characteristics and better photonic yield [133]. As a result, I believe this demonstrates an important refinement of previous observations, now including information as to what's happening during and immediately after mitosis.

The discovery of the dip, however, poses a serious question as to what is happening to Sas-6 and Ana2 molecules during mitosis, when a significant amount of protein appears to be lost from the centrosome. Due to the reliable positioning with respect to NEB and M/A, it is most likely that at some level this "dip process" is cell cycle regulated. However, the mechanism by which this occurs is particularly elusive. As the dip begins around NEB, when Cyclin B levels are highest, its likely to be Cdk1-dependent driven, however, Ana2 mutants lacking Cdk1 sites have previously been reported showing a dip process, and instead this deconvolutes it from the Ana2 specific drop in fluorescence pre-NEB [46]. Consequently, the dip process is unlikely to be Ana2-dependent, and if

based on Cdk1/Cyclin B it must work through an additional upstream factor.

As for why the dip occurs, the simplest explanation is it's the shedding of excess material. Recovery after the dip, particularly of Sas-6 doesn't appear to be complete, necessitating that, in the absence of extreme photobleaching, not all the material at the peak after initial incorporation forms part of the permanent cartwheel. Recently, super-resolution FRAP experiments have shown the Sas-6/Ana2 cartwheel does not turn over(*unpublished data, Alan Wainman),* this suggests that the sum of Sas-6 and Ana2 at the minima of the dip the sufficient to form the mature cartwheel and the prior peak is simply excess recruited to the centrosome to form a centriolar "primordial soup". This is particularly strange in the case of Ana2 as it would suggest that the level of Ana2 in the centre of the dip, combined with its large drop in fluorescence, is comparable to that at the minima immediately following centriole separation.

These results are directly incompatible with Ana2 beginning to incorporate at computed centriole separation, as either it would require Ana2 to refill into the mothers, or the amount of Ana2 to deplete in the centriole ad infinitum. Hypothetically, these could be explained through photobleaching reducing the true level over the course of a cycle, however, this appears unlikely to be the case due to the similar maxima

and minima of across multiples cycles within same embryo, thus requiring the levels of Ana2 at the centriole to actually be increasing cycle on cycle – again unlikely. Instead, what this likely suggests, is that Ana2 incorporation, occurs earlier, most likely as the recovery up from the dip, and then is masked by the overwhelming effect of centriole separation on centrosome intensity. This would suggest that Ana2 incorporation begins far earlier than previously believed, or is suggested by the daughter detection data. The discrepancy with the daughter detection data is reasonable, as it requires the level of protein at the daughter to get above background and sufficiently above background such that deconvolution and latter gaussian fitting doesn't combine it with the high intensity source of the mother centriole. This delay in observation, through the same logic, likely applies to Sas-6, meaning their relative position should be similar and that both Sas-6 and Ana2 will begin building into the cartwheel approximately at M/A. Notably absent is data regarding Sas4 incorporation, which would be predicted to be similar, however, fly lines couldn't be generated in time due to the lack of functional tagged Sas4 that sufficient to rescue Sas4 mutants.

My data suggests that Sas-6 and Ana2 load onto centrioles with different kinetics. First, they suggest that Ana2 loads slightly before Sas-6, this was shown both at standard and super-resolution. Despite the difference being small, this would fit with current literature in which Ana2 promotes

Sas-6 ring formation [9,10]. However, with how slight the differences are, it is entirely plausible that these are the result of slight differences in the signal:noise, ratio and ability to detect the daughter from the background, from protein to protein as a result of the amount at the centriole and the exact imaging conditions. Second, and more notably, is the difference in when the separation of Sas-6 and Ana2 appears to occur, Sas-6 staying on for longer. One explanation for this would be poor alignment of data, this is unlikely though as this varies between being aligned with M/A in the case of Ana2, but notably after in the case of Sas-6. If this effect is not due to alignment, it would suggest that Sas-6-NG centrioles are harder to resolve with a larger structuring factor than Ana2-NG centrioles. This, however, is difficult to pull apart, as it could suggest differing localisation between Ana2 and Sas-6 within the centriole and its surroundings, though could equally convoluted with imaging settings, the amount of protein present, the general background, and the health/microtubule state of the embryo. Consequently, this is particularly hard to comment on, and is unlikely of biological relevance.

Chapter 3: Beyond the Cartwheel Dynamics – Ana3, CEP135, Ana1

Following the success generating and aligning aggregated cartwheel protein data, I expanded the methodology to beyond the cartwheel proteins. Up until now these have remained more elusive, without significant efforts to quantify their assembly overtime instead of as snapshots. In this way I investigated Ana3-NG, CEP135-GFP, Ana1-GFP and Asl-GFP, again in comparison with Jupiter-mCherry (*Tables 5.1 & 5.2)*. Within this chapter I describe the centrosomal fluorescence intensity and centriole:centrosome ratio profiles of beyond the cartwheel proteins to infer differences the regulation of their assembly processes. In addition, I observe an asymmetry between old- and new-mothers in initiation of assembly of daughter centrioles, where Sas-6-NG and Ana2-NG are detected earlier at old-mother centrioles, however, this asymmetry is not observed in Ana3-NG nor Cep135-GFP. Finally, I show mutant Cep135 does not appear to be necessary for centrosomal Ana1-GFP recruitment, in contrast to previous thinking.

3.1 Centrosomal dynamics of beyond the cartwheel proteins

Consistent across all proteins they incorporate protein at the centrosome from centriole separation onwards (*Figures 3.1-3.5)*, then they experience a dip between NEB and M/A, similar to Sas-6-NG and Ana2-NG. In addition

to this, for all proteins, the time normalised cycles map neatly atop each other, again suggesting that their action is coordinated with the cell cycle and stretch uniformly as such. CEP135-GFP and Ana1-GFP appear very similar in timing (*Figures 3.2 & 3.3)*, however, CEP135-GFP levels at the centrosome are notably higher after the dip while Ana1-GFP appears largely symmetric directly about the dip and less clearly defined. Aligned comparisons (*Figure 3.5)* show Ana3 incorporating quickly from the initial computed separation, peaking earlier, while CEP135-GFP and Ana1-GFP take longer to incorporate at their maximal rates and also longer to peak. This suggests a putative order of Ana3 incorporating before CEP135-GFP and Ana1-GFP. Asl-GFP (*Figure 3.4*) appears to occupy a middle ground, incorporating quickly initially, more akin to Ana3, but then entering a slower phase of gradual accumulation, potentially with another sharp phase at following the dip. An unusual feature of the dip in Ana3 (*Figure 3.1)*, is a conserved dogtooth motif in the centre of it, suggesting a transient burst of incorporation that is almost immediately lost before later accumulation.

Figures 3.1-3.4 Centrosome Incorporation Profile of Ana3-NG, Cep135-GFP, Ana1-GFP and Asl-GFP (next 4 pages) *Mean centrosome fluorescence intensity plotted against time (composite & overlayed – seconds; individual - 12 second frames) across nuclear cycles. Nuclear cycles are defined by the computed fluorescence intensity minima caused by centriole separation. Composite & overlayed graphs consist of multiple embryo tracks aggregated via mean averaging of time and amplitude normalised aligned individual tracks. Nuclear envelope breakdown and the Metaphase/Anaphase transition are shown with blue/yellow and red/orange bands denoting the distribution of event timing within datasets. Standard error of the mean is shown as dashed lines or error bars.*
Composite number of embryos: Ana3 Cycle 11 – 8, Cycle 12 - 9, Cycle 13 – 6; Cep135 Cycle 11 – 3, Cycle 12 - 6, Cycle 13 – 4; Ana1 Cycle 11 – 8, Cycle 12 - 8, Cycle 13 – 8; Asl Cycle 11 – 6, Cycle 12 – 10, Cycle 13 – 2

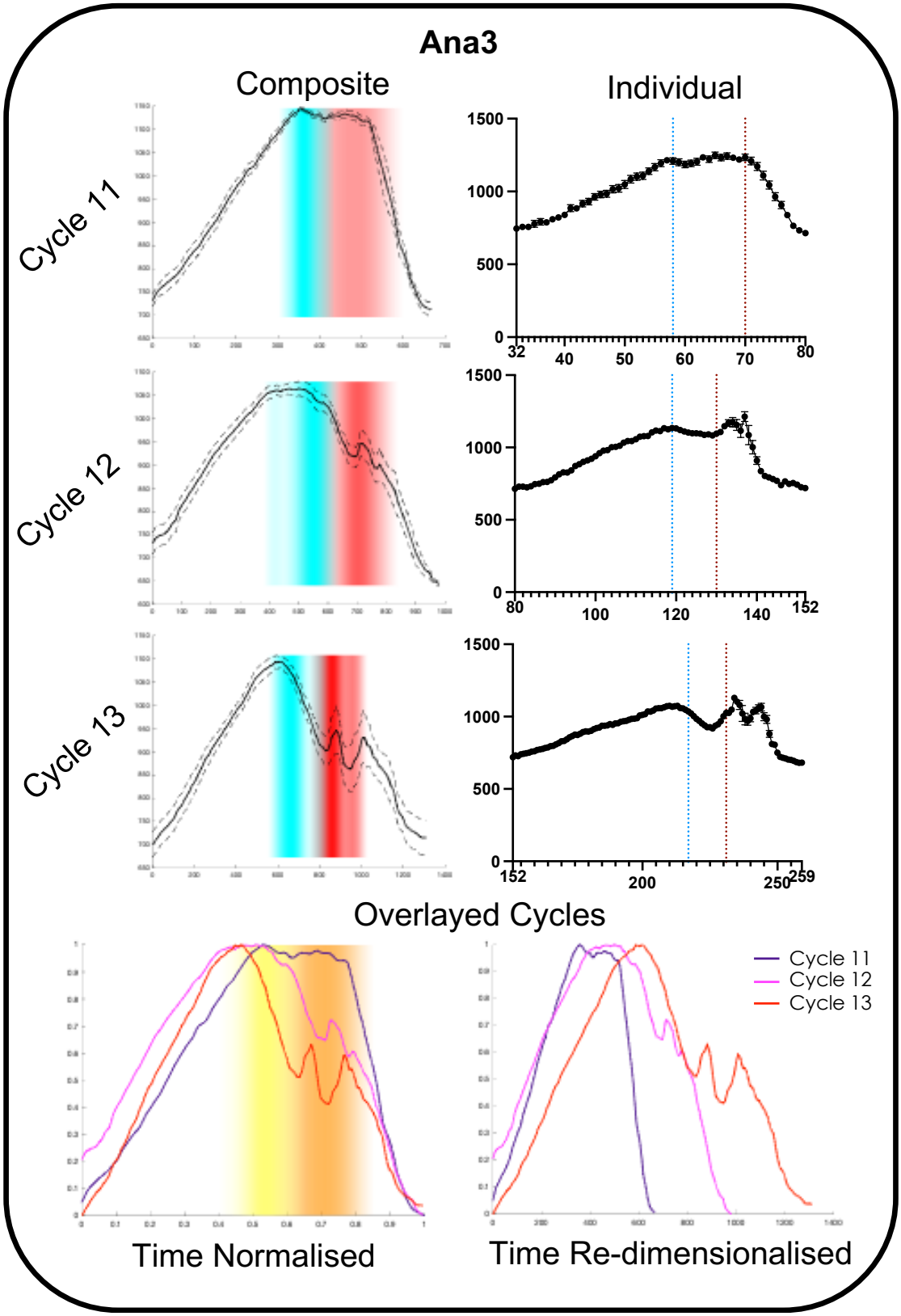
Ana3
Composite
Individual
Cycle 11
Cycle 12
Cycle 13
1500
1000
500
0
32
40
50
60
70
80
100
120
140
152
200
250
259
Overlayed Cycles
Cycle 11
Cycle 12
Cycle 13
Time Normalised
Time Re-dimensionalised

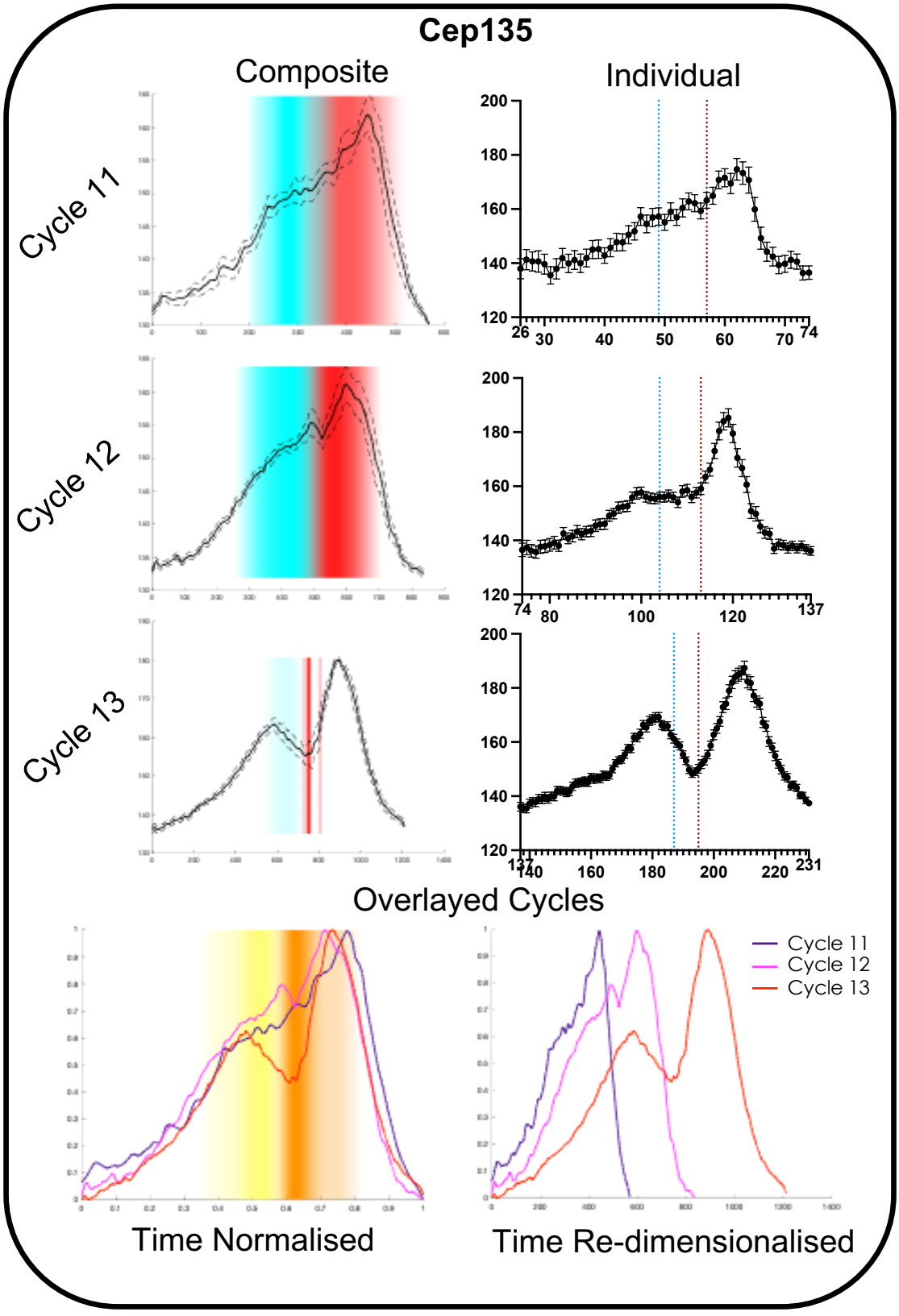
Cep135
Composite
Individual
Cycle 11
Cycle 12
Cycle 13
Overlayed Cycles
Cycle 11
Cycle 12
Cycle 13
Time Normalised
Time Re-dimensionalised

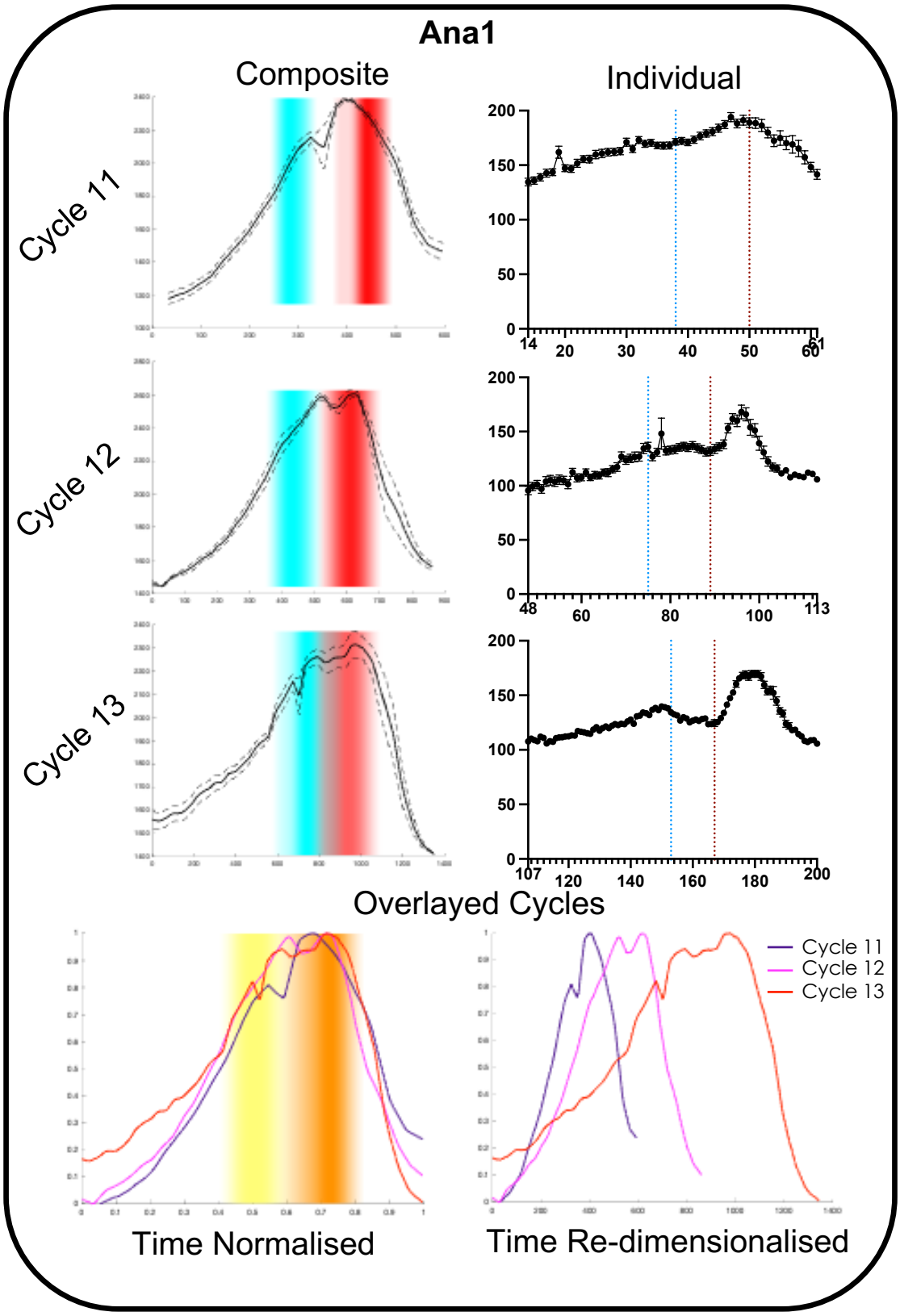
Ana1
Composite
Individual
Cycle 11
Cycle 12
Cycle 13
Overlayed Cycles
Cycle 11
Cycle 12
Cycle 13
Time Normalised
Time Re-dimensionalised

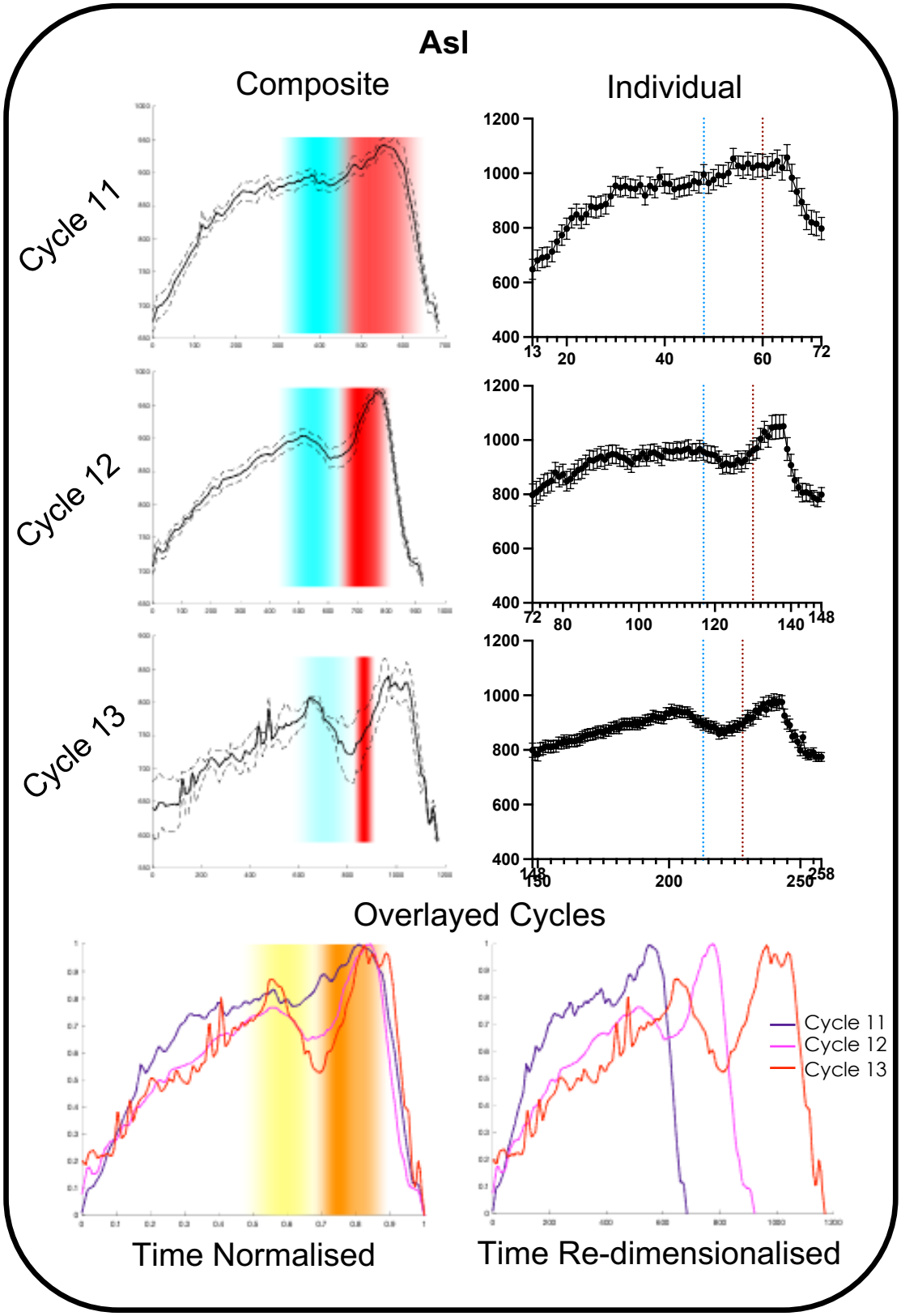
AsI
Composite
Individual
Cycle 11
Cycle 12
Cycle 13
1200
1000
800
600
400
13
20
40
60
72
72
80
100
120
140
148
148
150
200
250
258
Overlayed Cycles
Cycle 11
Cycle 12
Cycle 13
Time Normalised
Time Re-dimensionalised

Cycle 11

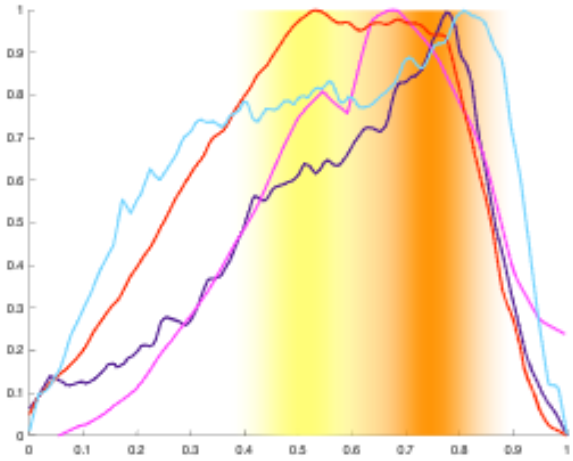

Cycle 12

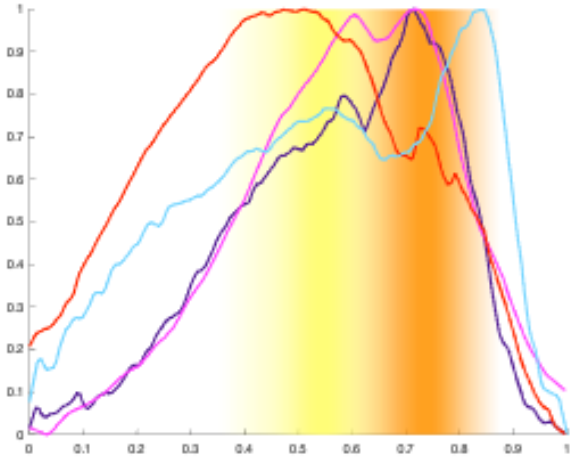

Cycle 13

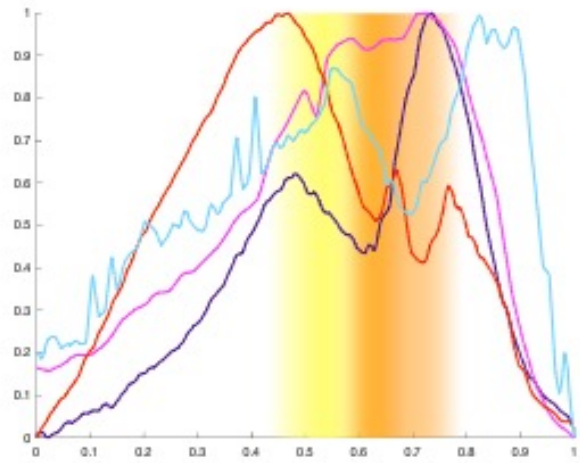

Figure 3.5 Comparison of Cep135-GFP, Ana1-GFP, Ana3-NG and Asl-GFP incorporation profiles (page before) *Overlayed composite incorporation trends showing the mean normalised fluorescence centrosome intensity verses progression of cycle of Cep135, Ana1, Ana3 and Asl across nuclear cycles. Nuclear cycles are defined by the computed fluorescence intensity minima caused by centriole separation. Timings of nuclear envelope breakdown and the metaphase/anaphase transition within the dataset are shown by yellow and orange distribution bands respectively.*
Composite number of embryos: Ana3 Cycle 11 – 8, Cycle 12 - 9, Cycle 13 – 6; Cep135 Cycle 11 – 3, Cycle 12 - 6, Cycle 13 – 4; Ana1 Cycle 11 – 8, Cycle 12 - 8, Cycle 13 – 8; Asl Cycle 11 – 6, Cycle 12 – 10, Cycle 13 – 2

3.2 Super-resolution characterisation of Ana3 & CEP135 daughter loading

To better understand probe the order of incorporation and what structures the incorporation could be assigned to, SoRa time-lapses of the Ana3-NG and Cep135-GFP fly lines were collected and analysed as described previously for Sas-6-NG and Ana2-NG. This analysis confirms the difference in when the daughter loads Ana3 vs CEP135 (*Figure 3.6.E&F*), showing Ana3 beginning loading at least 20% of the cycle length earlier than CEP135. Like Sas-6 and Ana2, Ana3 begins to show a daughter around computed centriole separation in line with when its incorporation appears to occur into the centrosome (*Figure 3.6.A&C)*. In contrast, CEP135 shows a daughter notably after incorporation into the centrosome is visible *(Figure 3.6.B&D)*, suggesting that this early phase of incorporation is actually going into the mother, not the daughter centriole. In later cycles CEP135's initial incorporation appears to have two rates of incorporation, potentially suggesting a switch from single to double centriole loading. This, however, is hard to see in cycles 11 and 12 so may be an exponential

trend as opposed to two linear increases. Similarly, to Ana2 and Sas-6, resolving centriole separation of CEP135 appears to occur after Ana3.

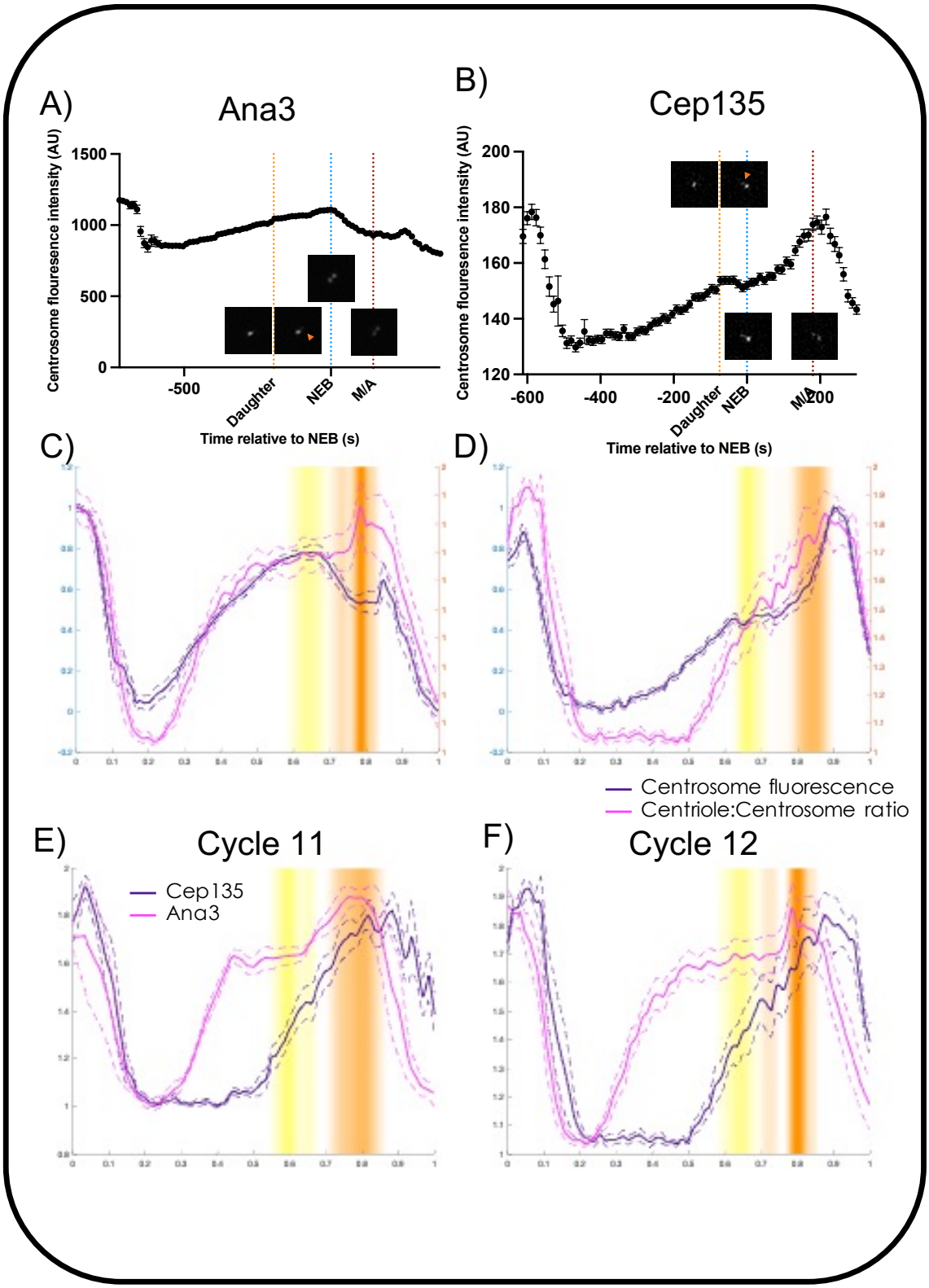

Figure 3.6 Super-resolution quantification of Ana3 & Cep135 appearance on the daughter (previous page) *A&B) Ana3 & Cep135 centrosomal incorporation across cycle 12 individual embryos, showing centrosome intensity over time in seconds, with nuclear envelope breakdown and the metaphase/anaphase transition annotated. Tracks are shown between M/A of cycle 11 and the midbody breakdown in cycle 13. Similar length cycle 12 super-resolution images have been aligned relative to NEB with the frame before and after the visual appearance of the daughter shown (Yellow line, Orange arrowhead) as well as the centriole state at NEB and M/A. C&D) Ana3 & Cep135 aggregated cycle 12 centrosomal incorporation (left axis) overlayed with the super-resolution centriole:centrosome ratio (right axis) between M/A of cycle 11 and the midbody breakdown in cycle 13. Standard error of the mean is shown by the dashed lines and NEB & M/A distribution is represented by the yellow and red distribution bars respectively. E&F) Comparison between Ana3 and Cep135 cycle 11 & cycle 12 quantifications of centriole:centrosome ratio shown between M/A the previous cycle and the midbody breakdown in the next. Standard error of the mean is shown by the dashed lines and NEB & M/A distribution is represented by the yellow and red distribution bars respectively.*
Composite number of embryos: Ana 3 Standard resolution Cycle 12 – 8, Super-resolution Cycle 11 – 3, Cycle 12 - 5; Cep135 Standard resolution Cycle 12 – 9, Super-Resolution Cycle 11 – 5, Cycle 12 – 5

3.3 Comparison of Cartwheel and Beyond cartwheel assembly dynamics

Using the aggregated datasets from cartwheel proteins and beyond the cartwheel proteins, the overall incorporation profile can be combined to generate a highly detailed picture of the order of centriole assembly. Comparing the standard resolution data from centriole proteins (*Figure 3.7 & supp. Figure 4)*, a clear order is established of centrosome incorporation is established with Sas-6, Ana2, Ana3 and Asl loading first into the centrosome, then later CEP135 and Ana1 being incorporated. Of note, Sas-6 and Asl appear to have similar patterns of inflection points and follow a similar trend of initial incorporation, despite Asl then peaking higher following the dip. Furthermore, the alignment further shows reasonable conservation of the positioning of the dip, further suggesting it's a conserved process across the entire centrosome.

Cycle 11

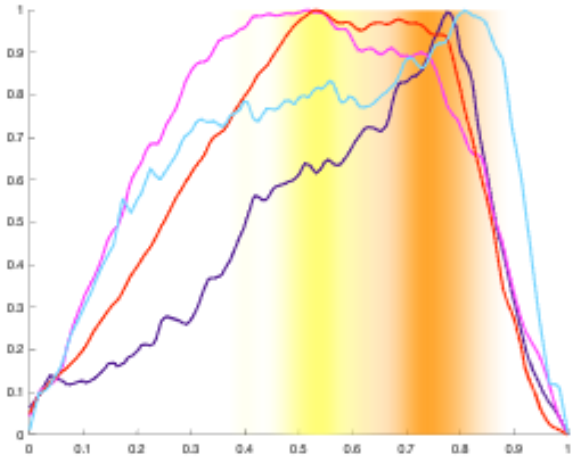

Cycle 12

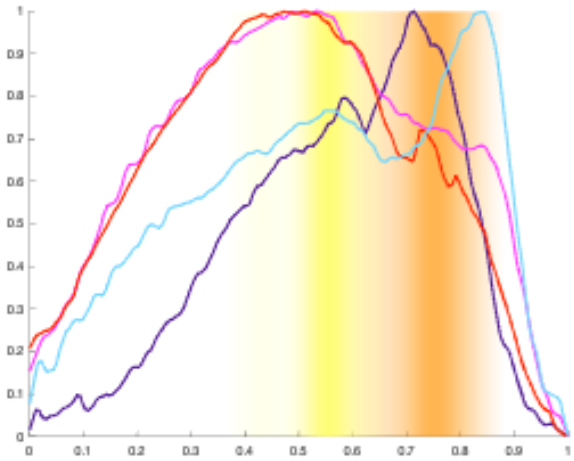

Cycle 13

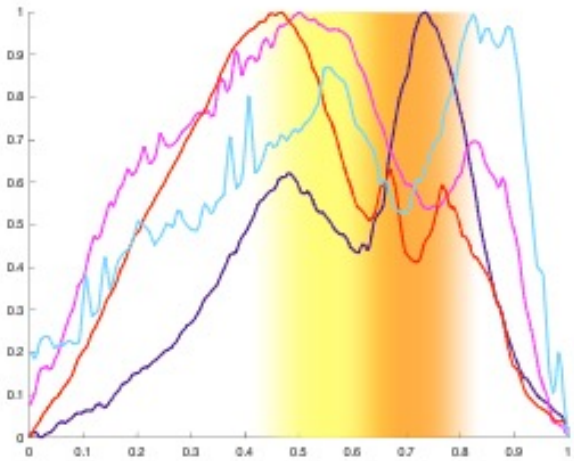

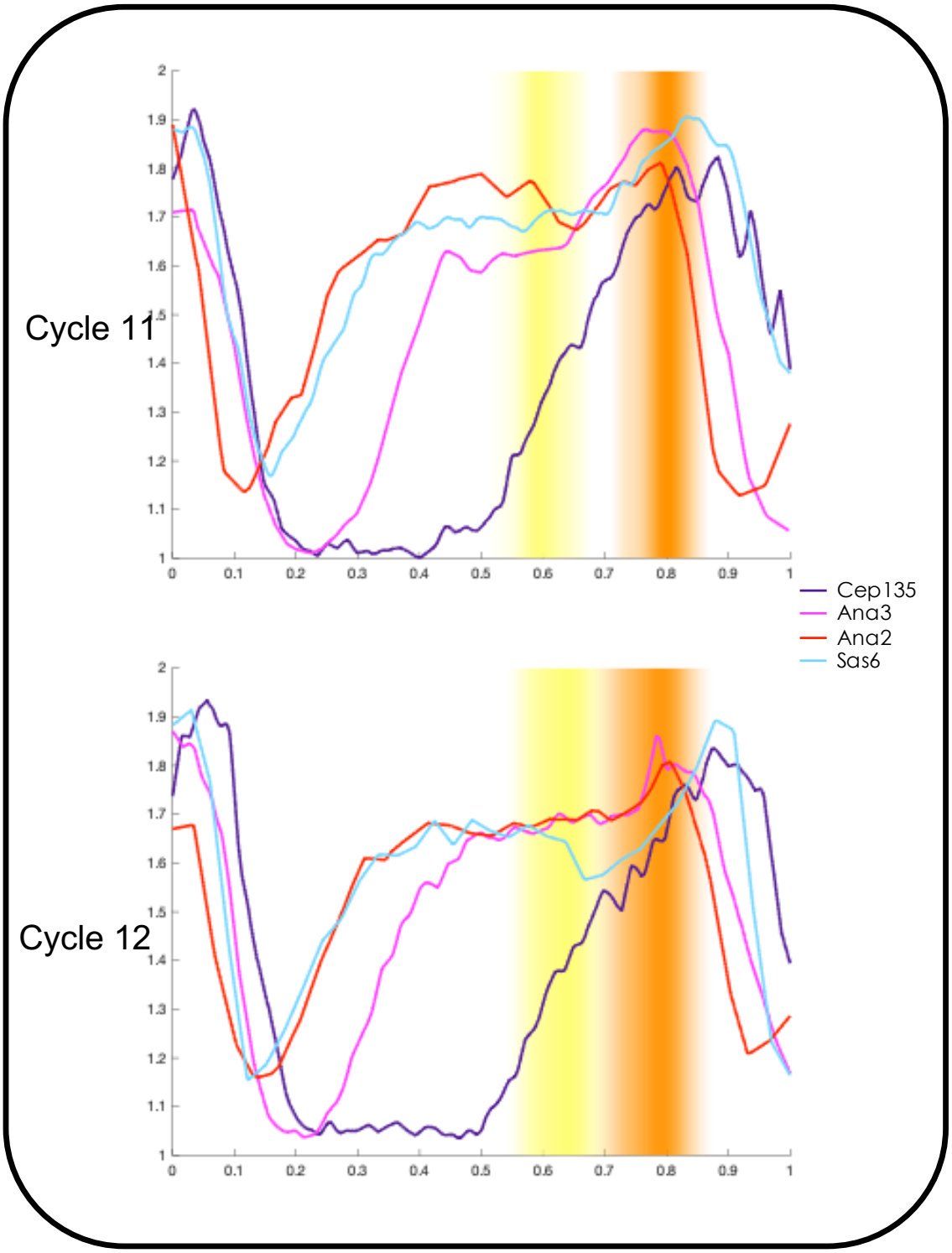
Cycle 11
Cycle 12
Cep135
Ana3
Ana2
Sas6

Figure 3.7 Comparison of Sas6-NG, Ana3-NG, Cep135-GFP and Asl-GFP incorporation profiles (2nd previous page) *Overlayed composite incorporation trends showing the mean normalised centrosome fluorescence intensity verses the cycle progression of cycle of Sas6, Ana3, Cep135 and Asl. Nuclear cycles are defined by the computed fluorescence intensity minima caused by centriole separation. Timings of nuclear envelope breakdown and the metaphase/anaphase transition within the dataset are shown by yellow and orange distribution bands respectively. Graphs consist of multiple embryo tracks aggregated via mean averaging of time and amplitude normalised aligned individual tracks.*
Composite number of embryos: Ana3 Cycle 11 – 8, Cycle 12 - 9, Cycle 13 – 6; Cep135 Cycle 11 – 3, Cycle 12 - 6, Cycle 13 – 4; Ana1 Cycle 11 – 8, Cycle 12 - 8, Cycle 13 – 8; Asl Cycle 11 – 6, Cycle 12 – 10, Cycle 13 – 2; Sas6 Cycle 11 – 9, Cycle 12 - 15, Cycle 13 – 8; Ana2 Cycle 11 – 3, Cycle 12 - 6, Cycle 13 - 4
Figure 3.8 Comparison of Cep135, Ana3, Ana2 and Sas6 appearance on the daughter (previous page) *Comparison between Cep135, Ana3, Ana2 and Sas6 cycle 11 & cycle 12 quantifications of centriole:centrosome ratio shown between M/A the previous cycle and the midbody breakdown in the next. Standard error of the mean is shown by the dashed lines and NEB & M/A distribution is represented by the yellow and red distribution bars respectively.*
Composite number of embryos: Cep135 Cycle 11 – 5, Cycle - 12; Ana3 Cycle 11 – 3, Cycle 12 – 5; Ana2 Cycle 11 – 2, Cycle 12 – 3; Sas6 Cycle 11 – 14, Cycle 12 - 2

Comparing the super resolution data (*Figure 3.8)*, the appearance of the daughter further refines the order of loading, such that Ana2 and Sas-6 show on the daughter earliest, then Ana3, and finally CEP135. Of note, Ana2 and Sas-6 show a higher initial probability of daughter centriole detection (exhibiting an in initial centriole:centrosome ratio of ~1.2 in early S-phase; Figure 3.8) than CEP135 and Ana3 (where this ration is just over 1.0; Figure 3.8). This suggests that Ana2 and Sas-6 may start loading onto the daughter centrioles prior to the detectable separation of the old and new-mother centrioles—so that some daughter centrioles are already detectable by the time the old- and new-mother centrioles can be resolved as two independent centrioles at the start of S-phase.

Finally, a manual "pedigree" analysis of the super resolution data (tracing back the history of the centrioles so that I could separate out the behaviour of old- and new-mothers) revealed a striking asymmetry in the timing of daughter centriole assembly. Sas-6 and Ana2 were both detectable on the daughters of the old-mother centrioles approximately 90 seconds before they were detectable on the daughters of the new-mother centrioles (*Figure 3.9.A&B*). This strongly suggests that new-mother centrioles, which only started to recruit Asl (the key protein that recruits PLK4 to initiate centriole assembly [9,60,85]) a few minutes previously, are slightly delayed in initiating centriole assembly compared to the old-mothers, which already have recruited a full complement of Asl. Interestingly, no such asymmetric loading was observed for Ana3 or Cep135 (*Figure 3.9.C-E*), further supporting the conclusion that Ana2 and Sas-6 start to load onto daughter centrioles at the very earliest stages of their assembly.

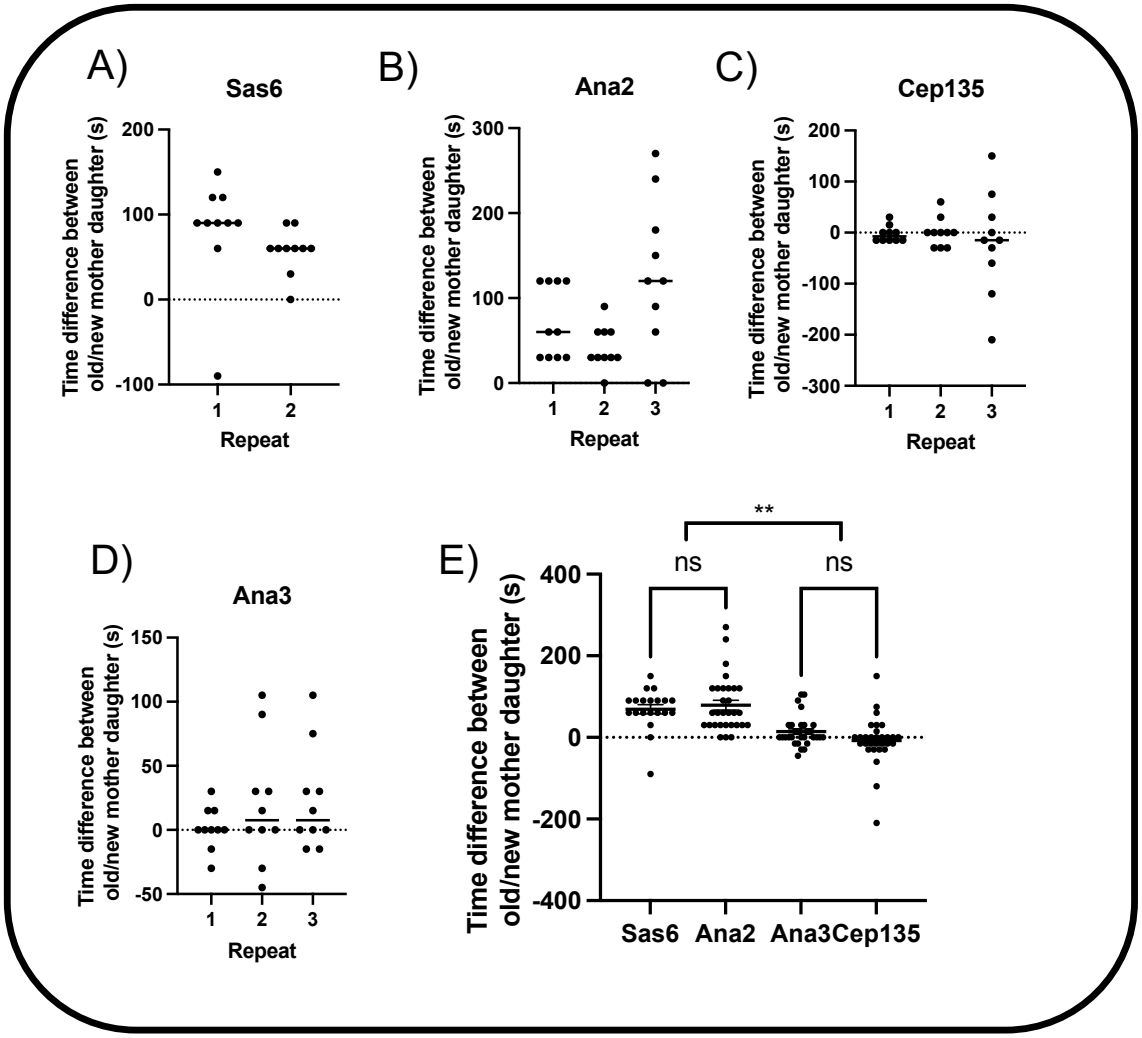

Figure 3.9 Asymmetry in daughter loading between old and new mother centrioles *A-D) Quantifications of time between protein loading onto the daughter of the old and new mother; positive numbers indicate the old mother loading first, while negative, the new mother first. Each repeat represents an independent embryo, within which 10 centrosome pairs were recorded. E) Aggregate comparisons of of time between protein loading onto the daughter of the old and new mother; positive numbers indicate the old mother loading first, while negative, the new mother first. No significant differences were found between Sas6 and Ana2 or Ana3 and Cep135, while inter-group comparisons are significantly different (One-way ANOVA with Tuckey's multiple comparisons, ** P<0.005)*

3.4 CEP135 is not necessary for centrosomal recruitment of Ana1

To better understand the role of CEP135 at the centriole, I decided to compare the recruitment of Ana1 in a mutant *CEP135* background where one copy had a complete N-terminal deletion while the other copy had the promoter inactivated via p-element insertion *(Tables 5.1 & 5.2)*. In both cycle 11 and cycle 12 mutant embryos showed no evidence of perturbed or reduced recruitment of Ana1 (*Figure 3.10*). In fact, in both cycles the peak before the dip was proportionally higher than after, which could suggest that perturbing CEP135 function lead to an earlier or more efficient incorporation of Ana1. This strongly refutes the claim that CEP135 is essential for the recruitment of Ana1 to centrioles [32].

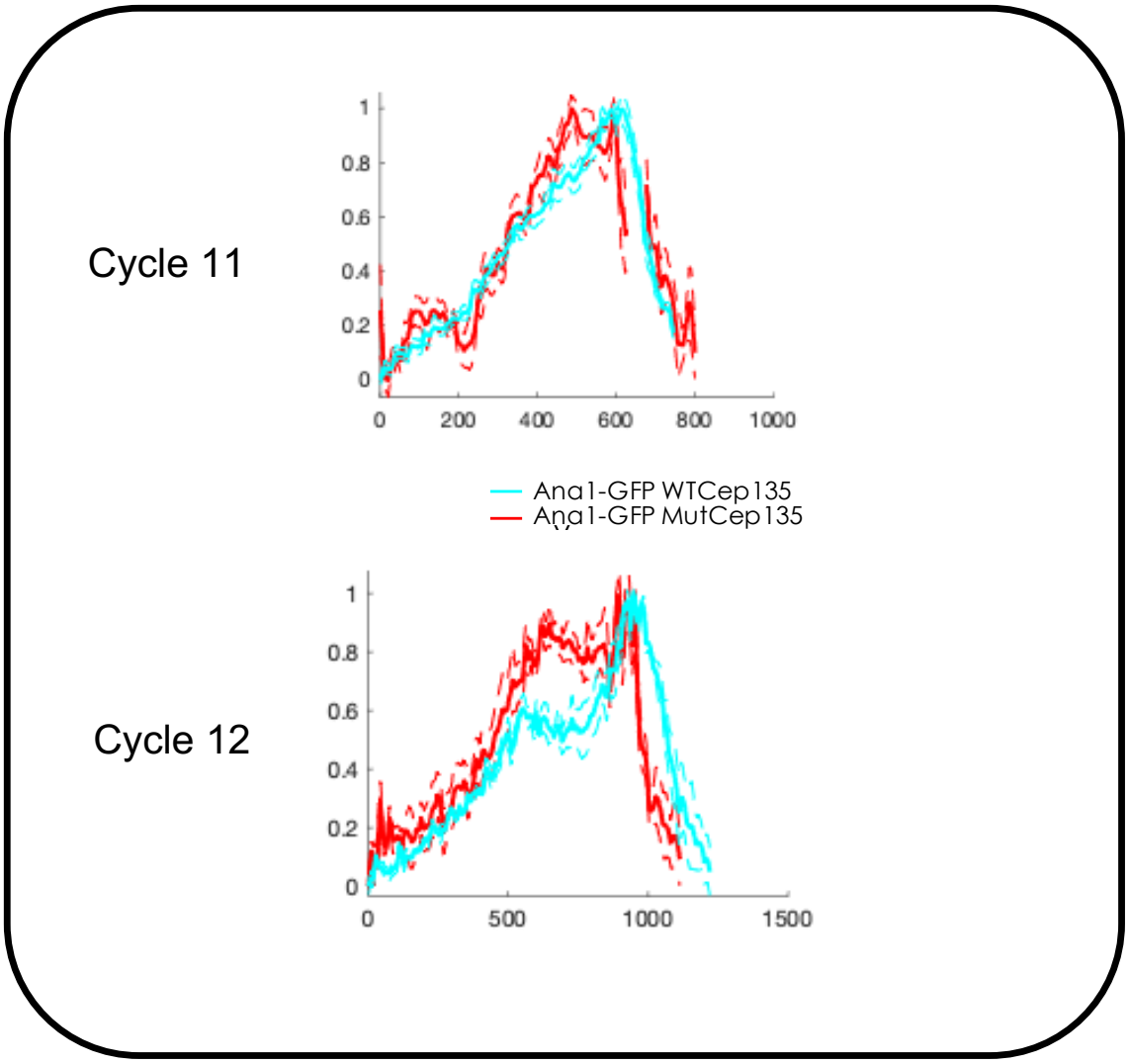

Figure 3.10 Effect of Mutant Cep135 on Ana1 incorporation *Overlayed composite incorporation trends showing the mean normalised fluorescence centrosome intensity verses time (seconds) in cycles 11 and 12 Ana1 in a wild type or mutant Cep135 background. Nuclear cycles are defined by the computed fluorescence intensity minima caused by centriole separation. Standard error of the mean is shown through dashed lines.*
Composite number of embryos: WTCep135 Cycle 11 – 7, Cycle 12 – 10; Mutant Cep135 Cycle 11 – 4; Cycle 12 - 5

3.5 Discussion

Alignment of super-resolution data quantifying the appearance of daughter centrioles has demonstrated a clear order of centriole assembly: Ana2, Sas-6, Ana3 then CEP135. Due to a lack of time, I could not generate the appropriate lines to test Sas4, Ana1 and Rcd4 in the same way, although plans are underway in the laboratory to do this. Previous data, however, suggests that Sas4 will incorporate into daughter centrioles with similar timing to Sas-6 and Ana2, due to begin an integral cartwheel component [3,11,15]. Rcd4 forms a functional complex with Ana3, so I would expect their incorporation timing to be similar [21,90]. Finally, I have shown that Ana1-GFP has a similar incorporation profile to CEP135-GFP, so I would predict their timings of loading onto the daughter would be similar.

Asl was imaged in super-resolution, however, the drastic asymmetry (Asl is much brighter on the old-mother than the new-mother) masked the low intensity daughter/new-mother and the centriole:centrosome ratio fell out of reasonable parameters. While this reduces the confidence in the Asl data, there is a clear hint in this data that daughter loading occurs just prior to centriole separation (i.e as the daughter is transitioning to a new-mother), which is consistent with expectations (*supp Figure 4)*. Consequently, this data can inform across the entire set of conserved centriole proteins.

The increased probability of initial Sas-6-NG and Ana2-NG daughter detection, verses Ana3-NG and CEP135-GFP, aligns with the standard resolution suggesting Ana2-NG and Sas-6-NG incorporate earlier, leading it to being caught partially incorporated at the point of detection, with the previous loading obscured by centriole separations. This may inform as to why Sas-6-NG, Ana2-NG and Ana3 all align roughly with computed centriole separation despite Sas-6 and Ana2 loading earlier. This also highlights limits of both methods as the dominant effect of centriole separation leads to significant convolution of what is actually going on at the centriole. Despite individual limitations, the combination of these methods appears to be able to better probe into this convolution: the more sensitive standard resolution data giving insight directly before separation, then the fully quantitative super-resolution data giving insight on assembly started during separation. Thus, while individually powerful, the combination clearly becomes "more the than sum of parts", enabled by the alignment process.

The asymmetric timing of cartwheel growth between new and old-mothers came as a surprise: if controlled solely by cell cycle regulators and global PLK4 levels then both daughters should begin cartwheel growth at similar times. As cartwheel growth is not synchronised, it suggests a rate limiting asymmetry in new-mothers. The two most likely candidates for asymmetry are PLK4 and Asl, as these are the key proteins directly

upstream of new cartwheel development. In the case of PLK4, to grow a new daughter, PLK4 accumulates around the centriole then symmetry breaks down to a focus [7,8]. Previously it has been suggested, this could leave a "bud scar" [77], which could then direct and accelerate future symmetry breaking, allowing the old-mother to grow a daughter cartwheel before the new-mother. While this is plausible, at time of writing there is no clear evidence for this process, leaving this as speculation. The more likely hypothesis, is that Asl is asymmetrically distributed between the old and new-mother [33], and consequently the old-mother has more capacity to recruit PLK4 until the new-mother finishes recruiting its full complement of Asl. This is visually apparent in the super-resolution data which showed distinct asymmetry between the old and new-mother. In addition, the attempted quantification of the timing of Asl loading places this just before centriole separation, which would give minimal time for the new-mother to recruit up to its full complement of Asl (presumably explaining why old- and new-mother centrioles are so asymmetric for Asl recruitment). Finally, the Sas-6 incorporation profile before NEB aligns well with features in the Asl profile up to NEB. This would be compatible with the Asl loading to the new-mother enabling increased recruitment of Sas-6.

As this asymmetry doesn't appear in Ana3 or CEP135, it suggests that their loading is independent of the timing of initial cartwheel appearance.

Simply, this could be explained as Ana3 and CEP135 loading being influenced by cell cycle regulators, and thus globally controlled. The alternative hypothesis would be that the cartwheel can adjust the rate it grows such that the asymmetry is lost by the time Ana3 or CEP135 loads. This is plausible as PLK4 levels have been suggested to influence the rate of Sas-6 incorporation: in shorter cycles, centriolar PLK4, peaks higher and confers a greater rate of cartwheel assembly [83,84]. Therefore, it's plausible that in new-mothers could have shorter, more intense, PLK4 peaks leading to faster cartwheel growth, CEP135 and Ana1 show similar trends of incorporation however show a notable the difference in the relative heights of their centrosomal intensities before and after centriole separation, in the case of CEP135 only reaching maximal intensity after while Ana1 managing before. This is easily explained for CEP135 as super-resolution data only resolves the daughter loading barely prior to NEB, and so following the dip this increase up to a maxima corresponds to the centrosome moving to a state with two CEP135 positive centrioles. This is particularly evident in cycle 13 where the gradient leading up to NEB and up from the dip appear steeper than immediately post centriole separation, this likely represents one vs two centriole loading of CEP135. In practice this would predict, at the start of the cycle a mother in each centrosome would be loading CEP135, then before NEB daughters begin loading CEP135, thus increasing the rate of incorporation. During the dip, CEP135 is released from the centrosome, then due to a similar rate of

incorporation is likely to be recovered both on the mother and daughter centriole. This, however, would require further FRAP or old/new-mother tracking to confirm.

In contrast to Cep135-GFP the Ana1-GFP data shows a less clearly defined dip in fluorescence, potentially slightly earlier, and in composites do not reach as high a second peak. This may be due to the reduced genetic quality of the Ana1-GFP fly line as only one copy of tagged Ana1 was present in a homozygous endogenous background (*Table 5.1&5.2)*. This leads to reduced overall contrast and the potential for Ana1-GFP to be excluded in favour of endogenous Ana1, potentially resulting in the minimised dip. Caveats in mind, the more balanced peaks in centrosomal intensity suggest recruitment to the daughter centriole may occur before that of CEP135. This is surprising as it opposes existing literature which suggests that CEP135 recruits Ana1 to the centriole thus implying that CEP135 would tend to load first [32].

Chapter 4: Discussion

4.1 Appraisal of Methodology

This work represents the first concerted effort to quantify and compare the incorporation of core centriole proteins into growing centrioles. Prior to this wide scale comparisons were primarily made via taking super-resolution snapshots of centrioles and comparing presence of co-expressed tagged proteins [32,72]. This lead to prior studies being particularly sensitive to the signal:noise ratio and prevented them from providing true temporal data to align with cell cycle events. Through measuring the fluorescence changes of hundreds of centrioles per embryo, this improved methodology [83] provides much higher sensitivity via the combination of large amounts of low bit-density data. This work has further improved this by allowing the aggregation of data across embryos, improving reliability through additional biological repeats, while also further honing sensitivity through increased numbers of centrioles. Within this work, I have demonstrated the capacity for composite data to preserve the individual features seen within individual tracks, this confirms the faithful aggregation of data and improves confidence that these features are not merely noise. A significant benefit of this analysis scheme is the ease of comparison between datasets. Within this work, it has been utilised both to flexibly compare between centriolar proteins, genetic backgrounds, and data types i.e., standard resolution fluorescence intensity and super-

resolution daughter detectability. This demonstrates the robustness and widespread applicability of this method for investigating centrioles and centrosomes within the *Drosophila* early embryo.

This work is a clear demonstration of the capability of SoRa spinning disk microscopes. As SoRA microscopy allows for reduced photobleaching relative to other super-resolution techniques, it enabled the practical capture of super-resolution timelapses across the timescales of early embryo nuclear divisions while maintaining high temporal resolution and image quality. This enabled continuous analysis of the appearance of individual proteins onto the daughter, giving previously unparalleled time resolution on when proteins load onto the daughter. While this data is unable to provide quantitative intensity data, its combination with standard resolution data, provides significant insight into centriole assembly, particularly improving the ability to deconvolute what is going on during the centriole separation "blind spots". The ability to perform fluorescence recovery after photobleaching (FRAP) on the SoRa, while not explored within this work, provides a powerful further tool to be explored in future. This can enable deconvolution of which centriole is loading protein and when, which played a key role in understanding the nature of Sas-6 and Ana2 incorporation and so should be similarly applied to beyond the cartwheel proteins, particularly CEP135, such that their incorporation can be structurally assigned.

4.2 Cartwheel Construction

This work significantly alters the previously understood paradigm of cartwheel construction (*Figure 4.1*). First, the incorporation of Sas-6 and Ana2 before computed centriole separation, around M/A, suggests the cartwheel may be being assembled earlier than previously thought within the *Drosophila* early embryo. Second, this work shows that a sizeable proportion of the Sas-6-NG, and essentially all of the Ana2-NG, incorporated into centrosomes during S-phase is subsequently lost from the centrosome as the embryos enter mitosis. This indicates the presence of a large transient fraction of protein at the centrosome, out of which the cartwheel is constructed, akin to a primordial "soup". Together, these pieces of information put into question the previous Aydogan et al. studies[83,84]. These studies are underpinned by the assumption that the daughter cartwheel is assembled between centriole separation and NEB proportional to the sum of Sas-6-GFP incorporated. The previously mentioned studies, had used Sas-6-GFP incorporation as a measure of cartwheel growth to investigate PLK4's regulatory role. While this study doesn't directly dispute the conclusions on PLK4's regulatory activity, it does raise questions to the previously mentioned assumption. This is because if cartwheel growth cannot be separated from incorporation into the soup: it is plausible that the cartwheel grows incredibly quickly, and later incorporation into the soup is merely a consequence of the PLK4

recruitment platform taking time to dissipate. If this is the case then PLK4's precise dynamics could be interpreted instead as regulating the soup rather than the cartwheel.

The discrepancy in data between embryos expressing Sas-6-NG and Sas-6-GFP serves as a caution to the study of endogenously tagged centriole proteins. While the differences between the two incorporation profiles may be due to variations in fluorescence characteristics of mNeonGreen and GFP, the degree of difference in the overall trend suggests a notable change in Sas-6 functionality based on the fluorophore it is fused to. The effect of fused fluorophores on Sas-6 functionality is further supported by the poor health of Sas-6-mCherry expressing embryos [84]. This, in turn, can be interpreted to suggest that the structure of the central cartwheel is spatially restrictive to the extent that it is particularly sensitive to the addition of fluorophores into this structure. Overall, this makes investigating the incorporation dynamics of the central cartwheel deceptively difficult and demonstrates the importance of developing and screening probes, such as fluorophores, to minimise their impact on the biology they are designed to observe. In this case NeonGreen is a smaller protein with improved fluorescent qualities over GFP [133]. In addition, within this study, Sas-6-NG was generated via a CRISPR knock-in at the endogenous locus rather than as a transgenic insertion as used with Sas-6-GFP. Together, this suggests that this study will benefit from expression

characteristics and Sas-6 function closer to that of wild-type embryos, however it is inherently difficult to confirm this.

Figure 4.1 Revised model of Centriole Assembly (next page) *Model centrosomal incorporation and daughter detection trends are shown aligned between computed centriole separations (CS). Approximate positioning of NEB and M/A are shown with yellow and orange dashed lines. Illustrations below the graphs show the progression of central cartwheel assembly and appearance of the "soup" throughout the cycle. Between M/A and NEB, the new and old mother centrioles disengage. First the old mother, then the new mother, begin growing daughter centrioles and accumulating "soup". Around the entry into the mitosis of the next cycle, their assembly is complete and the soup is shed from the daughter centrioles. These daughter centrioles will then disengage and become new mother centrioles to repeat the cycle.*

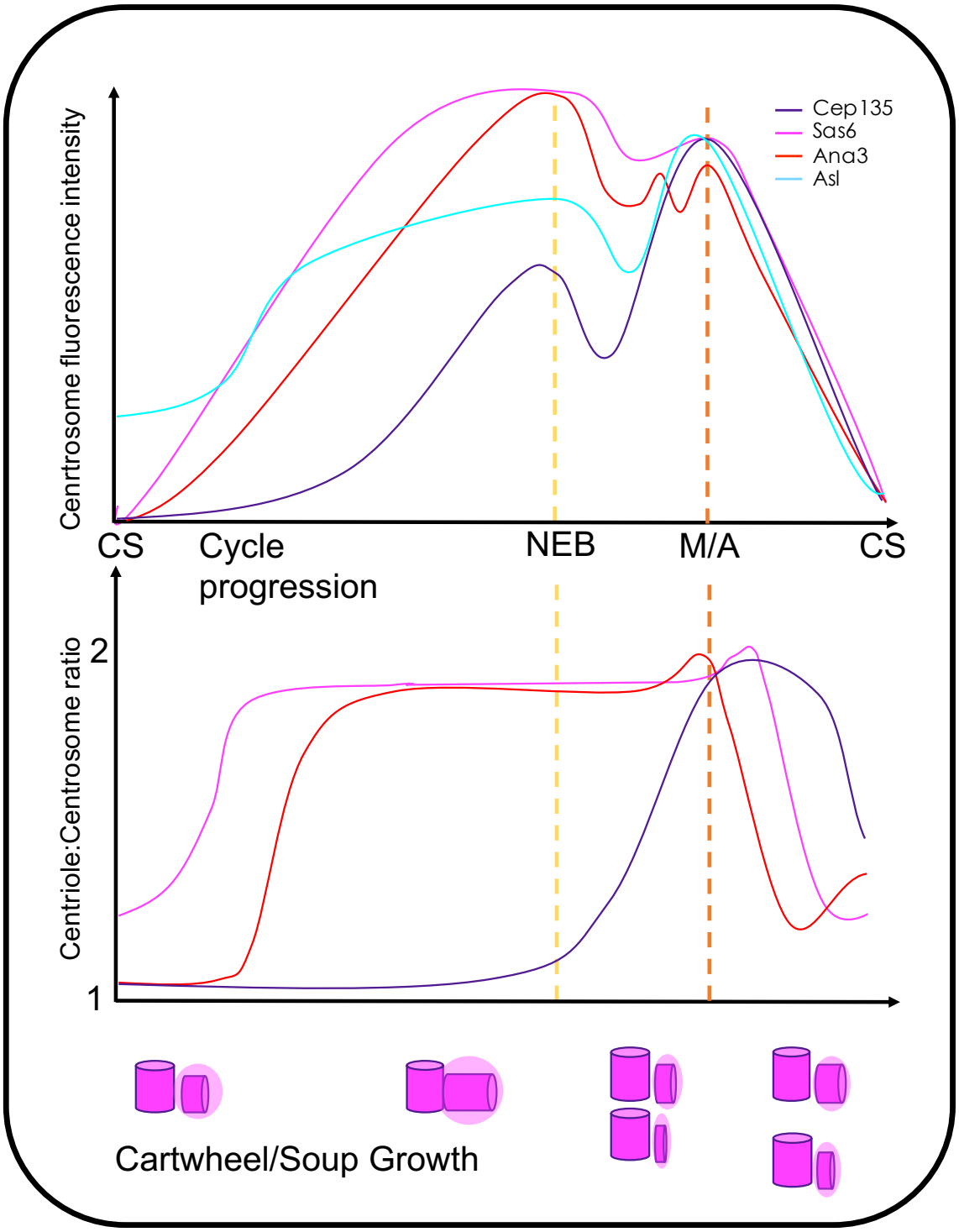
Cep135
Sas6
Ana3
Asl
Centrosome fluorescence intensity
CS
Cycle progression
NEB
M/A
CS
Centriole:Centrosome ratio
2
1
Cartwheel/Soup Growth

An obvious question is whether or not the soup has a specific function, or is just excess. On one hand, the sheer quantity of protein in the soup, particularly in the case of Ana2, could indicate there is a function for it, as otherwise it seems somewhat wasteful. On the other hand, it may instead be a symptom of needing rapid assembly of the cartwheel yet not having the evolutionary pressure to develop a system to dissociate excess material rapidly. This is further supported as centriole proteins appear to be in excess in the *Drosophila* early embryo [46], it is thus logical to assume the centrosome will then saturate upon becoming competent to recruit proteins such as Sas-6 and Ana2, potentially above the level that is required for cartwheel assembly. This may be a phenotype specific to the *Drosophila* early embryo, as its protein production relies on the initial injection of maternal mRNA [134]. Consequently, this degree of excess may be a function of the early embryo having the protein readily available to rapidly produce thousands of centrioles. This specific case would thus reduce the evolutionary pressure to add a further system to restrict levels at the centrosome, supporting the argument of it being biologically irrelevant, instead just a quirk of the system.

While asymmetry between the new and old-mother centrosome is not a new concept [135], this work shows the first convincing evidence showing asymmetry in the timing of daughter cartwheel assembly. While this is unlikely to have downstream functional purpose, it could provide

significant diagnostic value in understanding the latter stages of centriole assembly and the initiation of new cartwheel growth. This is because the asymmetry encodes the rate limiting step of cartwheel growth, therefore, by selectively arresting the cycle or by altering the concentrations/activities of Asl and PLK4 the limiting step can likely be found. The *Drosophila* early embryo context may be particularly important here, as there are not defined phases in interphase, and the embryo is permissive of centriole duplication immediately after mitosis. Potentially in somatic cells, the increased time between mitosis and centriole conversion and duplication may allow Asl levels to equilibrate potentially destroying the asymmetry.

4.3 Function and Dynamics of Beyond the Cartwheel Proteins

A notable surprise from this study was the relationship between CEP135 and Ana1. First, they appear to load at least coincidentally, with the plausible potential of Ana1 loading earlier. Second, and most shocking, was the negligible effect of mutant CEP135 on Ana1 recruitment. This is in contradiction to the conclusions of a prior study by Fu et al [32] which suggested CEP135 as an essential recruiter for Ana1 - sequentially forming a CEP135-Ana1-Asl complex that is essential for centriole assembly. The Fu study's conclusions are based on three main pieces of evidence. First, is the ordered co-localisation of CEP135-Ana1-Asl axis, showing overlap between adjacent proteins and radial alignment, while this suggests the

proteins are in proximity, it is not proof of a direct interaction. Second, they demonstrate via an in-vitro pulldown assay that Cep135 can interact with Ana1, and Ana1 can interact with Asl but Asl and Cep135 do not interact. While this may appear convincing, it is likely that due to the co-localisation of adjacent proteins they must naturally accommodate each other. As a result, it's not unreasonable for them to have contact domains which stabilise each other and the overall structure, but are not required for recruitment to the centrosome. Third, and most convincingly, they showed RNAi knockdown of *CEP135* drastically reduced the Ana1/CEP295 present at the centrosome in human U2OS cells. This third finding appears to directly contradict my observations in the *Drosophila* embryo; however, this could be explained by differences in the experimental system. First, by using an immortalised cell line taken from sarcomas, it is possible that wildtype function has been altered, this is particularly relevant when considering machinery directly linked to cell division. More notably, however, there are significant temporal and structural differences between the two systems. Temporally, *Drosophila* early embryos go through the cell cycle at a highly accelerated rate verses somatic cells [104]. Structurally, the *Drosophila* centriole maintains its central cartwheel while the human centriole loses it, this combined with the increased prevalence of cilia puts much higher demand on the stability of beyond the cartwheel components in humans [6,17]. Taken together, these differences allow the marriage of the results in the interpretation, in that

while *CEP135* may not be required to directly recruit Ana1 to the centriole, it may stabilise its position there. In the *Drosophila* system where cycles are rapid, and the centriole has more innate stability, this role is less relevant in comparison to the human cell which have greater stability requirements over drastically longer time periods. On an organismal level, the differing structures and mechanical loads, may also explain the lack of lethality of *CEP135* mutants in *Drosophila*, lack of expression in the early embryo of *C. elegans*, despite harsher phenotypes in humans [17,32,136].

4.4 An Updated Model of Centriole Assembly

On the basis of these results, I propose an updated model of centriole assembly. This study confirms the previously defined order of centriole assembly (*Figure 1.3*). While this was previously established via super-resolution of imaging of fluorescently-tagged proteins [32,72], my new data has true temporal resolution and explicitly places assembly events in context with the cell cycle. Of note Ana2 and Sas-6 appear to begin building the cartwheel drastically earlier than previously reported [83], following M/A of the previous nuclear division. This suggests M/A is a key stage in regulation of centriole duplication in the *Drosophila* early embryo. This may be due to the simplified cell cycle found in *Drosophila* early embryos, described as oscillating between M-Phase then an S-phase permissive periods [137]. This duplication timing correlates with the drop of Cyclin B/Cdk1 at M/A but also centriole separation at a nanometre scale.

This highlights the importance of understanding the chain of causality between centriole disengagement, cell cycle regulators and centriole duplication. The asymmetry in the initiation of daughter duplication strongly suggests that at this point, only the old-mother is competent to produce a daughter. As a result, the intervening period is of significant interest as the events of this approximately 90 second window include the critical threshold where the new-mother becomes competent to produce a daughter of its own.

Through the increased temporal resolution and ability to properly place assembly events on a timeline, Ana3's incorporation has been shown to be notably before that of CEP135 and Ana1. This suggests the two groups of proteins have differential regulation. However, due to the lack of notably asymmetry in either, the rate of cartwheel growth must either compensate or their regulation is linked to different cell cycle events. Going forwards, the methodology used within this work could be replicated alongside differential doses or activities of key regulators such as Polo, PLK4 and Cyclin B, to identity the exact regulation underpinning incorporation of beyond the cartwheel proteins.

The importance of M/A is emphasised by the consistency of a dip process correlating with its timing in the case of all proteins examined. While the incorporation following M/A appears largely explainable, with potentially

the exception of the Ana3 dogtooth pattern, the cause of the dip is particularly interesting as it is likely a single event affecting all centriole proteins at once. Cyclin B/Cdk1 activity provides a reasonable candidate as the dip begins coincidentally with NEB, where cyclin B/cdk1 activity is highest, however, if this is the case it likely acts via an intermediary upstream as while embryos expressing Cdk1-phosphonull Ana2 show a greatly reduced loss of Ana2 from the centrosome before NEB, they still appear to have a dip-like process between NEB and M/A [46]. Plk4 is another attractive candidate as it is involved in the recruitment of Sas-6 and Ana2 but also is observed to oscillate at the centriole, having drastically reduced by NEB [10,84]. PLK4 thus may act as the primary recruiting body of the soup, which may itself or indirectly, through transient Sas-6/Ana2, recruit beyond the cartwheel proteins. At NEB PLK4 levels would then fall below a critical threshold thus causing loss of the soup until M/A where PLK4 levels would increase again, above a threshold, evidenced by capacity for daughter cartwheel growth.

4.5 Summary of Future Work

- Reanalysis of PLK4 in the new context of the soup
- Expansion of the methodology across all remaining core centriole proteins – Ana1, Rcd4, Sas4
- SoRa FRAP & old/new-mother tracking to localise incorporation profiles
- Confirmation of CEP135's role at the centriole using knockouts rather than mutants
- Interrogation into the cause of cartwheel growth asymmetry
- Differential dosage/activity analysis of key assembly kinases and their effect on incorporation profiles of beyond the cartwheel proteins to identify assembly regulation

4.6 Conclusions

- Centriole duplication in *Drosophila* early embryos begins following M/A
- Initial centriole duplication is asymmetric, where the old-mother builds a cartwheel approximately 90 seconds before the new-mother
- Incorporation of CEP135 and Ana1 verses Ana3 are differentially regulation and independent of initial centriole asymmetry
- Across the cycle of nuclear division excess transient material composed of core centriole components accumulates at the centrosome
- CEP135 is not required for Ana1 recruitment, and may instead have roles in its stability at the centriole

Chapter 5: Methods

5.1 Fly husbandry & Stocks

Flies were cultured in plastic vials or flasks containing culture media (0.68% agar, 2.5% yeast, 6.25% cornmeal [maize], 3.75% molasses, 0.42% propionic acid, 0.14% tegosept, and 0.70% ethanol) maintained at 18 or 25 ℃. Embryos, used for imaging, were collected from egg-laying cages upon fruit-agar plates (0% cranberry-raspberry juice, 2% sucrose, and 1.8% agar) with single yeast drops. Embryos were collected for 1 hour, then incubated at 25 ℃ for 45-60 min. To prepare for imaging, embryos were manually dechorionated then glued to a 35-mm glass-bottom Petri dish with 14 mm micro-well (MatTek) and covered with Voltalef grade H10S oil (Arkema). Fly lines and alleles used detailed in Figure 5.1 & 5.2.

Table 5.1 Summary of fly lines and uses

Genotype	Use
Sas6NG//; Jupiter-mCherry//	All Sas6 data
Ana2NG//; Jupiter-mCherry//	All Ana2 data
Ana3NG//; Jupiter-mCherry//	All Ana3 data
Ana1-GFP/+;Jupiter-mCherry/+	Ana1 control & Ana1 timing data
Ana1-GFP/+;mCep135/Bld10ΔN	Ana1 Cep135 mutant data
Cep135-GFP//;mCep135,Jupiter-mCherry/Cep135Δa	All Cep135 data
GFP-Asl//; Jupiter-mCherry,Asl-B46//	All Asl data

Table 5.2 Summary of alleles used

Allele	Overview	Previous publication
Sas6NG	Endogenous CRISPR knock-in of mNeonGreen into the Sas6 locus	[138]
Ana2NG	Endogenous CRISPR knock-in of mNeonGreen into the Ana2 locus	[138]
Ana3NG	Endogenous CRISPR knock-in of mNeonGreen into the Ana3 locus	[138]
Ana1-GFP	P-element insertion of Ana1-GFP under endogenous promoter	[139]
Cep135-GFP	P-element insertion of Cep135-GFP under endogenous promoter	[139]
GFP-Asl	P-element insertion of GFP-Asl under endogenous promoter	[139]
Jupiter-mCherry	Trap insertion of mCherry into Jupiter locus	[140]
mCep135	P-element insertion into promoter of Cep135 disabling expression	[141]
Bld10ΔN	N-terminal deletion of Cep135	[142]
Cep135Δa	CRIPSR –terminal deletion of N-terminal exon of Cep135	Unpublished – Raff lab
Asl-B46	Mutant Asl	[143]

5.2 Live Embryo Standard Resolution Spinning Disk Confocal Microscopy

Living embryos were imaged at 22℃ using one of two microscopes, herby referred to as "Andor" and "Dragonfly".

Andor: Images were captured via an EM-CCD Andor iXon+ camera, mounted on a Nikon Eclipse TE200-E microscope, through a Plan-Apochromat 60x/1.42-NA oil immersion DIC lens.

Dragonfly: Images were captured via an EM-CCD iXon Ultra 888 camera, mounted on a Lecia DMi8 microscope, through a HC PL APO 63x/1.40 oil immersion lens.

Both microscopes were operated through Andor Fusion software (version 2.3). Fluorophores were excited using 488/561 (GFP & mNeonGreen/mCherry) and emission was selected for using [get from alan] bandpass filters. Images were taken every 12 seconds, across an 8 µm stack made of 0.5 µm slices.

Timelapses were processed using imageJ/FIJI[132]. Stacks were maximum intensity Z-projected, background subtracted (15 µm rolling ball). Embryos where the membrane autofluorescence obscured centrosomal signal underwent crude membrane stripping before Z-projection (code available supp. Table 1). Timelapses were assessed for photobleaching and corrected if needed using an exponential fit of sum intensity.

Centrosome intensity values were extracted via Trackmate [129]. Centrosomes were identified through a Laplacian of Gaussian filter with

an expected object size of 1.5 µm, anomalous identifications were excluded by eye using quality, contrast and spatial secondary filters. Trackmate exported data was then collated via custom designed code (supp. Table 1).

Centriole separation was scored visually, based on the GFP/Neongreen channel, and computationally through the minima of centrosome intensity over time graphs. M/A, NEB and midbody disassembly were scored visually using a Jupiter-mCherry reporter (Figure 2.1)

5.3 Live Embryo Super-Resolution SoRa Microscopy

Living embryos were imaged at 25℃ using a Photometrics Primer BSI camera, mounted on an Olympus IX-83 inverted frame, equipped with a Yokogawa SoRa super-resolution spinning disc module, through a Olympus UplanSApo 60x/1.30 Sil Lens.

Fluorophores were excited using a 488 nm (mNeonGreen) or 561 nm (mCherry) solid-state laser (OBIS), and fluorescence emission was selected using a 525/50 nm (mNeonGreen) or 617/73 nm (mCherry) bandpass filter. Images were processed for super-resolution (standard strength: Neongreen, Low strength: mCherry) and deconvoluted (constrained iterative, maximum likelihood, 5 iterations) using Olympus cellSens Dimension software (version 3.1.1).

Images were maximum intensity Z-projected using imageJ/FIJI[132]. Centrioles were identified and centrosomes were approximated using

Trackmate [129] with expected object size of 0.2 and 1.5 µm respectively, anomalous identifications were excluded by eye using quality, contrast and spatial secondary filters. Trackmate exported data was then collated, and a ratio of centrioles to centrosomes calculated via custom designed code (supp. Table 1). M/A, NEB and midbody disassembly were scored visually using a Jupiter-mCherry reporter (Figure 2.1).

5.4 Dataset alignment

Datasets were aligned and presented using Matlab. Frame indexes were converted to time values. Standard resolution data was mean averaged within each embryo, ignoring the highest and lowest 5% of values, on a frame-by-frame basis. The alignment region of interest was selected via defined bounds either: computed centriole separation to computed centriole separation or previous M/A to the following cycle's midbody disassembly. For each embryo, this region was linearly interpolated over 500 points, to time-normalise. Intensity for each embryo was normalised then mean averages, standard deviation and standard error of the mean were then calculated for each normalised dataset. Code available (supp. Table 1)

5.5 Centrosome Z-positioning analysis

Custom python code (supp. Table 1) using the OpenCV library, was used to process and analyse images. Raw timelapses were converted to 8-bit

greyscale .tif files using imageJ/FIJI[132]. Background was reduced using gaussian blur, then points of intensity were reinforced using tophat filtering. Contours were detected and filtered based on, size, shape, location and intensity, to include only centrosomes. Identified centrosomes then were linked across Z-stacks, the maximal intensity Z-stack was then recorded. Matlab was use to visualise data(supp. Table 1).

5.6 Quantification of daughter timing asymmetry

Centrosome pairs were identified at random from SoRa movies starting in cycle 12, these were followed back such and the time between the mothers showing a daughter was recorded. These were then tracked further back to score which of the pair was the new-mother/old-mother. 10 centrosome pairs were picked at random per embryo, if the embryo pair condensed to enable undiscernible rotation or was lost from the field of view, it was excluded and another found. Times were then recorded and aggregated on a 1-dimensional scale such that new-mother first was negative, and old-mother first was positive. GraphPad Prism 9 was used to calculate significance between aggregated data from each group, via one-way ANOVA with Tuckey multiple comparisons.

Acknowledgements

Alan Wainman – For providing SoRa timelapses, generating additional fly lines, providing microscope, fly and moral support

Zach Wilmot – For providing basis and troubleshooting for dataset alignments

Laura Hankins – For initial training of fly husbandry and early embryo imaging as well as collection of preliminary data

Jordan Raff – For providing personal funding and project supervision

Alberto Baena Lopez – For project supervision

Maria Eppey – For providing moral support throughout and collection of preliminary data

Raff lab – For providing lab space, fly lines and microscopes

References

1. Conduit PT, Wainman A, Raff JW: **Centrosome function and assembly in animal cells**. *Nature Reviews Molecular Cell Biology 2015 16:10* 2015, **16**:611–624.
2. Conduit PT, Raff JW: **Cnn Dynamics Drive Centrosome Size Asymmetry to Ensure Daughter Centriole Retention in Drosophila Neuroblasts**. *Current Biology* 2010, **20**:2187–2192.
3. Kirkham M, Müller-Reichert T, Oegema K, Grill S, Hyman AA: **SAS-4 is a C. elegans centriolar protein that controls centrosome size**. *Cell* 2003, **112**:575–587.
4. Conduit PT, Brunk K, Dobbelaere J, Dix CI, Lucas EP, Raff JW: **Centrioles regulate centrosome size by controlling the rate of Cnn incorporation into the PCM**. *Current Biology* 2010, **20**:2178–2186.
5. Banterle N, Gönczy P: **Centriole Biogenesis: From Identifying the Characters to Understanding the Plot**. *Annu Rev Cell Dev Biol* 2017, **33**:23–49.
6. Gupta A, Kitagawa D: **Ultrastructural diversity between centrioles of eukaryotes**. *The Journal of Biochemistry* 2018, **164**:1–8.

7. Yamamoto S, Kitagawa D: **Self-organization of Plk4 regulates symmetry breaking in centriole duplication**. *Nature Communications 2019 10:1* 2019, **10**:1–12.
8. Leda M, Holland AJ, Goryachev AB: **Autoamplification and Competition Drive Symmetry Breaking: Initiation of Centriole Duplication by the PLK4-STIL Network**. *iScience* 2018, **8**:222–235.
9. Dzhindzhev NS, Tzolovsky G, Lipinszki Z, Abdelaziz M, Debski J, Dadlez M, Glover DM: **Two-step phosphorylation of Ana2 by Plk4 is required for the sequential loading of Ana2 and Sas6 to initiate procentriole formation**. *Open Biol* 2017, **7**.
10. Dzhindzhev NS, Tzolovsky G, Lipinszki Z, Schneider S, Lattao R, Fu J, Debski J, Dadlez M, Glover DM: **Plk4 phosphorylates Ana2 to trigger Sas6 recruitment and procentriole formation**. *Curr Biol* 2014, **24**:2526–2532.
11. Gartenmann L, Vicente CC, Wainman A, Novak ZA, Sieber B, Richens JH, Raff JW: **Sas-6, Ana2 and Sas-4 self-organise into macromolecular structures that can be used to probe centriole/centrosome assembly**. *J Cell Sci* 2020, **133**.
12. Novak ZAA, Wainman A, Gartenmann L, Raff JWW: **Cdk1 Phosphorylates Drosophila Sas-4 to Recruit Polo to Daughter Centrioles and Convert Them to Centrosomes**. *Dev Cell* 2016, **37**:545.
13. Ramani A, Mariappan A, Gottardo M, Mandad S, Urlaub H, Avidor-Reiss T, Riparbelli M, Callaini G, Debec A, Feederle R, et al.: **Plk1/Polo Phosphorylates Sas-4 at the Onset of Mitosis for an Efficient Recruitment of Pericentriolar Material to Centrosomes**. *Cell Rep* 2018, **25**:3618-3630.e6.
14. Sharma A, Aher A, Dynes NJ, Frey D, Katrukha EA, Jaussi R, Grigoriev I, Croisier M, Kammerer RA, Akhmanova A, et al.: **Centriolar CPAP/SAS-4 Imparts Slow Processive Microtubule Growth**. *Dev Cell* 2016, **37**:362–376.
15. Tang CJC, Lin SY, Hsu W bin, Lin YN, Wu CT, Lin YC, Chang CW, Wu KS, Tang TK: **The human microcephaly protein STIL interacts with CPAP and is required for procentriole formation**. *EMBO J* 2011, **30**:4790–4804.
16. Lin Y-C, Chang C-W, Hsu W-B, Tang C-JC, Lin Y-N, Chou E-J, Wu C-T, Tang TK: **Human microcephaly protein CEP135 binds to hSAS-6 and CPAP, and is required for centriole assembly**. *EMBO J* 2013, **32**:1141–1154.
17. Roque H, Wainman A, Richens J, Kozyrska K, Franz A, Raff JW: **Drosophila Cep135/Bld10 maintains proper centriole structure but is dispensable for cartwheel formation**. *J Cell Sci* 2012, **125**:5881–5886.
18. Saurya S, Roque H, Novak ZA, Wainman A, Aydogan MG, Volanakis A, Sieber B, Pinto DMS, Raff JW: **Drosophila Ana1 is required for centrosome assembly and centriole elongation**. *J Cell Sci* 2016, **129**:2514–2525.
19. Alvarez-Rodrigo I, Wainman A, Saurya S, Raff JW: **Ana1 helps recruit Polo to centrioles to promote mitotic PCM assembly and centriole elongation**. *J Cell Sci* 2021, **134**.
20. Stevens NR, Dobbelaere J, Wainman A, Gergely F, Raff JW: **Ana3 is a conserved protein required for the structural integrity of centrioles and basal bodies**. *J Cell Biol* 2009, **187**:355–363.

21. Panda P, Kovacs L, Dzhindzhev N, Fatalska A, Persico V, Geymonat M, Riparbelli MG, Callaini G, Glover DM: **Tissue specific requirement of Drosophila Rcd4 for centriole duplication and ciliogenesis**. *Journal of Cell Biology* 2020, **219**.
22. Dobbelaere J, Josué F, Suijkerbuijk S, Baum B, Tapon N, Raff J: **A Genome-Wide RNAi Screen to Dissect Centriole Duplication and Centrosome Maturation in Drosophila**. *PLoS Biol* 2008, **6**:e224.
23. Chen HY, Wu CT, Tang CJC, Lin YN, Wang WJ, Tang TK: **Human microcephaly protein RTTN interacts with STIL and is required to build full-length centrioles**. *Nat Commun* 2017, **8**.
24. Wong S-S, Wilmott ZM, Saurya S, Alvarez-Rodrigo I, Zhou FY, Chau K-Y, Goriely A, Raff JW: **Centrioles generate a local pulse of Polo/PLK1 activity to initiate mitotic centrosome assembly**. [date unknown], doi:10.15252/embj.2022110891.
25. Alvarez-Rodrigo I, Steinacker TL, Saurya S, Conduit PT, Baumbach J, Novak ZA, Aydogan MG, Wainman A, Raff JW: **Evidence that a positive feedback loop drives centrosome maturation in fly embryos**. *Elife* 2019, **8**.
26. Tang N, Marshall WF: **Centrosome positioning in vertebrate development**. *J Cell Sci* 2012, **125**:4951.
27. Agircan FG, Schiebel E, Mardin BR: **Separate to operate: control of centrosome positioning and separation**. *Philos Trans R Soc Lond B Biol Sci* 2014, **369**.
28. Smith CEL, Lake AVR, Johnson CA: **Primary Cilia, Ciliogenesis and the Actin Cytoskeleton: A Little Less Resorption, A Little More Actin Please**. *Front Cell Dev Biol* 2020, **8**:1586.
29. Avasthi P, Marshall WF: **Stages of Ciliogenesis and Regulation of Ciliary Length**. *Differentiation* 2012, **83**:S30.
30. KlosDehring DA, Vladar EK, Werner ME, Mitchell JW, Hwang P, Mitchell BJ: **Deuterosome-mediated centriole biogenesis**. *Dev Cell* 2013, **27**:103–112.
31. al Jord A, Lemaître AI, Delgehyr N, Faucourt M, Spassky N, Meunier A: **Centriole amplification by mother and daughter centrioles differs in multiciliated cells**. *Nature* 2014, **516**:104–107.
32. Fu J, Lipinszki Z, Rangone H, Min M, Mykura C, Chao-Chu J, Schneider S, Dzhindzhev NS, Gottardo M, Riparbelli MG, et al.: **Conserved molecular interactions in centriole-to-centrosome conversion**. *Nature Cell Biology 2015 18:1* 2015, **18**:87–99.
33. Novak ZA, Conduit PT, Wainman A, Raff JW: **Asterless licenses daughter centrioles to duplicate for the first time in Drosophila embryos**. *Curr Biol* 2014, **24**:1276–1282.
34. Woods CG, Bond J, Enard W: **Autosomal recessive primary microcephaly (MCPH): A review of clinical, molecular, and evolutionary findings**. *Am J Hum Genet* 2005, **76**:717–728.
35. Phan TP, Holland AJ: **Time is of the essence: The molecular mechanisms of primary microcephaly**. *Genes Dev* 2021, **35**:1551–1578.
36. Hasenpusch-Theil K, Theil T: **The Multifaceted Roles of Primary Cilia in the Development of the Cerebral Cortex**. *Front Cell Dev Biol* 2021, **9**.

37. Andreu-Cervera A, Catala M, Schneider-Maunoury S: **Cilia, ciliopathies and hedgehog-related forebrain developmental disorders**. *Neurobiol Dis* 2021, **150**.
38. Phan TP, Maryniak AL, Boatwright CA, Lee J, Atkins A, Tijhuis A, Spierings DC, Bazzi H, Foijer F, Jordan PW, et al.: **Centrosome defects cause microcephaly by activating the 53BP1-USP28-TP53 mitotic surveillance pathway**. *EMBO J* 2021, **40**:e106118.
39. Marthiens V, Rujano MA, Pennetier C, Tessier S, Paul-Gilloteaux P, Basto R: **Centrosome amplification causes microcephaly**. *Nat Cell Biol* 2013, **15**:731–740.
40. Kalay E, Yigit G, Aslan Y, Brown KE, Pohl E, Bicknell LS, Kayserili H, Li Y, Tüysüz B, Nürnberg G, et al.: **CEP152 is a genome maintenance protein disrupted in Seckel syndrome**. *Nat Genet* 2011, **43**:23–26.
41. McIntyre RE, Lakshminarasimhan Chavali P, Ismail O, Carragher DM, Sanchez-Andrade G, Forment J v., Fu B, del Castillo Velasco-Herrera M, Edwards A, van der Weyden L, et al.: **Disruption of Mouse Cenpj, a Regulator of Centriole Biogenesis, Phenocopies Seckel Syndrome**. *PLoS Genet* 2012, **8**.
42. Zhang Y, Li H, Pang J, Peng Y, Shu L, Wang H: **Novel SASS6 compound heterozygous mutations in a Chinese family with primary autosomal recessive microcephaly**. *Clin Chim Acta* 2019, **491**:15–18.
43. Khan MA, Rupp VM, Orpinell M, Hussain MS, Altmüller J, Steinmetz MO, Enzinger C, Thiele H, Höhne W, Nürnberg G, et al.: **A missense mutation in the PISA domain of HsSAS-6 causes autosomal recessive primary microcephaly in a large consanguineous pakistani family**. *Hum Mol Genet* 2014, **23**:5940–5949.
44. Nakazawa Y, Hiraki M, Kamiya R, Hirono M: **SAS-6 is a Cartwheel Protein that Establishes the 9-Fold Symmetry of the Centriole**. *Current Biology* 2007, **17**:2169–2174.
45. Cottee MA, Muschalik N, Johnson S, Leveson J, Raff JW, Lea SM: **The homo-oligomerisation of both Sas-6 and Ana2 is required for efficient centriole assembly in flies**. *Elife* 2015, **4**:1–65.
46. Steinacker TL, Wong S-S, Novak ZA, Saurya S, Gartenmann L, van Houtum EJH, Sayers JR, Lagerholm BC, Raff JW: **Centriole growth is not limited by a finite pool of components, but is limited by the Cdk1/Cyclin-dependent phosphorylation of Ana2/STIL Affiliation**. *bioRxiv* 2022, doi:10.1101/2022.02.15.480489.
47. Cheng C, Yang Y, Zhu X, Yu X, Zhang T, Yang F, Chen F, Chen X, Zhao S, Guo J: **Novel compound heterozygous variants in the STIL gene identified in a Chinese family with presentation of foetal microcephaly**. *Eur J Med Genet* 2020, **63**.
48. Wu KS, Tang TK: **CPAP is required for cilia formation in neuronal cells**. *Biol Open* 2012, **1**:559–565.
49. Vásquez-Limeta A, Lukasik K, Kong D, Sullenberger C, Luvsanjav D, Sahabandu N, Chari R, Loncarek J: **CPAP insufficiency leads to incomplete centrioles that duplicate but fragment**. *J Cell Biol* 2022, **221**.
50. Al-Dosari MS, Shaheen R, Colak D, Alkuraya FS: **Novel CENPJ mutation causes Seckel syndrome**. *J Med Genet* 2010, **47**:411–414.
51. Khan NM, Masoud MS, Baig SM, Qasim M, Chang J: **Identification of Pathogenic Mutations in Primary Microcephaly- (MCPH-) Related Three Genes CENPJ,**

CASK, and MCPH1 in Consanguineous Pakistani Families. *Biomed Res Int* 2022, **2022**.

52. Hatzopoulos GN, Erat MC, Cutts E, Rogala KB, Slater LM, Stansfeld PJ, Vakonakis I: **Structural analysis of the G-box domain of the microcephaly protein CPAP suggests a role in centriole architecture**. *Structure* 2013, **21**:2069–2077.
53. Bamborschke D, Daimagüler HS, Hahn A, Hussain MS, Nürnberg P, Cirak S: **Mutation in CEP135 causing primary microcephaly and subcortical heterotopia**. *Am J Med Genet A* 2020, **182**:2450–2453.
54. Hussain MS, Baig SM, Neumann S, Nürnberg G, Farooq M, Ahmad I, Alef T, Hennies HC, Technau M, Altmüller J, et al.: **A Truncating Mutation of CEP135 Causes Primary Microcephaly and Disturbed Centrosomal Function**. *Am J Hum Genet* 2012, **90**:871.
55. Kraatz S, Guichard P, Obbineni JM, Olieric N, Hatzopoulos GN, Hilbert M, Sen I, Missimer J, Gönczy P, Steinmetz MO: **The Human Centriolar Protein CEP135 Contains a Two-Stranded Coiled-Coil Domain Critical for Microtubule Binding**. *Structure* 2016, **24**:1358–1371.
56. Vandervore L v., Schot R, Kasteleijn E, Oegema R, Stouffs K, Gheldof A, Grochowska MM, van der Sterre MLT, van Unen LMA, Wilke M, et al.: **Heterogeneous clinical phenotypes and cerebral malformations reflected by rotatin cellular dynamics**. *Brain* 2019, **142**:867.
57. Alazami AM, Shamseldin H, Manning M, Hashem A, Caluseiu O, Tabarki B, Esplin E, Schelley S, Innes AM, Parboosingh JS, et al.: **RTTN Mutations Cause Primary Microcephaly and Primordial Dwarfism in Humans**. *Am J Hum Genet* 2015, **97**:862–868.
58. Kia SK, Verbeek E, Engelen E, Schot R, Poot RA, de coo IFM, Lequin MH, Poulton CJ, Pourfarzad F, Grosveld FG, et al.: **RTTN mutations link primary cilia function to organization of the human cerebral cortex**. *Am J Hum Genet* 2012, **91**:533–540.
59. Archambault D, Cheong A, Iverson E, Tremblay KD, Mager J: **Protein phosphatase 1 regulatory subunit 35 is required for ciliogenesis, notochord morphogenesis, and cell-cycle progression during murine development**. *Dev Biol* 2020, **465**:1–10.
60. Sonnen KF, Gabryjonczyk AM, Anselm E, Nigg EA, Stierhof YD: **Human cep192 and cep152 cooperate in plk4 recruitment and centriole duplication**. *J Cell Sci* 2013, **126**:3223–3233.
61. Guernsey DL, Jiang H, Hussin J, Arnold M, Bouyakdan K, Perry S, Babineau-Sturk T, Beis J, Dumas N, Evans SC, et al.: **Mutations in Centrosomal Protein CEP152 in Primary Microcephaly Families Linked to MCPH4**. *Am J Hum Genet* 2010, **87**:40.
62. Boveri T: **Concerning the Origin of Malignant Tumours by Theodor Boveri. Translated and annotated by Henry Harris**. *J Cell Sci* 2008, **121**:1–84.
63. Serçin Ö, Larsimont JC, Karambelas AE, Marthiens V, Moers V, Boeckx B, le Mercier M, Lambrechts D, Basto R, Blanpain C: **Transient PLK4 overexpression accelerates tumorigenesis in p53-deficient epidermis**. *Nature Cell Biology 2015 18:1* 2015, **18**:100–110.

64. Vitrea B, Holland AJ, Kulukian A, Shoshani O, Hirai M, Wanga Y, Maldonado M, Cho T, Boubaker J, Swing DA, et al.: **Chronic centrosome amplification without tumorigenesis**. *Proc Natl Acad Sci U S A* 2015, **112**:E6321–E6330.
65. Godinho SA, Pellman D: **Causes and consequences of centrosome abnormalities in cancer**. *Philosophical Transactions of the Royal Society B: Biological Sciences* 2014, **369**.
66. Schvartzman JM, Sotillo R, Benezra R: **Mitotic chromosomal instability and cancer: mouse modelling of the human disease**. *Nature Reviews Cancer 2010 10:2* 2010, **10**:102–115.
67. Janssen A, van der Burg M, Szuhai K, Kops GJPL, Medema RH: **Chromosome segregation errors as a cause of DNA damage and structural chromosome aberrations**. *Science (1979)* 2011, **333**:1895–1898.
68. Caussinus E, Gonzalez C: **Induction of tumor growth by altered stem-cell asymmetric division in Drosophila melanogaster**. *Nature Genetics 2005 37:10* 2005, **37**:1125–1129.
69. Basto R, Brunk K, Vinadogrova T, Peel N, Franz A, Khodjakov A, Raff JW: **Centrosome Amplification Can Initiate Tumorigenesis in Flies**. *Cell* 2008, **133**:1032–1042.
70. Rivera-Rivera Y, Saavedra HI: **Centrosome – a promising anti-cancer target**. *Biologics* 2016, **10**:167.
71. Gönczy P: **Towards a molecular architecture of centriole assembly**. *Nat Rev Mol Cell Biol* 2012, **13**:425–435.
72. Tian Y, Wei C, He J, Yan Y, Pang N, Fang X, Liang X, Fu J: **Superresolution characterization of core centriole architecture**. *Journal of Cell Biology* 2021, **220**.
73. Pelletier L, O'Toole E, Schwager A, Hyman AA, Müller-Reichert T: **Centriole assembly in Caenorhabditis elegans**. *Nature* 2006, **444**:619–623.
74. Hilbert M, Noga A, Frey D, Hamel V, Guichard P, Kraatz SHW, Pfreundschuh M, Hosner S, Flückiger I, Jaussi R, et al.: **SAS-6 engineering reveals interdependence between cartwheel and microtubules in determining centriole architecture**. *Nat Cell Biol* 2016, **18**:393–403.
75. Hilbert M, Erat MC, Hachet V, Guichard P, Blank ID, Flučkiger I, Slater L, Lowe ED, Hatzopoulos GN, Steinmetz MO, et al.: **Caenorhabditis elegans centriolar protein SAS-6 forms a spiral that is consistent with imparting a ninefold symmetry**. *Proc Natl Acad Sci U S A* 2013, **110**:11373–11378.
76. Boese CJ, Nye J, Buster DW, McLamarrah TA, Byrnes AE, Slep KC, Rusan NM, Rogers GC: **Asterless is a Polo-like kinase 4 substrate that both activates and inhibits kinase activity depending on its phosphorylation state**. *Mol Biol Cell* 2018, **29**:2874–2886.
77. Carla Lopes AA, Chandra Jana S, Cunha-Ferreira I: **PLK4 trans-Autoactivation Controls Centriole Biogenesis in Space**. 2015, doi:10.1016/j.devcel.2015.09.020.
78. Dzhindzhev NS, Yu QD, Weiskopf K, Tzolovsky G, Cunha-Ferreira I, Riparbelli M, Rodrigues-Martins A, Bettencourt-Dias M, Callaini G, Glover DM: **Asterless is a scaffold for the onset of centriole assembly**. *Nature 2010 467:7316* 2010, **467**:714–718.

79. Gartenmann L, Wainman A, Qurashi M, Kaufmann R, Schubert S, Raff JW, Dobbie IM: **A combined 3D-SIM/SMLM approach allows centriole proteins to be localized with a precision of ~4–5 nm**. *Current Biology* 2017, **27**:R1054–R1055.
80. Nievergelt AP, Banterle N, Andany SH, Gönczy P, Fantner GE: **High-speed photothermal off-resonance atomic force microscopy reveals assembly routes of centriolar scaffold protein SAS-6**. *Nat Nanotechnol* 2018, **13**:696–701.
81. Gogendeau D, Hurbain I, Raposo G, Cohen J, Koll F, Basto R: **Sas-4 proteins are required during basal body duplication in *Paramecium***. *Mol Biol Cell* 2011, **22**:1035–1044.
82. Klein HCR, Guichard P, Hamel V, Gönczy P, Schwarz US: **Computational support for a scaffolding mechanism of centriole assembly**. *Sci Rep* 2016, **6**:1–9.
83. Aydogan MG, Wainman A, Saurya S, Steinacker TL, Caballe A, Novak ZA, Baumbach J, Muschalik N, Raff JW: **A homeostatic clock sets daughter centriole size in flies**. 2018, doi:10.1083/jcb.201801014.
84. Aydogan MG, Steinacker TL, Mofatteh M, Goriely A, Boemo MA, Raff JW: **An Autonomous Oscillation Times and Executes Centriole Biogenesis**. 2020, doi:10.1016/j.cell.2020.05.018.
85. Cizmecioglu O, Arnold M, Bahtz R, Settele F, Ehret L, Haselmann-Weiß U, Antony C, Hoffmann I: **Cep152 acts as a scaffold for recruitment of Plk4 and CPAP to the centrosome**. *Journal of Cell Biology* 2010, **191**:731–739.
86. Chu Z, Gruss OJ: **Mitotic Maturation Compensates for Premature Centrosome Splitting and PCM Loss in Human cep135 Knockout Cells**. *Cells* 2022, **11**:1189.
87. Giansanti MG, Bucciarelli E, Bonaccorsi S, Gatti M: **Drosophila SPD-2 Is an Essential Centriole Component Required for PCM Recruitment and Astral-Microtubule Nucleation**. *Current Biology* 2008, **18**:303–309.
88. Chou EJ, Tang TK: **Human microcephaly protein rttn is required for proper mitotic progression and correct spindle position**. *Cells* 2021, **10**.
89. Cho DG, Lee SS, Cho KO: **Anastral spindle 3/rotatin stabilizes sol narae and promotes cell survival in drosophila melanogaster**. *Mol Cells* 2021, **44**:13–25.
90. Sydor AM, Coyaud E, Rovelli C, Laurent E, Liu H, Raught B, Mennella V: **PPP1R35 is a novel centrosomal protein that regulates centriole length in concert with the microcephaly protein RTTN**. *Elife* 2018, **7**.
91. Bayless BA, Giddings TH, Winey M, Pearson CG: **Bld10/Cep135 stabilizes basal bodies to resist cilia-generated forces**. *Mol Biol Cell* 2012, **23**:4820–4832.
92. Jerka-Dziadosz M, Gogendeau D, Klotz C, Cohen J, Beisson J, Koll F: **Basal body duplication in Paramecium: The key role of Bld10 in assembly and stability of the cartwheel**. *Cytoskeleton* 2010, **67**:161–171.
93. Carvalho-Santos Z, Machado P, Alvarez-Martins I, Gouveia SM, Jana SC, Duarte P, Amado T, Branco P, Freitas MC, Silva STN, et al.: **BLD10/CEP135 Is a Microtubule-Associated Protein that Controls the Formation of the Flagellum Central Microtubule Pair**. *Dev Cell* 2012, **23**:412–424.
94. Cooper GM, Hauseman RE: *The Cell - A Molecular Approach 4th edition*. ASM Press; 2007.

95. Kuriyama R, Borisy GG: **Centriole cycle in Chinese hamster ovary cells as determined by whole-mount electron microscopy.** *Journal of Cell Biology* 1981, **91**:814–821.
96. Chrétien D, Buendia B, Fuller SD, Karsenti E: **Reconstruction of the Centrosome Cycle from Cryoelectron Micrographs**. *J Struct Biol* 1997, **120**:117–133.
97. Matsuura K, Lefebvre PA, Kamiya R, Hirono M: **Bld10p, a novel protein essential for basal body assembly in Chlamydomonas: localization to the cartwheel, the first ninefold symmetrical structure appearing during assembly**. *J Cell Biol* 2004, **165**:663–671.
98. Dutcher SK: **Elucidation of basal body and centriole functions in Chlamydomonas reinhardtii**. *Traffic* 2003, **4**:443–451.
99. Leidel S, Delattre M, Cerutti L, Baumer K, Gönczy P: **SAS-6 defines a protein family required for centrosome duplication in C. elegans and in human cells**. *Nature Cell Biology 2005 7:2* 2005, **7**:115–125.
100. O'Connell KF, Caron C, Kopish KR, Hurd DD, Kemphues KJ, Li Y, White JG: **The C. elegans zyg-1 Gene Encodes a Regulator of Centrosome Duplication with Distinct Maternal and Paternal Roles in the Embryo**. *Cell* 2001, **105**:547–558.
101. Leidel S, Gönczy P: **SAS-4 Is Essential for Centrosome Duplication in C. elegans and Is Recruited to Daughter Centrioles Once per Cell Cycle**. *Dev Cell* 2003, **4**:431–439.
102. Kemp CA, Kopish KR, Zipperlen P, Ahringer J, O'Connell KF: **Centrosome Maturation and Duplication in C. elegans Require the Coiled-Coil Protein SPD-2**. *Dev Cell* 2004, **6**:511–523.
103. Delattre M, Leidel S, Wani K, Baumer K, Bamat J, Schnabel H, Feichtinger R, Schnabel R, Gönczy P: **Centriolar SAS-5 is required for centrosome duplication in C. elegans**. *Nat Cell Biol* 2004, **6**:656–664.
104. Foe VE, Alberts BM: **Studies of nuclear and cytoplasmic behaviour during the five mitotic cycles that precede gastrulation in Drosophila embryogenesis**. *J Cell Sci* 1983, **61**:31–70.
105. Idema T, Dubuis JO, Kang L, Manning ML, Nelson PC, Lubensky TC, Liu AJ: **The Syncytial Drosophila Embryo as a Mechanically Excitable Medium**. *PLoS One* 2013, **8**:77216.
106. Sluder G: **One to only two: a short history of the centrosome and its duplication**. *Philosophical Transactions of the Royal Society B: Biological Sciences* 2014, **369**.
107. Winey M, O'Toole E: **Centriole structure**. *Philosophical Transactions of the Royal Society B: Biological Sciences* 2014, **369**.
108. Klena N, Guennec M le, Tassin A-M, Hoek H van den, Erdmann PS, Schaffer M, Geimer S, Aeschlimann G, Kovacik L, Sadian Y, et al.: **Architecture of the centriole cartwheel-containing region revealed by cryo-electron tomography**. *EMBO J* 2020, **39**:e106246.
109. Chen F, Tillberg PW, Boyden ES: **Expansion microscopy**. *Science (1979)* 2015, **347**:543–548.

110. Chozinski TJ, Halpern AR, Okawa H, Kim HJ, Tremel GJ, Wong ROL, Vaughan JC: **Expansion microscopy with conventional antibodies and fluorescent proteins**. *Nature Methods 2016 13:6* 2016, **13**:485–488.
111. Gambarotto D, Zwettler FU, le Guennec M, Schmidt-Cernohorska M, Fortun D, Borgers S, Heine J, Schloetel JG, Reuss M, Unser M, et al.: **Imaging cellular ultrastructures using expansion microscopy (U-ExM)**. *Nature Methods 2018 16:1* 2018, **16**:71–74.
112. Kong D, Loncarek J: **Analyzing Centrioles and Cilia by Expansion Microscopy**. *Methods Mol Biol* 2021, **2329**:249.
113. Gustafsson MGL: **Surpassing the lateral resolution limit by a factor of two using structured illumination microscopy**. *J Microsc* 2000, **198**:82–87.
114. Rust MJ, Bates M, Zhuang X: **Stochastic optical reconstruction microscopy (STORM) provides sub-diffraction-limit image resolution**. *Nat Methods* 2006, **3**:793.
115. Hell SW: **Toward fluorescence nanoscopy**. *Nature Biotechnology 2003 21:11* 2003, **21**:1347–1355.
116. Klein T, Löschberger A, Proppert S, Wolter S, van de Linde S, Sauer M: **Live-cell dSTORM with SNAP-tag fusion proteins**. *Nature Methods 2011 8:1* 2010, **8**:7–9.
117. Wainman A: **Expansion microscopy on Drosophila spermatocyte centrioles**. *Methods Cell Biol* 2021, **161**:217–245.
118. Zwettler FU, Reinhard S, Gambarotto D, Bell TDM, Hamel V, Guichard P, Sauer M: **Molecular resolution imaging by post-labeling expansion single-molecule localization microscopy (Ex-SMLM)**. *Nature Communications 2020 11:1* 2020, **11**:1–11.
119. Azuma T, Kei T, Betzig E, Patterson GH, Sougrat R, Lindwasser OW, Olenych S, Bonifacino JS, Davidson MW, Lippincott-Schwartz J, et al.: **Super-resolution spinning-disk confocal microscopy using optical photon reassignment**. *Optics Express, Vol 23, Issue 11, pp 15003-15011* 2015, **23**:15003–15011.
120. Xu Y, Wu T, Gao F, Charlton JR, Bennett KM: **Improved small blob detection in 3D images using jointly constrained deep learning and Hessian analysis**. *Scientific Reports 2020 10:1* 2020, **10**:1–12.
121. Wang G, Lopez-Molina C, de Baets B: **Automated blob detection using iterative Laplacian of Gaussian filtering and unilateral second-order Gaussian kernels**. *Digit Signal Process* 2020, **96**:102592.
122. Sage D, Neumann FR, Hediger F, Gasser SM, Unser M: **Automatic tracking of individual fluorescence particles: Application to the study of chromosome dynamics**. *IEEE Transactions on Image Processing* 2005, **14**:1372–1383.
123. Meijering E, Dzyubachyk O, Smal I: **Methods for Cell and Particle Tracking**. *Methods Enzymol* 2012, **504**:183–200.
124. Rogers SS, Waigh TA, Zhao X, Lu JR: **Precise particle tracking against a complicated background: polynomial fitting with Gaussian weight**. *Phys Biol* 2007, **4**:220.
125. Enwei Z, Feng C, Weidong Z: **A novel particle filter based background subtraction method**. *2006 International Conference on Computational Intelligence and Security, ICCIAS 2006* 2006, **2**:1837–1840.

126. Benezeth Y, Jodoin P-M, Emile B, Laurent H, Rosenberger C: **Comparative study of background subtraction algorithms**. *https://doi.org/101117/13456695* 2010, **19**:033003.
127. Garcia-Garcia B, Bouwmans T, Silva AJR: **Background subtraction in real applications: Challenges, current models and future directions**. *Comput Sci Rev* 2020, **35**:100204.
128. Isard M, MacCormick J: **BraMBLe: A Bayesian multiple-blob tracker**. *Proceedings of the IEEE International Conference on Computer Vision* 2001, **2**:34–41.
129. Ershov D, Phan MS, Pylvänäinen JW, Rigaud SU, le Blanc L, Charles-Orszag A, Conway JRW, Laine RF, Roy NH, Bonazzi D, et al.: **TrackMate 7: integrating state-of-the-art segmentation algorithms into tracking pipelines**. *Nature Methods 2022 19:7* 2022, **19**:829–832.
130. Lindeberg T: **Feature Detection with Automatic Scale Selection**. *International Journal of Computer Vision 1998 30:2* 1998, **30**:79–116.
131. Bay H, Tuytelaars T, van Gool L: **SURF: Speeded up robust features**. *Lecture Notes in Computer Science (including subseries Lecture Notes in Artificial Intelligence and Lecture Notes in Bioinformatics)* 2006, **3951 LNCS**:404–417.
132. Schindelin J, Arganda-Carreras I, Frise E, Kaynig V, Longair M, Pietzsch T, Preibisch S, Rueden C, Saalfeld S, Schmid B, et al.: **Fiji: an open-source platform for biological-image analysis**. *Nature Methods 2012 9:7* 2012, **9**:676–682.
133. Tanida-Miyake E, Koike M, Uchiyama Y, Tanida I: **Optimization of mNeonGreen for Homo sapiens increases its fluorescent intensity in mammalian cells**. *PLoS One* 2018, **13**.
134. Bai S, Fu K, Yin H, Cui Y, Yue Q, Li W, Cheng L, Tan H, Liu X, Guo Y, et al.: **The maternal-to-zygotic transition revisited**. *Development* 2019, **146**.
135. Chen C, Yamashita YM: **Centrosome-centric view of asymmetric stem cell division**. *Open Biol* 2021, **11**.
136. Holzer E, Rumpf-Kienzl C, Falk S, Dammermann A: **A modified TurboID approach identifies tissue-specific centriolar components in C. elegans**. *PLoS Genet* 2022, **18**:e1010150.
137. Farrell JA, O'Farrell PH: **From egg to gastrula: How the cell cycle is remodeled during the Drosophila mid-blastula transition**. *Annu Rev Genet* 2014, **48**:269.
138. Steinacker TL: **Investigation of the cytoplasmic pool of centriolar and centrosomal proteins**. 2021,
139. Blachon S, Gopalakrishnan J, Omori Y, Polyanovsky A, Church A, Nicastro D, Malicki J, Avidor-Reiss T: **Drosophila asterless and Vertebrate Cep152 Are Orthologs Essential for Centriole Duplication**. *Genetics* 2008, **180**:2081–2094.
140. Callan MA, Cabernard C, Heck J, Luois S, Doe CQ, Zarnescu DC: **Fragile X protein controls neural stem cell proliferation in the Drosophila brain**. *Hum Mol Genet* 2010, **19**:3068–3079.
141. Mottier-Pavie V, Megraw TL: **Drosophila Bld10 is a centriolar protein that regulates centriole, basal body, and motile cilium assembly**. *Mol Biol Cell* 2009, **20**:2605–2614.

142. Singh P, Ramdas Nair A, Cabernard C: **The Centriolar Protein Bld10/Cep135 Is Required to Establish Centrosome Asymmetry in Drosophila Neuroblasts**. *Current Biology* 2014, **24**:1548–1555.
143. Baumbach J, Anna Novak Z, Raff JW, Wainman A: **Dissecting the Function and Assembly of Acentriolar Microtubule Organizing Centers in Drosophila Cells In Vivo**. *PLoS Genet* 2015, **11**:1005261.

Appendices

Supplementary Table 1 Summary of Custom Code used

Code	Overview	Usage	Available at
Trackmate Datahandler	A lightweight app for extraction and processing of data from Trackmate files	All data quantified over time	https://github.com/RaffLab/TrackMateDataHandler
Matlab alignment code	A suite of matlab files for alignment of standard and superresolution data from embryos	All data quantified over time	https://github.com/RaffLab/TessAlignmentMatlab/
SLT height adaption	Python script enabling the analysis of the Z-positioning of centrosomes with respect to parameters such as their intensity	Dip investigations	https://github.com/RaffLab/SLT-Height-adaption

Supplementary Figures 1-3 Processing Graphs of Standard Resolution Data (next 3 pages) Graphs show the entirety of the datasets and the progressive alignment of the standard resolution centrosomal fluorescence data. Each protein and cycle is arranged as a set of 6 graphs of fluorescence intensity vs time, individual graphs as follows: Top left – Middle 90th percentile means of individual embryo fluorescence intensity at centrosomes**;** Top middle – As top left, cropped to the cycle of interest; Top right – Time normalised middle 90th percentile means of aligned cycles; Bottom left – As top right, amplitude normalised; Bottom middle – mean aggregate of bottom left; Bottom right – As bottom middle, re-dimensionalised

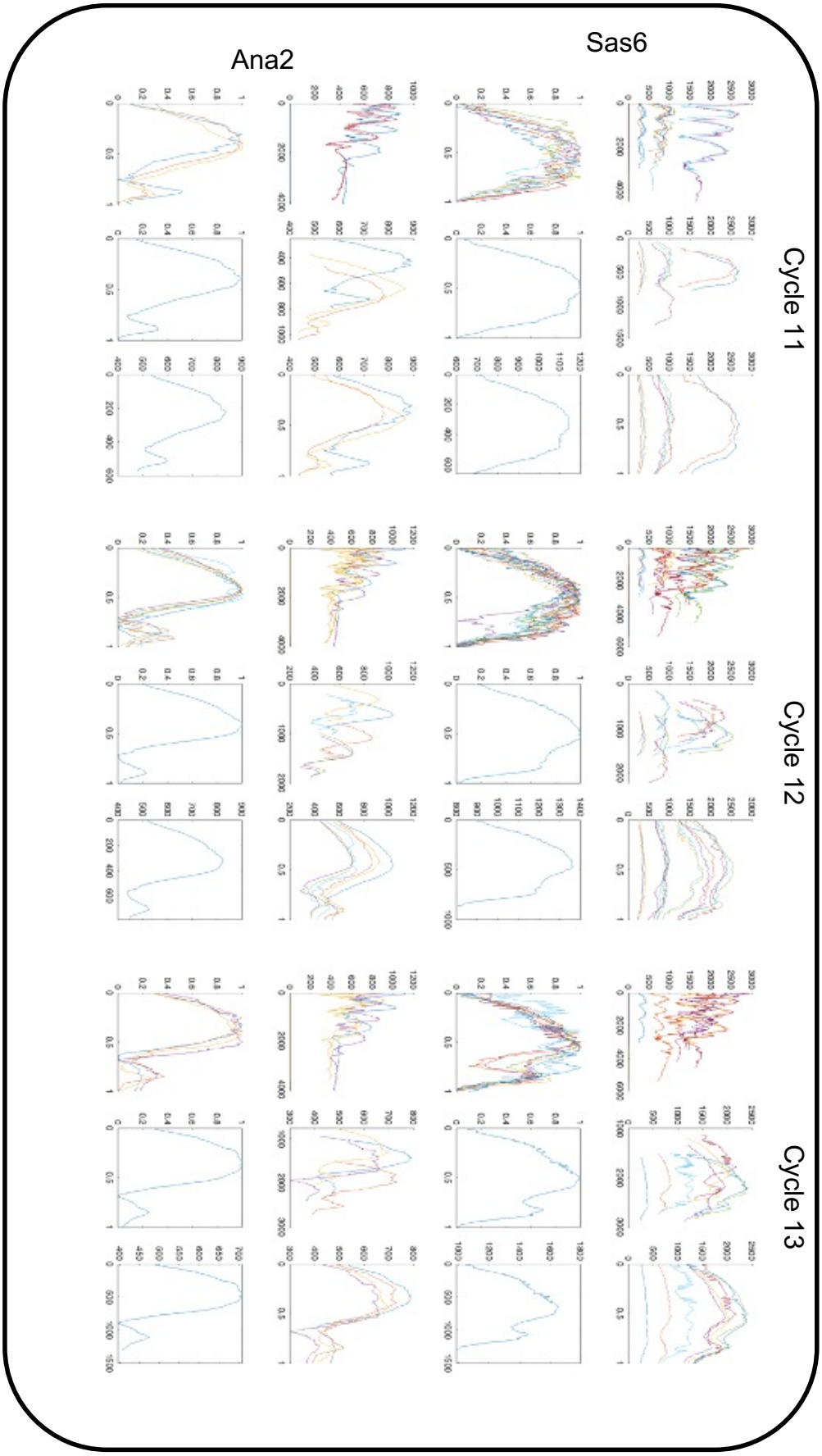
Sas6
Ana2
Cycle 11
Cycle 12
Cycle 13

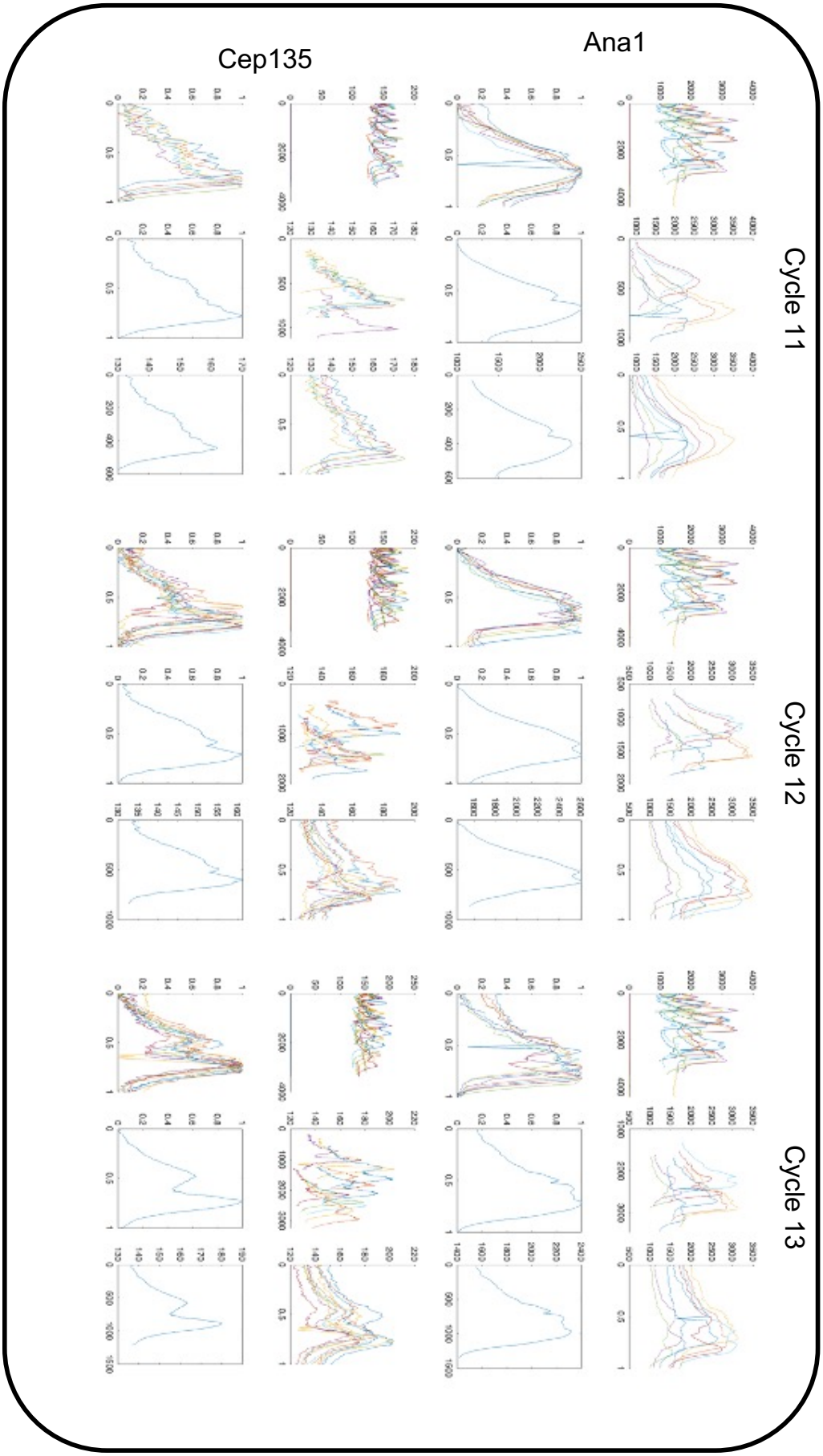
Ana1
Cep135
Cycle 11
Cycle 12
Cycle 13

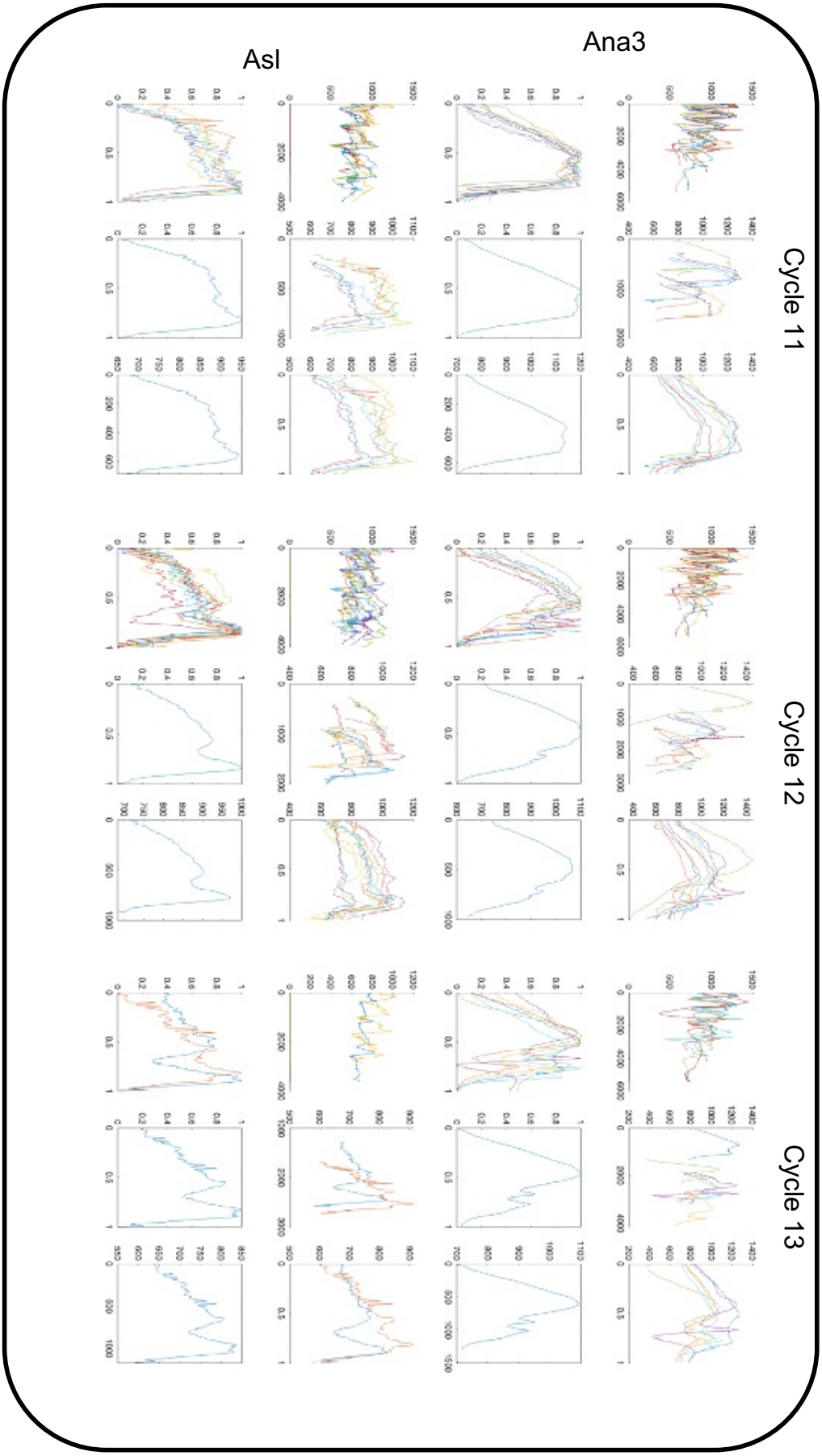
Ana3
Asl
Cycle 11
Cycle 12
Cycle 13

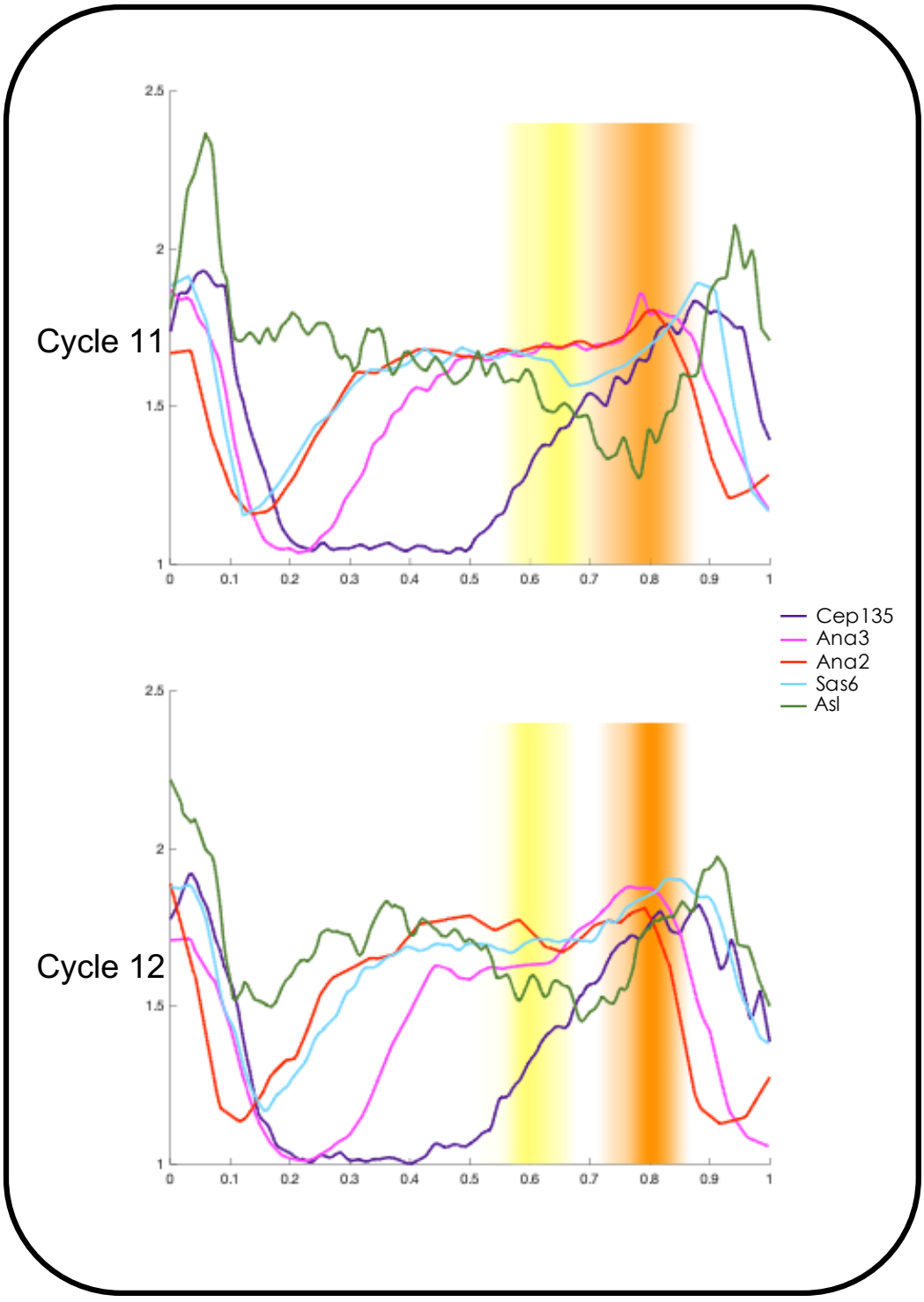

Supplementary Figure 4: Comparison of Cep135-GFP, Ana3-NG, Ana2-NG, Asl-GFP and Sas6-GFP appearance on the daughter *Comparison between Cep135, Ana3, Ana2, Asl and Sas6 cycle 11 & cycle 12 quantifications of centriole:centrosome ratio shown between M/A the previous cycle and the midbody breakdown in the next.*
Composite number of embryos: Cep135 Cycle 11 – 5, Cycle - 12; Ana3 Cycle 11 – 3, Cycle 12 – 5; Ana2 Cycle 11 – 2, Cycle 12 – 3; Sas6 Cycle 11 – 14, Cycle 12 – 2; Asl Cycle 11 – 6, Cycle 12 - 3